Supercritical water gasification

Decomposition of lipids forming a substantial part of sewage sludge

D. W. de Leeuw

TU Delft

Supercritical water gasification

Decomposition of lipids forming a substantial part of sewage sludge

by

D. W. de Leeuw

to obtain the degree of Master of Science
at the Delft University of Technology,
to be defended publicly on Monday November 13, 2017 at 1:00 PM.

P & E report number:	2859	
Student number:	4152867	
Project duration:	January, 2017 – November, 2017	
Thesis committee:	Prof. dr. ir. W. de Jong,	TU Delft, supervisor
	Dr. ir. P. V. Aravind,	TU Delft
	Dr. ir. H. B. Eral,	TU Delft
	Dr. H. W. Nugteren,	TU Delft
	Prof dr. ir. H. J. Heeres,	RuG

An electronic version of this thesis is available at http://repository.tudelft.nl/.

Cover picture by Dmitri Ma [1].

TU Delft

Abstract

Supercritical water gasification is a process in which wet biomass is converted to bio-syngas. In this process the temperature and pressure are raised above the critical point of water (374°C, 221 bar), creating a supercritical medium in which a high conversion and energetic efficiency of biomass to bio-syngas is realized. Due to these high efficiencies supercritical water gasification has received much attention as a potential treatment technique for sewage sludge from wastewater treatment plants.

To design a supercritical water gasification process kinetic models are used. They provide predictions on the decomposition products of the organic components of the biomass during treatment. However, kinetic data on lipids, which can make up to 25% of the organic matter in sewage sludge, are not available yet. This study aims to identify main reaction pathways and corresponding kinetic parameters that describe the decomposition of lipids in supercritical water.

Experiments were performed to provide data of decomposition products yields and find the dominant reaction pathways. Oleic acid was used as a model compound for lipids from sewage sludge. Experiments were conducted in a stainless steel batch reactor which was heated by immersion in a fluidized hot sand bath. Investigated temperatures and residence times were 400, 420, 460 and 520°C and 15, 35 and 65 min, respectively. Oleic acid feed concentration was 10 wt% and a pressure of 25 MPa was applied.

From experimental results the decomposition of oleic acid into aliphatic hydrocarbons and shorter chain fatty acids was identified. With increasing time and temperature these products would either gasify or the aliphatic hydrocarbons would dehydrogenate to cyclic and (poly)-aromatic compounds. A remarkably high selectivity towards the light hydrocarbon gases (C_2H_6, C_2H_4, C_3H_8, C_3H_6) compared to an earlier study into the decomposition of oleic acid in supercritical water was observed for all temperatures and residence times.

Parameters for a kinetic model, build up from the identified reaction paths, were fitted to the experimental data using Matlab. The Arrhenius equation was used to describe the reaction constants as function of temperature. For the oleic acid decomposition an activation energy of 151 kJ/mol was fitted first with a percentage output variation of 82% between 420°C and 520°C. Parameters for the other reactions were fitted using this activation energy as constraint.

Qualitative trends on the gas and liquid decomposition products distribution over time and temperature were predicted well by the model, but predictions on the quantitative yield of them were concluded to be inaccurate. Largest differences between experimental and model yields were observed for CH_4 and the light hydrocarbon gases.

One reason for these model errors is the scarcity of data points in the 0-15 min time-scale, where the process was highest in reactivity. Also some of the reaction pathways in the model might have been oversimplified, neglecting certain dominant decomposition reactions.

Contents

List of Symbols

Roman symbols

A	Arrhenius equation pre-exponential
C	Feed concentration
E_a	Arrhenius equation activation energy
K	Equilibrium constant
k	Reaction rate constant
P	Pressure
T	Temperature
v	Molar volume
x	Molar fraction
y	Species concentration

Greek symbols

σ	Standard error
$\sum_i$	Summation over all elements i
τ	Residence time
ζ	Conversion rate

Sub- and superscripts

mix	Mixture
mod	Model
sum	Summed

Abbreviations

mol%	Percentage by mole
ppm-by-mass	Parts per million by mass
vol%	Percentage by volume
wt%	Percentage by weight

List of Abbreviations

2D-GC	Two Dimensional Gas Chromatography
AD	Anaerobic Digestion
APR	Aqeous Phase Reforming
CGE	Carbon Gasification Efficiency
COD	Chemical Oxygen Demand
DBE	Di-n-Buthyl Ether
FA	Fatty Acid
FAME	Fatty Acid Methyl Esther
FID	Flame Ionization Detector
FIT	Percentage output variation
GC	Gas Chromatograph
GE	Gasification Efficiency
HC	Hydrocarbon
HTL	Hydrothermal Liquefaction
IP	Ionic Product
KIT	Kalsruher Institut für Technologie
LFA	Long-chain Fatty Acid
MS	Mass Spectometer
ODE	Ordinary differential equation
PAH	Poly-Aromatic Hydrocarbon
RF	Response Factor
RRF	Relative Response Factor
SCW	Supercritical Water
SCWG	Supercritical Water Gasification
SSE	Sum of Squared Errors
SSNE	Sum of squared normalized errors
STOWA	Stichting Toegepast Onderzoek Waterbeheer
TAG	Tryacylglyceride
TCD	Thermal Conductivity Detector
TG	Thermal Gasification
TMSH	Trymethylsulfonium hydroxide
TOC	Total Organic Carbon
VFA	Volatile Fatty Acid
WGS	Water-Gas-Shift

1

Introduction

Following the International Energy Outlook of the U.S. Energy Information Agency a worldwide energy consumption rise of 48% is predicted from 2012 to 2040 [3]. Currently the major sources of energy production are fossil fuels and depletion of their reserves combined with the increasing energy demand drives the transition to switch to renewable sources for energy production. Utilizing the energy stored in waste-streams can contribute to this transition.

In Energieagenda [4], a report of the Dutch Government on the transition towards a sustainable energy driven future, an important role is given to bio-fuels. Fuels that are produced from waste biomass should be used for transportation on a large scale. Gasification of biomass can produce such fuels. Besides usage as a transportation fuel, bio-syngas can also be used as a sustainable alternative to natural gas. Currently 40% of primary energy use in the Netherlands is provided by natural gas. One of the waste-streams gaining attention as a source of bio-syngas is sewage sludge, produced in wastewater treatment plants as by-product.

Sewage sludge has a medium high calorific value (8.5-17 MJ/kg on a dry basis [5]) and it is abundant: in the European Union production is more than 10.7 million tons annually based on dry sludge [6]. Conventional treatment methods of this sludge are anaerobic digestion (AD) or thermal gasification (TG). TG uses heat to decompose biomass to combustible gases under the presence of air or an inert gas. However, because of the high moisture content of sewage sludge (70-90 wt% [7, 8]) a drying step is required, which consumes a high amount of energy. This drying step is not needed for AD, but the process is relatively slow, in the order of weeks. These long residence times result in high costs for equipment and land.

A novel technique for the conversion of wet biomass into bio-syngas is supercritical water gasification (SCWG). Water is used as the reaction medium, so a drying step is not needed. Furthermore, at the conditions of supercritical water, reaction rates are accelerated resulting in required residence times in the order of minutes [7]. Yoshida et al. [9] evaluated the use of SCWG and other processes to produce combustible gases such as hydrogen and methane from wet biomass and calculated the total efficiency for heat utilization processes[1]. Figure 1.1 shows a comparison between these efficiencies of the different treatment techniques. Above a moisture content of 30 wt% SCWG has the highest thermal efficiency.

In order to design and operate a commercial SCWG plant that can treat sewage sludge, a good understanding on the reaction pathways and kinetics of the sludge is needed. Kinetic models

[1] total efficiency of heat utilization = $\frac{\text{heat from combustion of product gases}}{\text{energy in the biomass + net energy consumed by process}}$

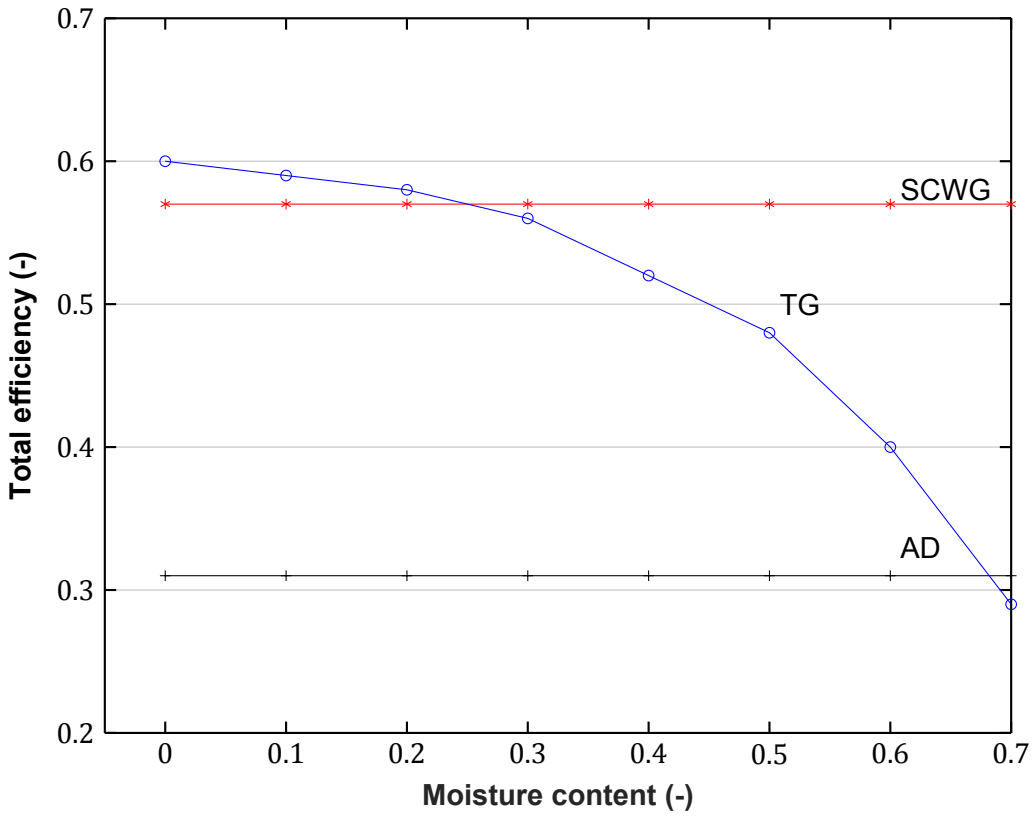

Figure 1.1: Total efficiency of heat utilization processes versus biomass moisture content [9].

can predict what residence times, process conditions and concentrations lead to the highest gasification efficiency (GE) and carbon gasification efficiency (CGE) for a specific reactor. The CGE and GE are defined as follows:

$$\text{Gasification Efficiency (GE)} = \frac{\text{mass of formed gas}}{\text{mass of dry feed}} \tag{1.1}$$

$$\text{Carbon Gasification Efficiency (CGE)} = \frac{\text{mass of carbon in formed gas}}{\text{mass of carbon in feed}} \tag{1.2}$$

Gensos BV is currently working on setting up a commercial SCWG plant for the gasification of different types of wet biomass. The integrated kinetic model developed by Yakaboylu et al. [10] is used for making predictions on CGE and GE. This model was made for the gasification behaviour of lignocellulosic biomass, containing cellulose, hemicellulose, lignin and proteins as main biochemical compounds. It does however not account for the presence of lipids, which can make up to 25% of the organic matter in sewage sludge [2].

Lipids kinetic decomposition in SCW should be implemented in the model, for the model to be able to give reliable predictions on the gasification behaviour of sewage sludge. Kinetic data on the decomposition of lipids in SCW conditions however has not been published in literature yet. Therefore an experimental study is needed that identifies and quantifies the main decomposition products of lipids in a SCWG process over a range of temperatures and times. The experimental data can then be used to extract from them reaction pathways and

corresponding reactions kinetics that can model the conversion of lipids in supercritical water.

This master thesis presents the results and conclusions of such a study into the decomposition of lipids in supercritical water. The main research question of this thesis is:

- *What are the main reaction pathways and corresponding kinetics of lipid decomposition in supercritical water, thereby improving the modeling of conversion of a sewage sludge SCWG process?*

Embedded in this question are the following subquestions that will be answered in this thesis:

- Which compound can act as a representative model compound for the SCWG of lipids from sewage sludge?
- What experiments and analyses are needed to build-up a kinetic model consisting of the main reactions of the SCWG of the model compound?
- Which reaction products are found from the experiments and what main reaction pathways can explain their presence?
- Which kinetic parameters can be fitted to these reaction pathways?
- Under which conditions and for what purposes can this kinetic model be used?

The structure of this thesis is as follows: in Chapter 2 a technical background on lipids and SCWG will be presented, followed by a review of published literature on the decomposition of lipids in SCW and related processes. In Chapter 3 the used experimental methodology is described. The results from these experiments and the reaction pathways identified from them are outlined in Chapter 4. The resulting kinetic decomposition model and its predictions based upon these reaction pathways will be discussed in Chapter 5. The conclusions of this thesis and recommendations for further research are given in Chapter 6.

2

Lipid SCWG background

This chapter presents a technical background and literature review on the SCWG of lipids, in order to find a proper model compound that can represent lipids as part of sewage sludge in experiments. Furthermore from literature a suggestion on how lipids decompose in a SCWG process is extracted.

In this chapter, the first section gives an explanation on what lipids are, and in what form they occur in sewage sludge. The second section presents the theory of using supercritical water to gasify wet biomass. In the third section experimental results of SCWG in general are discussed. The fourth section provides a literature review on possible decomposition pathways of lipids in SCW and related processes. This chapter concludes by presenting which model compound is chosen for the experiments and which decomposition pathways and products can be expected, based on literature.

2.1. Lipids in sewage sludge

Lipids can refer to any kind of natural occurring hydrophobic molecule. In biomass, the predominant amount of lipids are fats, which biochemically are tryacylglycerides (TAGs) [11]. These molecules consist of a glycerol group which is esterified with three fatty acids groups. Figure 2.1 shows an example of such a TAG. While the glycerol structure is well defined, the fatty acid (FA) groups carbon chain length can vary both in length and in degree of saturation. The majority of fatty acids in fats and oils consist of 12,16 or 18 carbon atoms [12, 13].

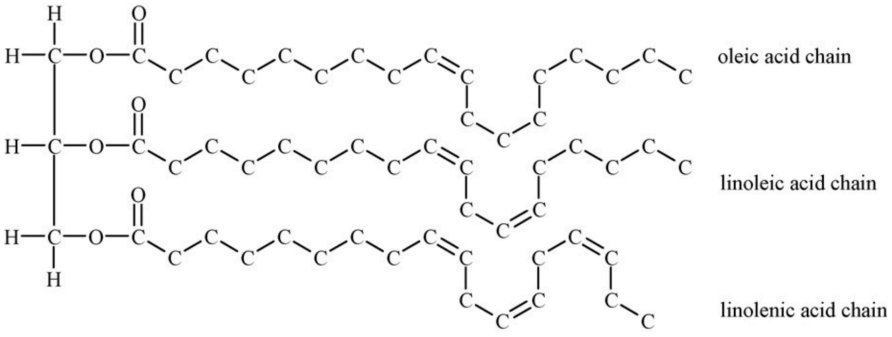

Figure 2.1: Molecular structure of a vegetable oil (example applies for rapeseed oil). This oil consist out of mono-unsaturated (oleic) and poly-unsaturated (linoleic and linolenic) C18 fatty acids [14].

Research into the characterization of fatty acids in lipids in sewage sludge shows that sewage sludge contains three main fatty acids. Boocock et al. characterized the composition of lipids in sewage sludge. Stearic (C18:0) and palmitic acid (C16:0) appeared to be the main fatty acids present, while also a significant amount of oleic acid (C18:1) was found [15]. This is in accordance with Réveillé et al. who identified the predominant components of the free fatty acids in sewage sludge as palmitic- and oleic acids [16].

2.2. Supercritical water gasification theory

Besides the fact that SCWG is relatively energy-efficient in comparison to other gasification techniques, as was shown in Chapter 1, the process also benefits from a change in physical properties when water is near or in its supercritical state, which is described first. Next, the chemical theory on SCWG and a comparison between theoretical and experimental results will be discussed.

2.2.1. Supercritical water properties

Water is in supercritical state when it has exceeded its critical point at 374 °C and 221 bar [17]. Near and at this state some thermodynamic properties of water change in such a way that water plays a role as reactant, solvent and catalyst for gasification of biomass [18]. Figure 2.2 shows the phase diagram including the critical point of water and important thermodynamic properties of water as a function of temperature.

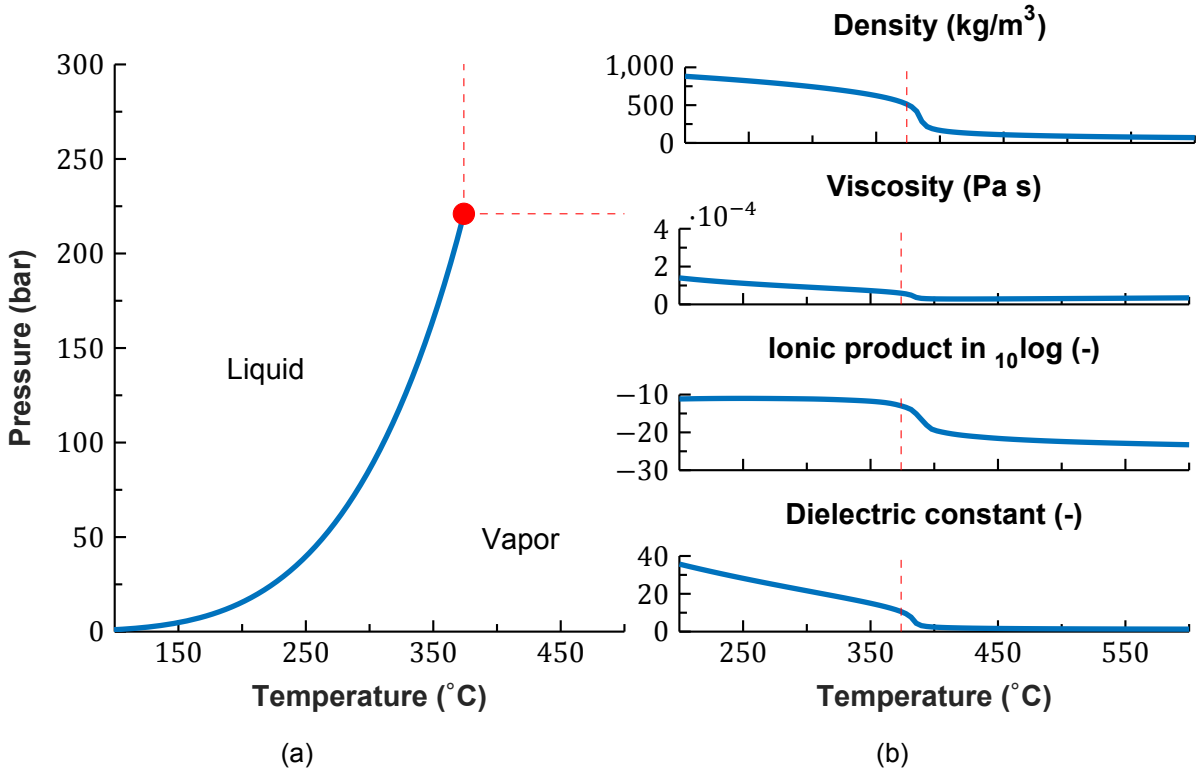

Figure 2.2: Phase diagram of water, showing the critical point of water (a) and important physical properties of water in sub- and supercritical conditions at 250 bar (b) [17, 19, 20]. Borders of the supercritical region are indicated with red dashed lines

The role of these physical properties and their influence on gasification behaviour is:

- **Density** Although the density of water significantly decreases above the critical point, it still has a typical liquid-like value. This relatively high density for these temperature levels enhances the solvation of compounds [21].
- **Viscosity** Mass transfer is limited by the viscosity. The decrease in viscosity of supercritical water to a gas-like viscosity thus causes an increase in mass transfer [21].
- **Ionic Product** The ionic product (IP) of water is an indication for the type of reactions that are dominant. At subcritical conditions the IP is relatively high, order 10^{-11}, resulting in mainly ionic reaction pathways. In these reactions water acts as an acid/base catalyst and can be a reactant itself. An example of these reactions is hydrolysis [22]. Beyond the critical point the IP decreases to 10^{-23}, indicating that the main reaction pathways are radical based. Water now merely acts as a transporter for free radicals and reactions are pyrolytic-like, such as cracking [14, 22].
- **Dielectric constant** Under standard conditions water is an excellent polar solvent due to its high dielectric constant; most salts are highly soluable in water [23]. Therefore miscibility with non-polar substances such as gases and hydrocarbons is low. The drastic decrease in dielectric constant of water when in the supercritical phase makes the water behave as a non-polar solvent. Hydrocarbons and gases are now completely miscible in water, while salts have poor solubility. King et al. [24] found that canola oil solubility in water increases with temperature and water and the oil become an homogeneous phase at 339 °C. When a compound is completely miscible in water there are no phase boundaries anymore, which increases mass transfer by diffusion. This then leads to fast and complete reactions between the water and biomass components [22]. Furthermore, because the solvation properties of the water can be tuned with temperature near the critical region, partitioning of products or by-products into seperate phases can be used to separate and purify products [25].

In order to quantify and compare results from different gasification processes the following parameters, besides the CGE (Equation 1.2) and GE (Equation 1.1), are often used:

$$\text{Total Organic Carbon (TOC)} = \frac{\text{mass of organic carbon in liquid effluent}}{\text{volume of liquid effluent}} \tag{2.1}$$

$$\text{Chemical Oxygen Demand (COD)} = \frac{\text{mass of oxygen needed to completely oxidize liquid effluent}}{\text{volume of liquid effluent}} \tag{2.2}$$

2.2.2. SCWG chemical theory

Theoretically SCWG can be seen as an aqueous phase reforming (APR) method, producing hydrogen from biomass, as a potential, clean combustion, bio-fuel [26]. The general reaction can be written down as:

$$\mathrm{CH_xO_y} + (1-\mathrm{y})\mathrm{H_2O} \longrightarrow \mathrm{CO} + (1 - \mathrm{y} + \frac{1}{2}\mathrm{x})\mathrm{H_2} \tag{2.3}$$

Because of the high temperature of the process the water-gas shift (WGS) Reaction 2.4 and methanation Reactions 2.5 and 2.6 also play an important role in redistributing the gases.

$$CO + H_2O \longleftrightarrow CO_2 + H_2 \tag{2.4}$$

$$CO + 3\,H_2 \longleftrightarrow CH_4 + H_2O \tag{2.5}$$

$$CO_2 + 4\,H_2 \longleftrightarrow CH_4 + 2\,H_2O \tag{2.6}$$

Youssef et al. [2] performed an equilibrium calculation on the SCWG of oleic acid as a model compound of lipids in sewage sludge. Figure 2.3 shows the amount of moles of the different gas products formed per mol of oleic acid as a function of temperature. For these calculations a 100% oleic acid conversion was assumed. At higher temperatures the formation of H_2 is favored over the formation of CH_4 which is reported as a general trend in SCWG [26].

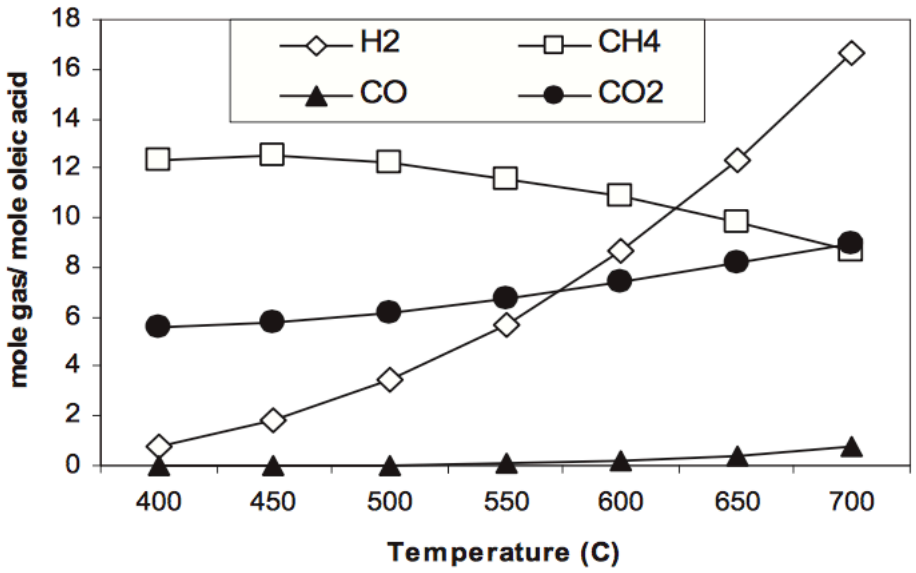

Figure 2.3: Calculated equilibrium gas yield as a function of temperature at 28 MPa and 10 wt% oleic acid [2]

From non-catalytic experiments between 400-500°C in a batch reactor for 30 minutes, four important observations were made:

1. The H_2 gas yield increased with temperature
2. The oleic acid was not fully converted as assumed in the equilibrium calculations.
3. Even when accounting for the converted oleic acid only, H_2 yields were between 40-60% lower than calculated.
4. Significant amounts of residual liquid products are formed, such as aromatics.

It can thus be concluded that equilibrium calculations can predict just general trends in gasification behaviour. Besides the simple Reactions 2.3 to 2.6 other side-reactions play a significant role in SCWG processes.

To improve predictions based on equilibrium calculations Yakaboylu et al. [27] proposed a constrained equilibrium model, in which additional values such as the CGE and the yields of gases such as hydrogen and methane form a constraint for solving the equations. This model

showed to give good predictions on distribution of product gases of SCWG experimental data, without the need to know all the side-reactions. The constraints that are needed for this model are however very process specific, which means that additional experiments are still needed to make reliable predictions.

The conclusion that can be drawn from this is that to make good predictions on formed products, experimental research is needed to identify the detailed decomposition reaction pathways and their kinetics. Process parameters and catalysts that suppress the unwanted side-reactions and promote the gasification reactions can then be found, which is one of the necessary steps to develop SCWG into a commercial process.

2.3. SCWG experimental studies

One of the first significant experimental results on SCWG of biomass was presented by Modell [28], who quickly immersed wood sawdust into supercritical water. The sawdust quickly decomposed to tars and gases without the formation of chars. This was an important breaktrough, since char is an unwanted byproduct of gasification and so far gasification of wood sawdust without char formation was not reported [29].

Research into the SCWG of different types of wet biomass followed. Corn- and potato-starch gels were gasified by Antal et al. [29] in tubular reactors using activated carbon as a catalyst at temperatures higher then 650°C and a pressure of 28 MPa. The results were very promising, showing GE values exceeding 100%, which is possible since some of the hydrogen formed originates from water, and a maximum CGE of 89% for potato-starch was reported. Other wet biomass types that have been subject of SCWG research experiments are for instance algae, manure and sewage sludge.

2.3.1. Sewage sludge

The first results of SCWG of sewage sludge were presented by Xu and Antal [30]. Using an activated carbon catalyst from coconut shell they continuously gasified mixtures of sewage sludge and corn starch. They were able to gasify the mixtures at 650°C and 28 MPa, with hydrogen as main gas product: 0.42 mol/mol gas. However, even at low solid loadings (2.1 wt% sludge and 5.1 wt% starch) plugging occurred within a couple of hours due to the high ash content of the sludge.

To overcome this plugging Chen et al. [31] used a fluidized bed reactor to continuously gasify sludge in SCW. They also looked at the influence of temperature on the hydrogen yield, gasifying at temperatures between 480-540°C. The highest hydrogen yield as well as the highest CGE was reported at the highest temperature of 540°C.

Increasing the SCWG temperature of sewage sludge however also promotes the formation of toxic poly-aromatic hydrocarbons (PAHs) as Xu et al. [32] showed. They found that when the temperature exceeded 400°C and residence times were longer then 60 min the formation of PAHs from the SCWG of sewage sludge was promoted. Adding H_2O_2 as an oxidant to the process was proposed as method to promote the degradation of PAH molecules. Gong et al. [8] followed up on this research and looked at the PAH formation of 10 different sewage sludge sources during SCWG. Comparing these sources and their gasification products it was concluded that the crude fat and carbohydrate content can promote lower-molecular-weight PAH formation, while lignin and humic substance content can promote higher-molecular-weight PAH formation. This indicates that the organic matter composition in raw sludge has a high impact on the PAH distribution.

Stichting toegepast onderzoek waterbeheer (STOWA), a Dutch research group in the field

of water management, have let the Karlsruher Institut für Technologie (KIT) perform SCWG tests with sewage sludge from the Netherlands [33]. KIT has its own pilot plant for SCWG, VERENA, which has a feed limit of 100 kg/h. Figure 2.4 shows the processcheme of VERENA. The VERENA pilot plant was tested with a continuous sewage sludge feed of 48-50 kg/h, gasifier temperatures between 470-650° and pressures between 270-280 bar. Two continuous operational test of 5.4 and 7.5 h were realized. The results on the carbon gasification efficiency were promising, realizing values as high as 57% . However plugging of the reactor and the formation of significant amount of PAHs were stated as some of the main issues that deserve further attention before scaling up the process. Gaining knowledge on sludge decomposition in SCW to locate the possible source(s) of these issues, is therefore vital.

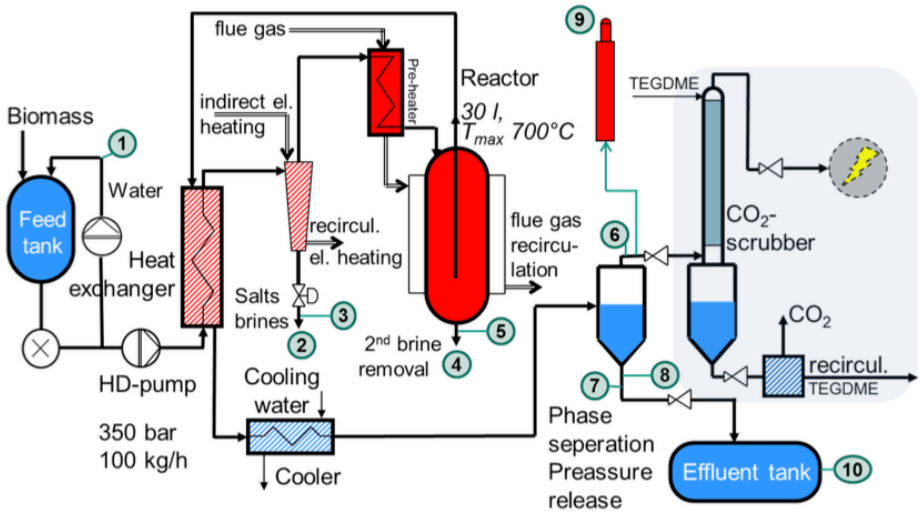

Figure 2.4: Processcheme VERENA of KIT [33]

2.3.2. Model compounds

Real biomass most of the time consists out of a multitude of organic compounds, which makes the decomposition chemistry complex. To obtain a better understanding of the reactions that occur when gasifying biomass in supercritical water, research into the SCWG of organics that can act as model compounds for real biomass is necessary. The main biochemical compounds of sewage sludge are proteins (about 40%), lipids (10-25%), carbohydrates (about 14%) and lignin (about 17%) [7][34]. Often used models for these compounds are glycine, fatty acids and glycerol, glucose and guaicol, respectively. Main reaction pathways and kinetics for glycine [35], glycerol [36], glucose [37] and guaicol [38] decomposition in supercritical water have been proposed, but not for fatty acids.

As presented in 2.2.2 Youssef et al. [2] performed both catalytic and non-catalytic gasification experiments in supercritical water with oleic acid as model compound for lipids in sewage sludge. The aim of this study was a catalyst screening and only three non-catalytic experiments were performed at a temperature of 400, 450 and 500°C, pressure of 280 bar and residence time of 30 min. Because of this single residence time kinetic parameters cannot be found from their experimental data. Possible reaction pathways were identified nonetheless, as shown in Appendix A.

Azadi et al. [39] performed a comparison on the SCWG behaviour of different model compounds resembling compounds in sewage sludge, which can give an idea on the reaction rates

for gasification of fatty acids in comparison to other model compounds. They used glucose, glycine, glycerol, lauric acid and humic acid, representing carbohydrates, proteins, alcohols, fatty acids and humic substances in sewage sludge, respectively. It was found that humic acid had the lowest CGE, followed by lauric acid. It can be expected then, that the reaction rates for gasification of fatty acids are generally lower than for carbohydrates, proteins, alcohols and lignin.

2.4. Lipids decomposition pathways

The absence of reported main decomposition pathways and corresponding kinetics of lipids in supercritical water for gas production, leads to the investigation of related processes in which lipids are decomposed. Hydrothermal liquefaction (HTL) and pyrolysis are such related processes and the decomposition of lipids to bio-based fuels and chemicals using these techniques has been subject of many research papers.

In HTL a biomass is liquified in subcritical water, which is water at temperatures between its atmospheric boiling point and its critical point. The reactor is pressurized, so that the water stays in liquid phase. This way HTL benefits from some of the same physical properties as pointed out in Section 2.2.1, such as a high density and low dielectric constant. The relatively high ionic product of subcritical water accelerates ionic reactions which resembles reactions in a SCWG process in near-critical regions.

Pyrolysis is a process that occurs within the same temperature range of SCWG, 300-600°C, but at lower pressures, 1-10 bar. Furthermore water is not present as a reaction medium. The biomass is pyrolyzed in a inert atmosphere to prevent oxidation. The main reaction pathways are radical based, as are the reaction pathways of SCWG at high temperatures, as was described in Section 2.2.1.

Much research into the decomposition and reaction kinetics of glycerol, the backbone of a lipid, in SCW has been performed. Because of rising bio-fuel production, with glycerol as main by-product, glycerol prices have been dropping. This drives investigation into their decomposition into fuels and base-chemicals [40]. Buhler et al. [41] looked at both ionic and free radical pathways of glycerol in SCW in great detail. An extensive kinetic model was proposed. The scope of this thesis however is aimed more at the fatty acid conversion in SCW, since this is much less understood. Therefore a further detailed literature overview of glycerol SCWG experimental results will not be given here.

In this section a literature review on the HTL of lipids will be presented first. Secondly, results on the pyrolysis of lipids will be discussed. From both processes a prediction on possible lipid decomposition pathways in SCW can be made, where HTL represents reactions at near-critical conditions and pyrolysis represents reactions at high temperature supercritical conditions.

2.4.1. Lipid hydrothermal liquefaction

In a hydrothermal reaction medium TAGs, the lipids in biomass, quickly hydrolyse into their corresponding free fatty acids and glycerol [11]. Holliday et al. [42] did pioneering work on the hydrolysis of vegetable oils in hydrothermal media. They reported a 97% conversion of oils into free fatty acids between 15-20 min at temperatures between 270-280 °C. At these temperatures the free fatty acids were stable. When the temperature was increased to 300-375 °C the decomposition of fatty acids into a dark brown oil was observed for reaction times between 8-15 min.

This further fatty acid decomposition was studied by Fu et al. [43] who reported on the

hydrogenation and decarboxylation of fatty acids at 330°C with a Pt/C catalyst and residence times ranging from 0.5-2.5 h. It was shown that stearic acid, palmitic acid and lauric acid decarboxylized into heptadecane at the same rate, indicating that the carbon chain length of a fatty acid did not influence the decarboxylation reaction. Oleic acid, a mono-unsaturated fatty acid, was expected to yield a high amount of heptadecene, while this decomposition mainly produced stearic acid and heptadecane. Linoleic acid decomposition showed a similar reaction pathway, however significant amounts of heavy liquid products were detected, such as aromatic and cyclic compounds. This lead to conclude that the degree of unsaturation strongly influences the decarboxylation reactions. A reaction scheme was proposed, see Figure 2.5, where hydrogenation is preferred over decarboxylation, with main product heptadecane. Hydrogen was assumed to be formed in-situ by APR. For poly-unsaturated fatty acids cyclization and aromatization also occured.

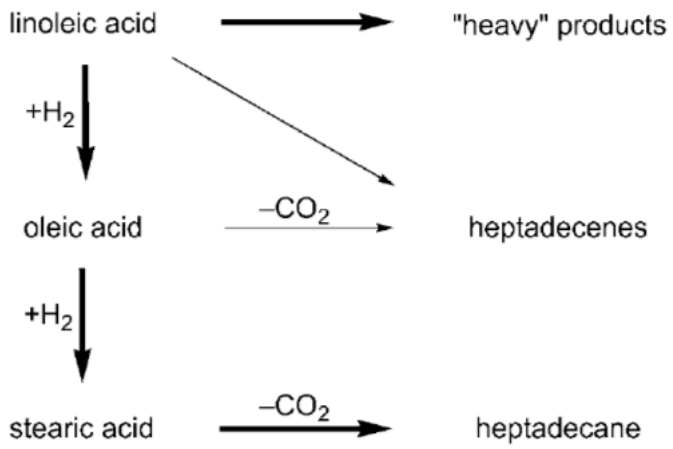

Figure 2.5: Hydrothermal catalytic reaction pathways for C18 fatty acids [43]

To speed up the deoxygenation of fatty acids into alkanes for continuous biodiesel production, Popov and Kumar [44] looked into the use of formic acid as an in situ source of hydrogen, so unsaturated fatty acid oleic acid would rapidly hydrogenate to stearic acid. Activated carbon was used as a catalyst at temperatures of 350-400°C and a residence time of 21 min, while pressure was mainted at 24.1 MPa. Indeed, addition of formic acid for in-situ hydrogen production resulted in heptadecane yields as high as 70% at 380°C. From this temperature on significant amount of gases started to form and at 400°C 22 wt% of the products were gases. Table 2.1 shows the distribution of gaseous products at 380°C.

Table 2.1: Yields of gaseous products from activated carbon catalyzed hydrothermal decomposition of oleic acid at 380°C and 24.1 MPa [44]

Compound	**Yield (wt%)**
Hydrogen	25.0 ±2
Methane	8.3 ±2
Carbon monoxide	3.5 ±1
Carbon dioxide	37.5 ±3
Ethane	4.0 ±1
Propane	21.7 ±2

It was concluded that one group of gases (H_2,CO,CO_2) arose from decomposition and deoxygenation of oleic and formic acids. The other group (CH_4,C_2H_6,C_3H_8) arose from the cracking of fatty acids and alkanes.

Vardon et al. [11] performed a similar experiment as Popov and Kumar. They used a somewhat lower temperature of 300°C in HT conditions, Pt-Re/C catalyst and glycerol for in situ hydrogen production. The reaction pathways presented were similar to Popov and Kumar, and it was concluded that with a natural 3:1 oleic acid:glycerol ratio oleic acid hydrogenation to stearic acid was completed within 15 min. When extra hydrogen was added to the process, reduction products from stearic acid, such as octadecane, were detected. This indicated the presence of the reduction reaction of the carboxylate group, as a secondary deoxygenation pathway, besides decarboxylation.

2.4.2. Lipid pyrolysis

In order to produce relatively light liquid fuels for transportation Dupain et al. [14] looked into the thermal and catalytic cracking of rape-seed oil and stearic and oleic acid as fatty acid model compounds. For rapeseed oil at 525°C the decomposition of the TAGs to fatty acids is fast: within 5.8 s TAG conversion was 91 wt%. The conversion of fatty acids to gasoline products is significantly lower however. A decomposition very similar to rapeseed oil was found with oleic acid, which could be expected as 60 wt% of rape-seed oil consists out of oleic acid. Stearic acid pyrolysis however resulted in a much higher gas and gasoline yield and lower aromatic yield compared to oleic acid. It was therefore concluded that the rate of aromatisation is highly dependent on the olefinicity of the fatty acid. The serial cracking to light hydrocarbon (HC) products (C_3 and C_4) was limited by the aromatisation of gasoline products.

Oleic acid was pyrolyzed at temperatures between 390 and 450°C and pressures between 1.0 and 3.1 MPa by Asomaning et al. [45]. Opposed to Dupain et al., who looked at residence times of 0-8 s, they used larger residence times of 0.5-8 h. An almost complete conversion of oleic acid was reported at 450°C after 4 h. Increasing the temperatures resulted in a significant rise in gas products and aromatic compounds formed. From the specific carbon chain lengths of the alkane and alkene formed products it was stated that the cleavage of the weak allylic C-C bond compared to other C-C bonds was preferred over other cleavage reactions. This was reasoned from the selectivity to C_6 to C_9 alkanes, C_6 to C_{10} alkenes and the absence of C_{12} to C_{15} alkenes as shown in Figure 2.6.

2.5. Conclusion

From the literature presented in this chapter, it was shown that SCWG has a high potential for converting wet biomass, and more specifically sewage sludge, to hydrogen and other high calorific gases. The thermodynamic and chemical theory on SCWG presented SCW as a highly reactive medium for the gasification of biomass, which is endorsed by experimental results. The level of knowledge on the decomposition of sludge in SCW that is needed to scale up this process is however not yet reached. Especially the decomposition and kinetics of the lipid compounds in sewage sludge in a SCW environment has not been described yet. Therefore to effectively model the kinetic decomposition of lipids in SCW experiments are needed. For performing experiments that can lead to a reaction model, a suitable model compound was chosen, which will be presented here. Furthermore an overview on possible reaction pathways of fatty acid SCWG will be shown.

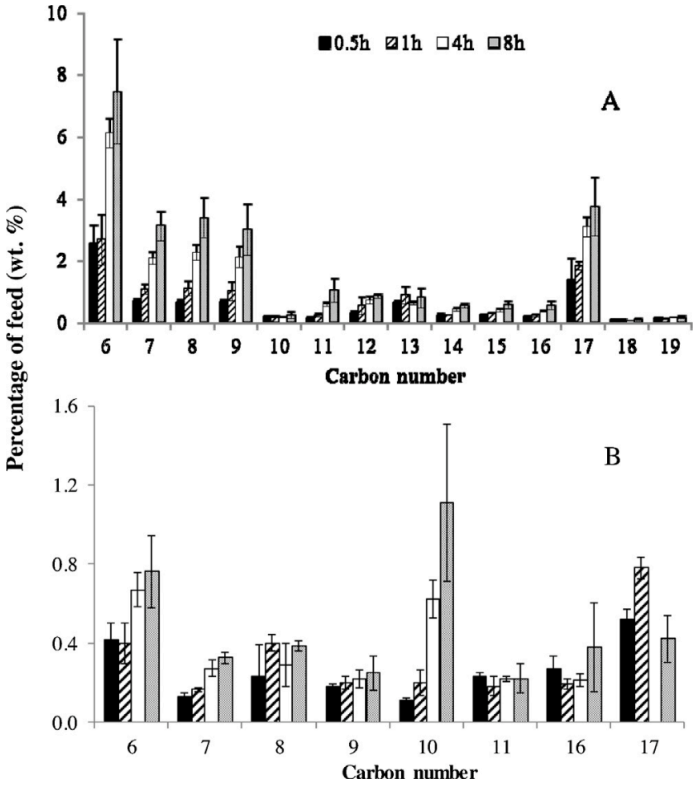

Figure 2.6: Percentage of alkanes (A) and alkenes (B) from oleic acid pyrolysis at 390°C as a function of carbon number and reaction time [45].

2.5.1. Model compound

Since the first decomposition step in SCWG is often a fast hydrolysis step [26], a model compound is normally chosen as the product of this hydrolysis. This enables a reaction model to be simpler in the chemistry, while still being representative. For instance, glucose is the main product of the hydrolysis of carbohydrates. As discussed in Section 2.3.2, glucose is commonly used in literature as model compound for carbohydrates.

It is presented in Section 2.4.1 that lipids quickly hydrolyze to FAs and glycerol in hydrothermal water. SCWG of glycerol has been covered by literature very well, but SCWG of FAs, which are the main products of the hydrolysis, has not. The model compound for lipid SCWG was therefore chosen to be a fatty acid.

In choosing a FA for building up a kinetic model on lipid SCWG, three main requirements were set:

1. The fatty acid should be a significant component of the lipids found in sewage sludge.
2. The fatty acid decomposition should be subject of multiple studies.
3. The fatty acid should be commercially available.

Based on these demands the preferred model compounds would be oleic acid or stearic acid. The noncatalytic decomposition of oleic acid in SCW has been studied before by Youssef et al. [2], while this has not been done for stearic acid. Therefore oleic acid was chosen as a model compound, so a good comparison between experimental results could be made.

2.5.2. Reaction pathways

From literature shown in this chapter on SCWG in general and on the HTL and pyrolysis of lipids, possible decomposition pathways of fatty acids in SCW have been bundled. Since the chosen model compound is oleic acid, the decomposition of this mono-unsaturated fatty acid was highlighted.

Oleic acid can decompose via C-C bond cleavage, decarbonylation and decarboxylation to shorter chain FAs and aliphatic hydrocarbons. If hydrogen is present the unsaturated oleic acid can also hydrogenate to the saturated stearic acid. The short chain FA and saturated FA both decompose through decarboxylation and decarbonylation to aliphatic hydrocarbons. At higher temperatures and residence times the aliphatic hydrocarbons will form cyclic hydrocarbons and aromatics, thereby producing H_2.

Production of CO,CO_2 and H_2 gases besides the reactions mentioned above will most likely come from gasification reactions of short chain FAs. Methane and other light hydrocarbon gases, such as ethane and propane, are formed via the cracking of short fatty acids or aliphatic hydrocarbons. The aromatics are more stable and do not decompose to gases.

A schematic overview of this reaction scheme can be seen in Figure 2.7 and the names of the reactions numbered in the Figure can be found in Table 2.2.

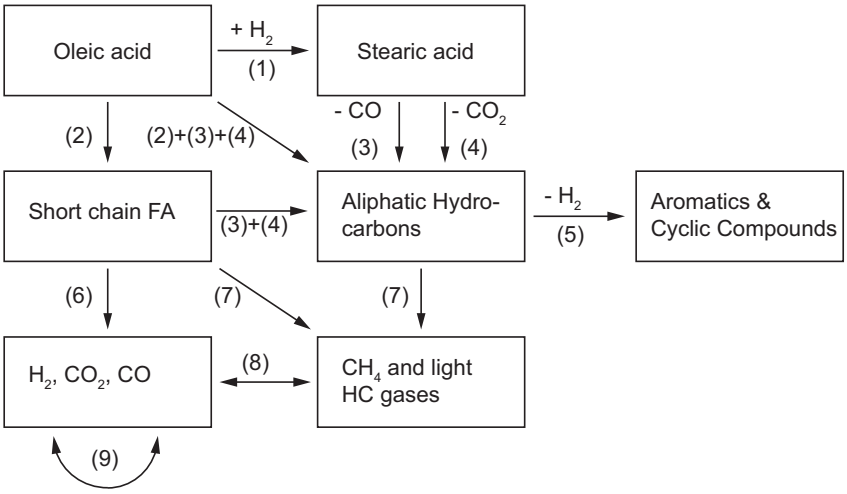

Figure 2.7: Expected decomposition pathways of SCWG of fatty acids based on HTL and pyrolysis experiments

Table 2.2: Reactions as proposed in Figure 2.7

Number	Reaction
1	Hydrogenation
2	C-C bond cleavage
3	Decarbonylation
4	Decarboxylation
5	Aromatization and Cyclization
6	Gasification
7	Cracking
8	Methanation
9	Water-gas-shift

This expected reaction scheme is in good accordance with the proposed possible reaction scheme of Youssef et al. [2]. Besides the reactions listed in Table 2.2 their reaction scheme includes a more detailed cyclic and aromatic formation route and the thermal decomposition of hydrocarbon molecules splitting into its elements was also proposed as a reaction pathway to gaseous products. Furthermore dehydrogenation of fatty acids was identified as possible formation route to the production of detected linoleic acid. Their reaction scheme is presented in Figure A.1 and Table A.1 in Appendix A.1.

Experimental data are needed to identify from all these reactions the ones that describe the non-catalytic decomposition of oleic acid in SCW the best. The next chapter will therefore present a methodology on experiments and analyses that can provide these experimental data.

3

Experimental methodology

In order to find to which products oleic acid decomposes and what their yields are in a non-catalytic SCWG process, experiments were conducted. In this chapter an overview and explanation on the used methodology for the experiments and chemical analyses is given.

In the first section the conditions applied in the experiments will be explained and presented. The second section describes the methods and materials used to accommodate the desired experimental conditions. The third section presents the used techniques to sample and analyze the liquid and gaseous products from the reactor after the experiment. The last section presents results of a test to validate the experimental set-up using glycerol.

3.1. Experimental conditions

The conditions applied in these experiments should be representative for real sewage sludge SCWG processes. Furthermore, these conditions should be varied to allow for the formation of a kinetic model from the experimental results. The important parameters used by a SCWG process are feed concentration, temperature and residence time.

It was chosen to use a single feed concentration, while varying temperature and residence time. The choice for the specific values of these three parameters is discussed in this section. Since compared to the effect of pressure, temperature and residence time play a more important role in gas composition [7], it was chosen to use a constant pressure of 25 MPa for all experiments.

3.1.1. Feed concentration

Feed concentration has a significant effect on the SCWG of biomass, where in general a higher feed concentration leads to more polymerization reactions of intermediate products, lowering the gasification efficiency. Approximately 80 wt% of sewage sludge is water, and of the remaining 20 wt% solids about 50 wt% is organic matter. The other solids are ashes [8].

The relative amount of gasifiable and reactive products that are present in the reactor should resemble the real sludge availability of reactive products. Since volatile matter is the organic matter in sewage sludge, the experiments are performed with a 10:90 model compound:water mass ratio. This also gives the opportunity to be able to compare results with Youssef et al. [2] who used 10 wt% oleic acid for their experiments.

3.1.2. Temperature

In SCWG processes biomass is generally brought to supercritical conditions by heating the pressurized feed from room temperature to the desired temperature. Figure 3.1 shows the temperature of water as a function of enthalpy at constant pressure. What is most important to notice is that around the critical point the temperature curve flattens.

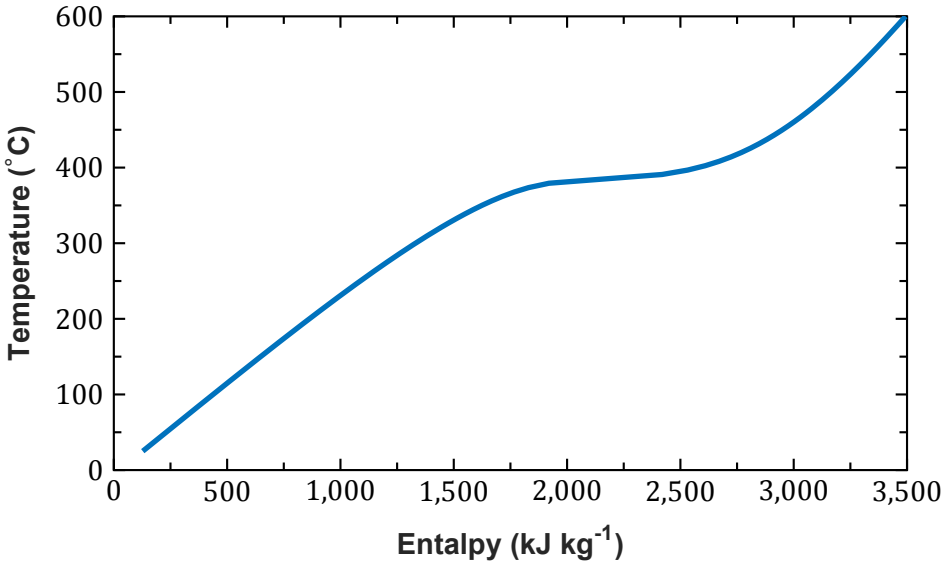

Figure 3.1: Temperature as a function of enthalpy for water at a pressure of 25 MPa [17]

This implies that the transition from sub- to supercritical takes a great amount of energy. Delivering this energy to the feed takes time, as shown in the Figure 3.2. The residence time is plotted here as a function of temperature for the pilot process of Gensos. The time needed to reach the higher temperature supercritical reactions is a significant part of the overall residence time. This implies that decomposition reactions in near-critical regions play an important role in the gasification process, besides the reactions in the higher temperature supercritical region.

Section 2.2.1 showed that reaction mechanisms at subcritical and supercritical conditions are ionic and radical based, respectively. Decomposition reactions in the near-critical regions can be a combination of radical and ionic reactions. Therefore to ensure experimental work that is representative for the Gensos process different temperature levels from near-critical to high temperature supercritical have to be examined. Four conditions, related to temperature levels, were chosen:

1. Near-critical condition (400°C)
2. Low temperature supercritical condition (420°C)
3. Average temperature supercritical condition (460°C)
4. High temperature supercritical condition (520°C)

3.1.3. Residence time

Reaction kinetics describe the concentration of compounds over time. It is thus vital to perform experiments at varying residence times, so reaction pathways can be identified and the proceedings of compounds concentration in time can be used to fit parameters of the kinetic

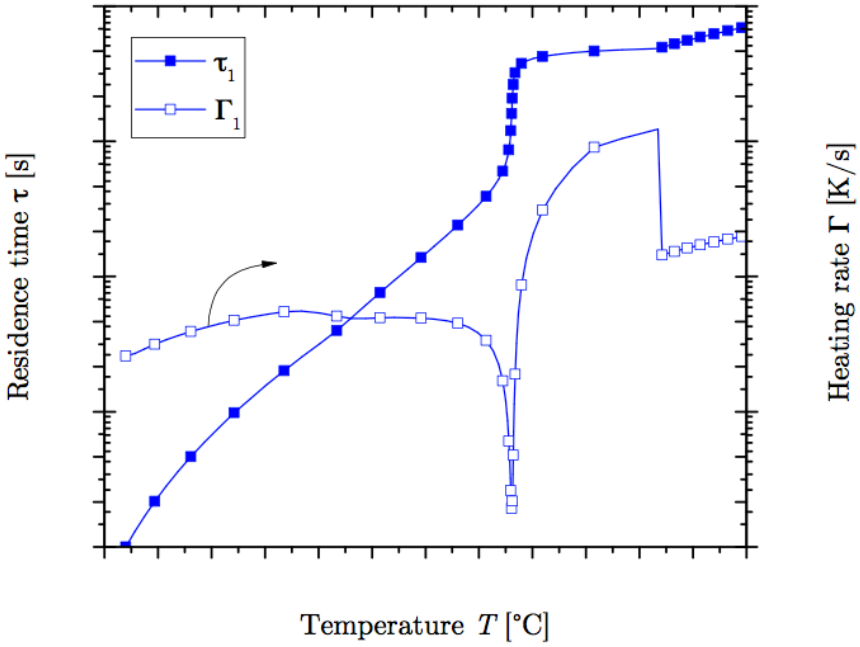

Figure 3.2: Residence time and heating rate of the feed as a function of temperature for the Gensos pilot plant [46]. Axis labels have been removed because of confidential information.

model. At a temperature of 500 °C and a residence time of 30 min, the SCWG of oleic acid reached a 52% CGE [2]. Higher CGEs are needed to make an SCWG process a competitive alternative for conventional gasification techniques. Higher residence times will generally lead to higher CGEs and therefore Gensos is also looking to extend residence times up to 60 min. For this reason the desired residence times are 10, 30 and 60 min. To allow for heat-up and cooling time, as will be described in Section 3.2.4, the experimentally used residence times are 5 min longer than theoretically desired residence times.

Table 3.1 gives an overview of the applied experimental conditions.

Table 3.1: Applied process conditions for the performed experiments

Process Condition				
Temperature (°C)	400	420	460	520
Residence time (min)	15	35	65	
Feed concentration (wt%)	10			

3.2. Materials and experimental setup

The used equipment, materials and methods to accommodate the desired experimental conditions are discussed in this section. The used chemicals and equipment for the SCWG process will be first described. This is followed by a description on the method of loading the reactor and inserting and removing it from the sand bath. Finally the measurements and calculations used to find the heat-up- and cool-down times are presented.

3.2.1. Chemicals used

Oleic acid, the model compound used in this study, and glycerol were purchased from Sigma-Aldrich. Both had a purity of ≥99% and were used without further purification. A list of other chemicals used for analysis can be found in Appendix C.4

3.2.2. Equipment setup

The SCWG process was conducted in a cylindrically shaped batch reactor, made from 316 SS with an inner diameter of 16.5 mm and height of 59.5 mm. This reactor vessel was connected to a pressure indicator and valve via Swagelok tube fittings, having a total length of 410 mm and 3.6 mm inner diameter. The volume of the whole connected reactor system was determined experimentally by removing the air from the empty closed reactor using a vacuum pump and subsequently attaching a water hose to the valve. The reactor would then be completely filled with water. The weight difference between an empty reactor and reactor filled with water was a measure for the total volume. This volume was determined to be 16.4 mL.

The desired reactor temperature was obtained by immersing the reactor in a fluidized sand bath until just above the valve and pressure indicator, since they could not withstand the high temperatures. The particles in the bath were made of aluminum oxide. Three heating elements were actively controlled using measurements from a thermocouple placed in the sand bath.

Figure 3.3 shows a schematic drawing of the used experimental setup.

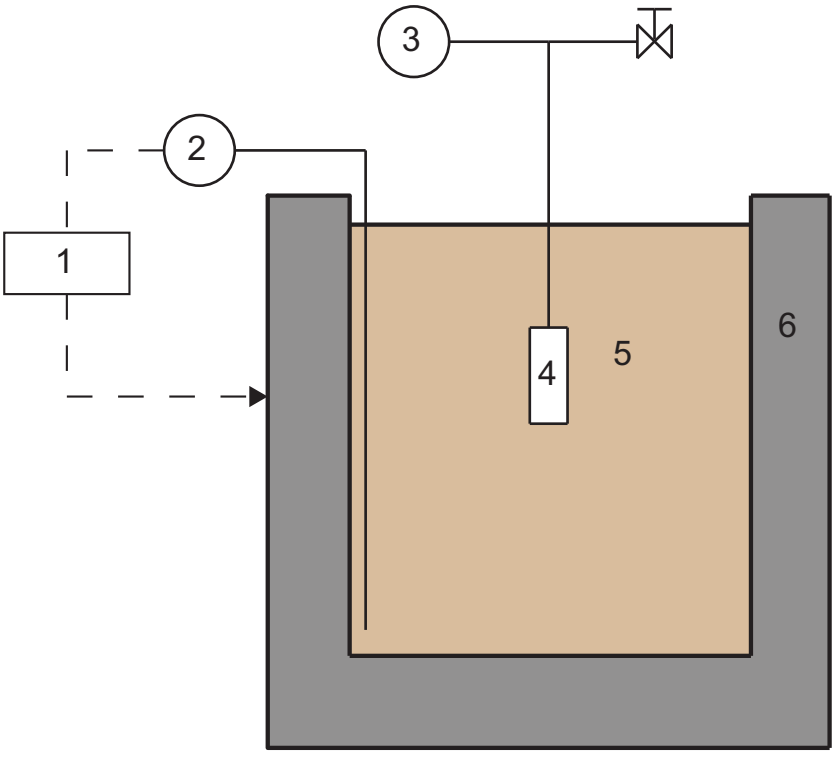

Figure 3.3: Schematic drawing of used experimental setup. 1: PID-control scheme; 2: Temperature reader; 3: Pressure reader; 4: Reactor; 5: Fluidized sand bath; 6: Heating elements

3.2.3. Experimental design

The first step in an experiment was to load the amount of demineralized water and oleic acid specific for that temperature level into the reactor. Hereafter the reactor was closed and oxygen present in the system was removed by purging with nitrogen three times. The reactor

was then weighed, pressurized with N_2 and weighed again. This was done to know the exact amount of nitrogen in the reactor, since it would be used later as an internal standard for the gas products analysis. The total amount of mixture supplied to the reactor was adapted to obtain the desired pressure of 25 MPa at the specific experimental temperature.

The amounts of products in the mixture added to the reactor for different temperature levels is shown in Table 3.2. These amounts were found by a trial and error approach using thermodynamic software calculations as a first trial. The calculations and measurements performed to obtain the initial reactor mixture loading can be found in Appendix A.2.

Subsequently the reactor was placed in the fluidized sand bath. After the desired reaction time had elapsed, the reactor was removed from the sand bath and quickly immersed in another sand bath at room temperature. After 30 min the cooled down reactor was removed from the cold sand bath for sampling. Results of pressure measurements performed during the experiments can be found in Appendix B.1

Table 3.2: Initial loading of N_2, water and oleic acid into the reactor

Temperature (°C)	Water (g)	Oleic Acid (g)	N_2 Pressure (MPa)
400	2.3	0.256	3.1
420	1.9	0.211	3.1
460	1.5	0.167	4
520	1.2	0.133	3.3

3.2.4. Heat-up and cool-down times

Heat-up- and cool-down times need to be defined to correct the residence time in the sand bath to an actual residence time at desired temperature, because of the thermal inertia of the reactor system. For clarity the term residence time will be used from here on as the actual time the reactor has spent in the heated sand bath. Reaction time will be used for the correction of the residence time for heat-up and cool-down times.

Temperature profiles during heat-up and cool down at different sand temperatures were determined using a similar reactor as described in Section 3.2.2 equipped with an extra thermocouple inside the reactor. This reactor was loaded with the same amount of nitrogen and water as in the experiments and the inner reactor temperature over time in the sand bath was recorded. Figure 3.4a shows the results of the temperature recordings at 520°C sand temperature. The heat-up time was defined as the intersection of the initial slope and final temperature line. Cool-down time was defined as the time needed for the reactor to reach 300°C. From Holliday et al. [42] it is known that that is the temperature below which FAs are stable.

To validate that the reactor used for the experiments and the reactor used for the temperature recordings actually have a similar heat-up profile, the pressure over time graphs of both the reactors are plotted in one figure for 520°C sand temperature (Figure 3.4b). The pressure is normalized with the final pressure to account for minor differences in nitrogen loading between measurements. Since the addition of oleic acid and its decomposition products have only a very small influence on the pressure (see Appendix A.2) and the reactors have equal water and nitrogen loadings, pressure is only dependent on temperature. Thus, if the pressures inside of both reactors are equal, so are the temperatures. Indeed, the two reactors show a similar pressure rise, and therefore temperature rise, over time during heat-up. Pres-

sure measurements of all experiments can be found in Appendix B.1.

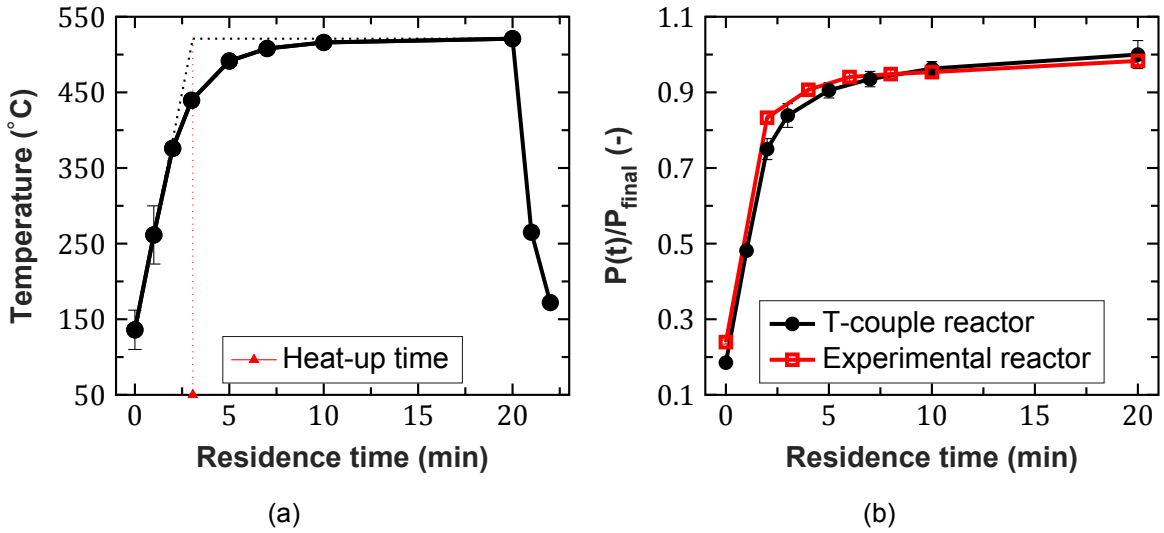

Figure 3.4: Inner reactor temperature over time in sand bath, indicating the defined heat-up time (a). Normalized pressure versus time of the temperature recordings and of the SCWG experiments with oleic acid (b). Both are at a sand temperature of 520°C

From preliminary experiments a heat-up time of 5 min was assumed. These 5 min were thus added to the desired reaction time to have the correct residence time of the reactor in the sand bath. These residence times were shown earlier in Table 3.1.

Measurements carried out with the thermocouple reactor and subsequent analysis as described earlier in this section resulted in heat-up times between 2-4 min. The calculated heat-up times for experiments at temperatures of 400, 420, 460, 520°C were 152, 192, 175 and 184 s, respectively. Cool-down times were indeed negligible compared to the studied reaction times. Measurements on heat-up and cool down times for all four temperature levels can be found in Appendix B.2.

3.3. Sampling and chemical analysis

After the reactor was cooled down by the cold sand bath different methods and techniques were used to sample the liquid and gaseous products and analyze them. Hereafter a gas bag, 1 L Tedlar Sample Bag from SKC, was connected to the reactor valve to obtain a gas sample. The valve was opened and the gas bag was filled with gas until the reactor pressure was equal to the atmospheric pressure.

The reactor was then opened, to obtain a liquid effluent sample. Since the liquid effluent consisted of an aqeous polar phase and a hydrocarbon a-polar phase, which sticked to the reactor walls, a solvent was needed to remove all phases from the reactor. Acetone was used as a solvent, so a homogeneous one phase sample would be acquired. First the liquid remaining in the reactor was poured into a 10 mL glass vial. Next the reactor was rinsed with approximately 2 mL of acetone, and poured into the same glass vial. This process was repeated one more time, to ensure that all liquid products were removed from the reactor and sampled into the glass vial. Before and after the sampling the reactor and glass vial were weighed. This ensured that the amount of products and acetone added could be quantified. The glass vial was closed tightly with a screw cap and stored at 7°C to prevent any acetone or decomposition products from evaporating out of the sample.

3.3.1. Gaseous product analysis

The gas product from the gas bags was analyzed for the presence of H_2, CH_4, CO, CO_2, C_2H_4, C_2H_6, C_3H_6 and C_3H_8. A HP 5890 series II gas chromatograph (GC) equipped with a thermal conductivity detector (TCD) was used. The system used a Varian CP-PoraBOND Q 50 m long column, with an internal diameter of 0.53 mm and film thickness of 10 µm and a Agilent Technologies HP-Molesieve column of length 30 m, an internal diameter of 0.53 mm and film thickness of 50 µm. The oven temperature was programmed as follows: initially at 40 °C for 3 min and raised with 20 °C min^{-1} to 90°C, which was held for 8 min. The injector was operated at 110°C, while the detector was operated at 200°C.

The GC was calibrated using a standard gas mixture of know composition containing H_2, CH_4, CO, CO_2, C_2H_4, C_2H_6, C_3H_6 and C_3H_8. Pure nitrogen gas was used to calibrate the N_2. This calibration was repeated each time before gas samples would be analyzed. An extra calibration report was made to validate the linear relationship between the product gas molar fraction and peak area. This report can be found in Appendix C.1.

Helium was used as a carrier gas for all components but hydrogen, for which nitrogen was used as a carrier gas. To quantify the exact molar amount of each produced gaseous component, the known amount of nitrogen added to the reactor for pre-pressurizing was used as an internal standard. Each calibration and gas sample measurement was repeated twice for consistency.

3.3.2. Liquid product analysis

Unconverted oleic acid in the liquid product was analyzed using a HP 6890 series GC equipped with the HP 5973 series mass spectometric detector. The column used was a Restek Rxi-5Sil MS being 30 m in length, having an inner diameter of 0.25 mm and a film thickness of 0.25 µm. The initial oven temperature was 45°C and was held for 2 min. It was then raised with 10°C min^{-1} to 280°C which was held for 5 min. Helium was used as a carrier gas and both injector and detector were operated at 280°C.

In order to allow for a good quantification of the oleic acid a trymethylsulfonium hydroxide (TMSH) solution was added 1:1 with the liquid sample in a separate GC sample vial. The TMSH would react with the FAs in the sample and their accompanied fatty acid methyl esther (FAME) would be formed. These FAMEs result in a sharper and smaller peek from the detector than the FAs, thereby increasing the accuracy of the analysis. A calibration line was made using three mixtures of a known amount of oleic acid with added TMSH. In both the calibration mixtures and sample mixtures hexadecane was used as an internal standard for quantification. A measurement report on the calibration mixtures can be found in Appendix C.2.

For the identification of main decomposition pathways it is more interesting to analyse for organic compound groups, such as cycloalkanes and aromatics, instead of individual organic components, such as cyclohexane and benzene. Identification of different compound groups present in the liquid sample was performed using a Thermo Finnigan Trace GC Ultra GCxGC (or 2D-GC), which was connected to a flame ionization detector (FID). Groups that were analyzed were:

- Small aliphatic hydrocarbon chains, with a carbon numer of 7 or lower.
- Cycloalkanes, Non-aromatic cyclic HC groups.
- Aromatics

- Volatile fatty acids (VFAs), with a carbon number of 7 or lower.
- Alcohols & ketones
- Large aliphatic hydrocarbon chains, with a carbon number exceeding 7.
- Methylesthers
- Naphtalenes; also including other poly-aromatic products.
- Long-chain fatty acids (LFAs), with a carbon number exceeding 7.

The first column in this GC was a Restek Rtx 1701 being 30 m in length, having an inner diameter of 0.25 mm and a film thickness of 0.25 µm. The product from that column was then injected in the second column every 6 s by a modulator using liquid CO_2. The second column was a Restek Rxi-5Sil MS with a length of 1.2 m, 0.10 internal diameter and 0.10 µm film thickness. The oven temperature program was set to start at 40°C, holding for 5 min, than raising to 280°C with 10°C min^{-1}. This final temperature was held for 5 min. Both detector and injector were operated at 280°C and helium was used as a carrier gas.

To calibrate the 2D-GC a mixture of known amounts of certain organic compounds representing a certain compound group was used. These compounds and their accompanied groups are shown in Table 3.3. In both the calibration mixtures and liquid samples di-n-butylether (DBE) was used as an internal standard for quantification. The calibration report for this 2D-GC analysis can be found in Appendix C.3.

Table 3.3: Chemical components used for calibrating the GCxGC analysis of the liquid sample and their representative compound group

Compound	Represented compound group(s)
Acetic Acid (glacial)	VFAs and LFAs
Cyclo-octane	Cycloalkanes
Hexadecane	Large aliphatic HCs
n-Heptane	Small aliphatic HCs
o-Xylene	Aromatics & naphthalenes
Propiophenone	Ketones & alcohols

Figure 3.5 shows the result of one analysis projected on a 2D-plane and the compound groups that were identified. One can see the individual peaks as dots with a different color intensity, which represent the height of the peak. Compounds within the same class have similar residence times in 1D, and lie within a range of residence times in the other dimension. A mapping can be made, in which components within a certain area belong to the same compound group. Individual peaks are integrated and summed up within the same compound group. 2D-plots from experiments at other temperatures and residence times are presented in Appendix C.5.

3.4. Glycerol test of set-up

In their work on the hydrothermal processing of glycerol, Muller and Vogel [47] use an experimental set-up that is comparable to the one used in this thesis. They performed experiments with glycerol in a hydrothermal, non-catalytic environment using small batch reactors that were placed in a fluidized sand bath. Two of their experiments were reproduced with the set-up and

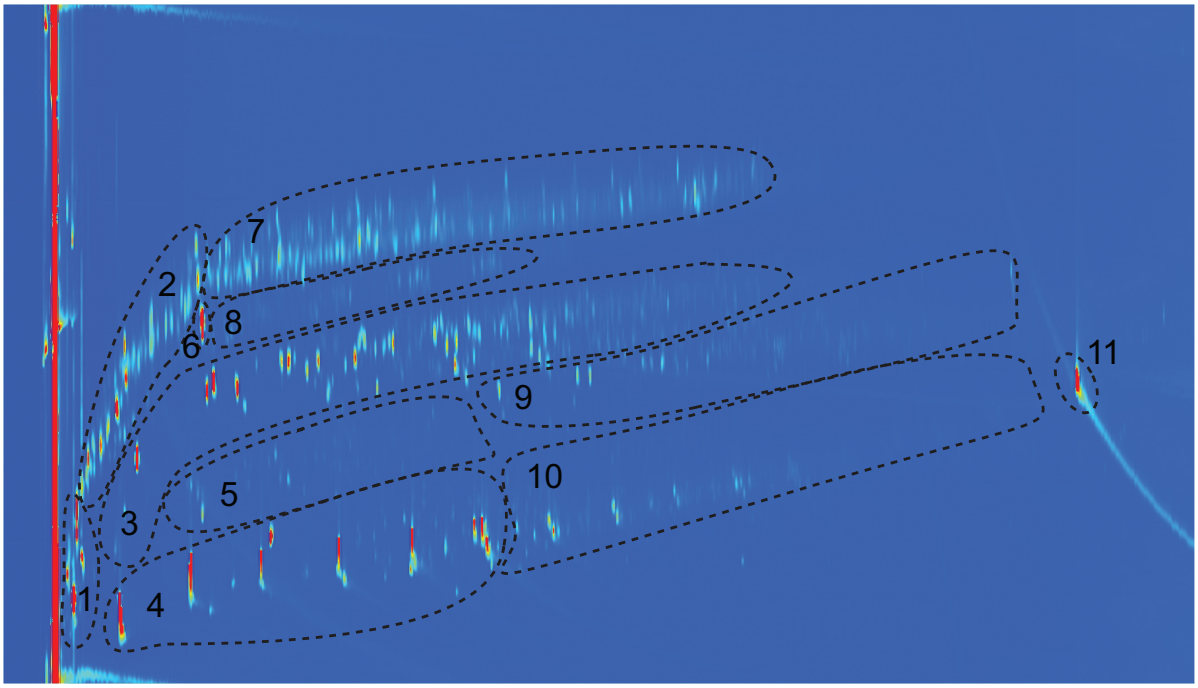

Figure 3.5: 2D-plot of 2D-GC analysis performed on effluent liquid from an experiment at T = 460°C and residence time of 35 min. Labeled compound groups represent: 1: Small aliphatic HCs 2: Cycloalkanes, 3: Aromatics, 4: VFAs 5: Alcohols & ketones, 6: DBE (internal std.) 7: Large aliphatic HCs, 8: Methylesthers, 9: Naphtalenes, 10: LFAs, 11: Oleic acid

procedure as presented in this thesis, to check if the experimental results from this set-up are reliable.

For a good comparison between this work and that of Muller and Vogel, the sampling and analysis of the liquid products deviated from what was described in Section 3.3. They looked at the distribution of carbon over different phases. Therefore the aqueous phase and the non-aqueous phase were sampled and analyzed individually for carbon content. After gas sampling the reactor was opened and the liquid phase was poured over a cellulose paper filter, only allowing the aqueous products to go through. This water solution was analyzed for TOC using a TOC-V_{SCN} Shimadzu TOC analyzer. The filter residue was weighed after drying of the filter and its amount was added to the amount of non-aqueous products.

The reactor was then flushed with acetone to sample the non-aqueous residue that was left. This sample was poured into a vacuum flask, and the acetone was evaporated out using a vacuum distiller. An elemental analyses was performed on the residual tarry product to find the average carbon weight percentage of the non-aqueous products.

Table 3.4 shows the results and characteristics of the glycerol experiments performed in this work and a comparison with the experimental results of Muller and Vogel. The carbon mass balance as presented is defined as:

$$\text{Carbon mass balance} = \frac{\text{total mass of carbon in product samples}}{\text{total mass of carbon in feed}} \tag{3.1}$$

The results of this work as presented in the Table 3.4 are in good accordance with the work of Muller and Vogel.

Furthermore, a comparison between the yields of the individual gas products found by Muller and Vogel and found here was also made, as can be seen in Figure 3.6. Although Muller and Vogel report slightly higher amounts of produced gas, which can also be noticed from the CGE values in Table 3.4, the distribution of gases is very similar. Both experimental works identify CO and CO_2 as the major produced gases and report on relatively low production of H_2, CH_4 and light HC gases[1]. The experimental procedure as described in Section 3.2 is therefore regarded a reliable method to perform hydrothermal processes.

Table 3.4: Characteristics and carbon distribution over different phases of the glycerol experiments performed here and by Muller and Vogel [47]. Feed concentration = 20 wt%.

	T (°C)	t (min)	P (bar)	CGE (%)	C aq. (%)	C non-aq. (%)	C mass bal. (%)
This work	350	35	275	3.0	45	36	84
Muller	350	35	295	4.0	48	36	88
This work	350	65	303	5.4	39	52	97
Muller	350	65	305	7.0	36	45	88
This work	460	35	251	35	46	12	93

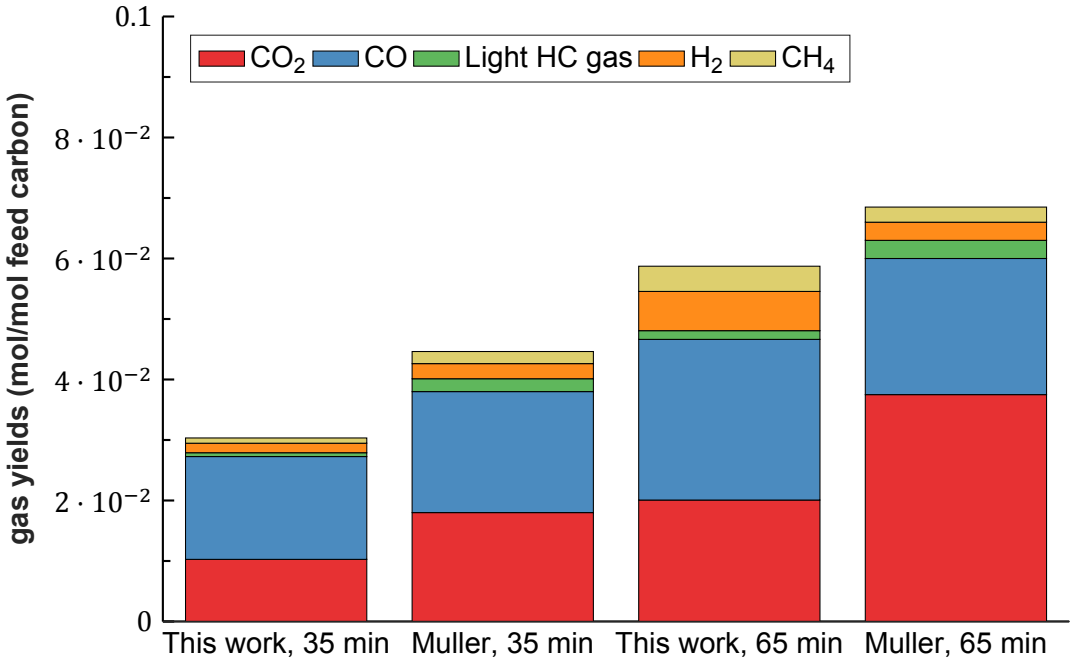

Figure 3.6: Comparison between the yields of the gas products of glycerol experiments at T = 350°C found in this work and by Muller and Vogel [47] at different residence times

An experiment at a supercritical temperature of 460°C was also performed. Following the trends described by Muller and Vogel, the change from subcritical to supercritical water for processing of glycerol should go with a drastic increase in carbon in the gas phase and a drastic decrease in carbon in the non-aqueous phase. From Table 3.4 this change in carbon distribution between 350 and 460°C is noticed. It can thus be concluded that the experimental set-up is capable of creating desired SCW conditions.

[1]The light HC gases analyzed for by Muller and Vogel are C_2H_6,C_3H_8 and C_4H_{10}. The light HC gases analyzed for in this work are C_2H_4,C_2H_6,C_3H_6 and C_3H_8

4

Experimental results

In this chapter the results that were obtained using the experimental setup, procedure and analyzing techniques described in Chapter 3 will be presented.

In the first section the results for the conversion of oleic acid and the CGE will be discussed, as they are important measures for the reactivity of oleic acid and its selectivity towards gas formation in SCW. In the second section the components found in the liquid effluent after reaction will be presented and reaction pathways that can explain the formed components are proposed. The third section will show the results from the gaseous product analysis and these results also will be translated in further possible reaction pathways that occur during the SCWG of oleic acid. In the fourth section the carbon mass balance found from the experimental analysis will be discussed. The expected decomposition scheme presented in Section 2.5.2 will be adjusted to the reaction pathways identified in this chapter in the fifth section. In the last section the results of an equilibrium analysis are compared to the experimental results. This comparison is used to justify that kinetic parameters can indeed be found from the experimental data presented in this chapter.

Table 4.1 shows a list of experiments that have been performed and how the liquid and gas samples have been analyzed. Three duplo experiments have been carried out at temperatures and residence times of 400°C and 65 min, 460°C and 15 min and at 520°C and 35 min. Error bars shown in the figures for these duplo experiments indicate the difference between values found for the duplos. At 400°C an extra experiment was carried out to get a better view of the oleic acid conversion over time.

4.1. Oleic acid conversion and CGE

The results for the conversion of oleic acid and the CGE can give a good view on the general behaviour of this SCWG process over time and at different temperatures. Furthermore, as mentioned in Section 2.2, the CGE is one of the important parameters based on which SCWG processes can be compared with each other. Figures 4.1 and 4.2 show the conversion of oleic acid and the CGE from the experiments for different temperatures as a function of residence time.

From Figure 4.1 it can be seen that at temperatures below 460°C significant amounts of unconverted oleic acid are still present. Oleic acid as fatty acid from a lipid is thereby less readily converted in SCW compared to the lipid backbone glycerol, which is almost fully converted (> 99%) after 40 min at 400°C and a pressure of 30 MPa [36]. At comparable

Table 4.1: List of experiments and analyses that have been performed

Temperature (°C)	Residence time (min)	Analyzed on:
400	10	GC-MS
400	15	GC-MS, 2D-GC & Gas-GC
400	35	GC-MS, 2D-GC & Gas-GC
400	65	GC-MS, 2D-GC & Gas-GC
400	65	GC-MS, 2D-GC & Gas-GC
420	15	GC-MS, 2D-GC & Gas-GC
420	35	GC-MS, 2D-GC & Gas-GC
420	65	GC-MS, 2D-GC & Gas-GC
460	15	GC-MS, 2D-GC & Gas-GC
460	15	GC-MS, 2D-GC & Gas-GC
460	35	GC-MS, 2D-GC & Gas-GC
460	65	GC-MS, 2D-GC & Gas-GC
520	15	GC-MS, 2D-GC & Gas-GC
520	35	GC-MS, 2D-GC & Gas-GC
520	35	GC-MS, 2D-GC & Gas-GC
520	65	GC-MS, 2D-GC & Gas-GC

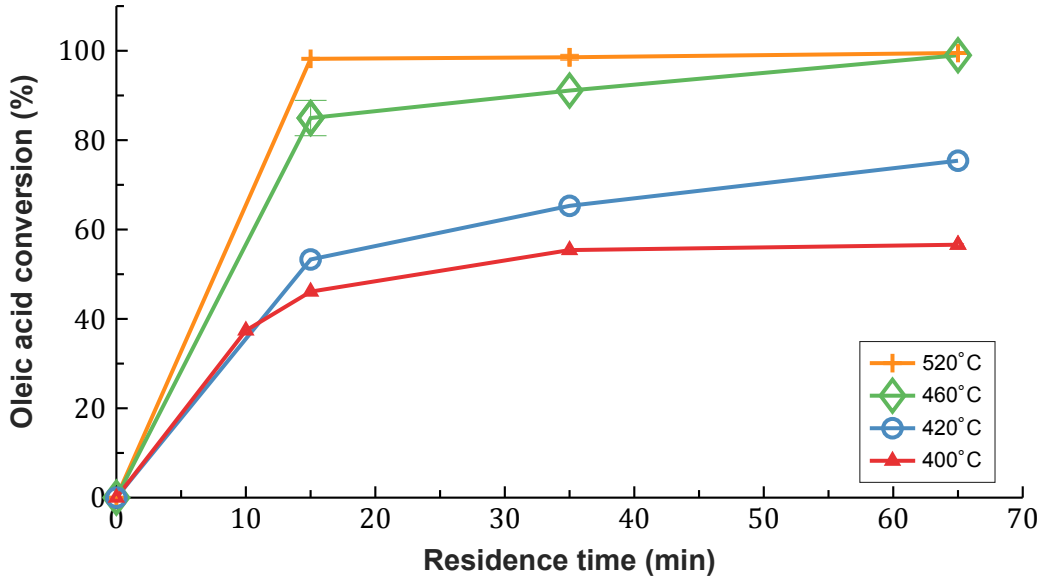

Figure 4.1: Oleic acid conversion at different reaction temperatures and residence times

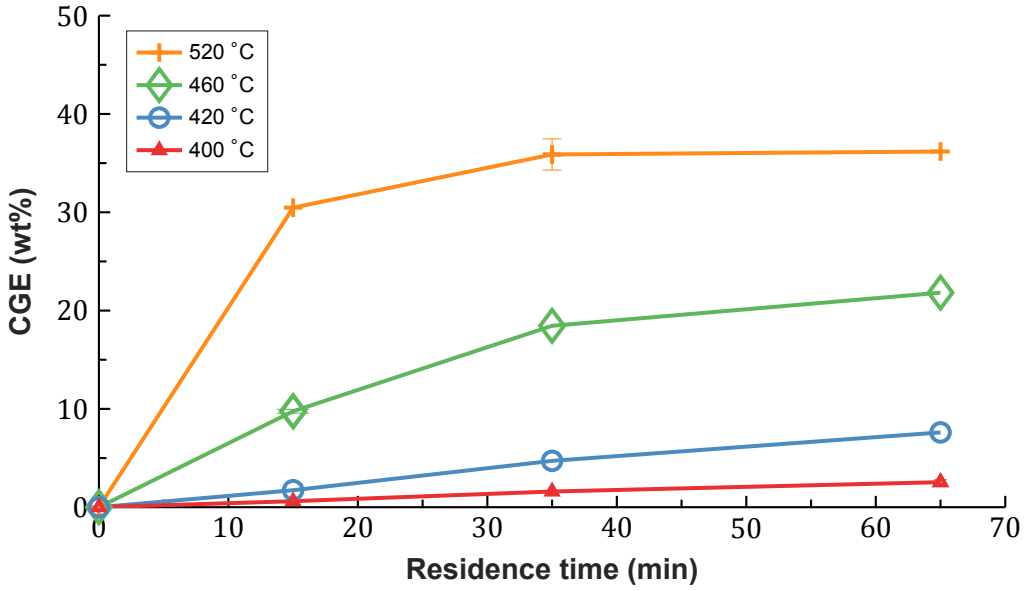

Figure 4.2: Carbon gasification efficiency at different reaction temperatures and residence times

reaction conditions of 400°C, after 35 min and at a pressure of 25 MPa the conversion of oleic acid is 55%.

At the highest temperature of 520°C an almost full conversion of oleic acid is reached, which indicates the large influence of temperature on the decomposition of oleic acid. It is thus expected that the decomposition of oleic acid can be modeled assuming Arrhenius-like temperature dependence. The concentration values of oleic acid from which the conversion was calculated can be found in Appendix C.6.

Two important conclusions can be drawn from the CGE results as shown in Figure 4.2. At first, the CGE seems to be more sensitive to temperature than residence time. Especially at higher temperatures the CGE does not increase much with residence time. This suggests a shift in formation of gases at a short residence time, to the formation of a more stable liquid product from liquid intermediates at a long residence time.

Secondly, CGE values reported are lower than for the non-catalytic oleic acid experiments of Youssef et al. [2]. They presented CGEs of 10, 25 and 52% for reaction temperatures of 400, 450 and 500°C respectively. Their residence time was 30 min, at a pressure of 28 MPa. At a pressure of 25 MPa, a residence time of 35 min and with comparable reaction temperatures of 400, 460 and 520°C CGEs of 1.6, 18.5 and 35.9% respectively were found in current experiments.

A reason for the current reported CGE values to be consistently lower is the influence of reactions during heat-up time. Youssef et al. used a reactor that was preheated to the desired temperature and subsequently the oleic acid was injected. In current experiments the oleic acid underwent a heat-up path. During this short heat-up time some of the oleic acid may convert to more stable liquid products, while it would be converted to gases at the desired reaction temperature. This effect was also suspected by Guan et al. [48] who gasified algae in SCW and found that their carbon yields were lower than reported by an earlier study with similar reaction conditions.

4.2. Liquid analysis results

This section presents the results of the analyses performed on the liquid effluent from the reactor after the experiments. The visual appearance of the liquid samples will be discussed first. Next, the liquid product yields at different temperatures and residence times are shown. Decomposition pathways than can explain the appearance of these products will be proposed.

4.2.1. Sample appearance

Figure 4.3 shows a photograph of the liquid samples taken from reactions at 460°C. With increasing time the sample liquids got a more intense yellow/brown color, which would suggest the formation of darker and heavier oils. The samples turned to an even darker brown/yellow color at 520°C, while samples at lower temperatures were almost colorless.

Small char particles were also visible in all liquid samples at 520°C. The quantification of these chars was performed for one experiment at a temperature of 520°C and residence time of 65 min. The liquid sample was poured over a filtration paper that was weighed after evaporation in a vacuum oven. The amounts of char were negligible (< 0.01 g/g oleic acid feed). Therefore these char particles were not analyzed further.

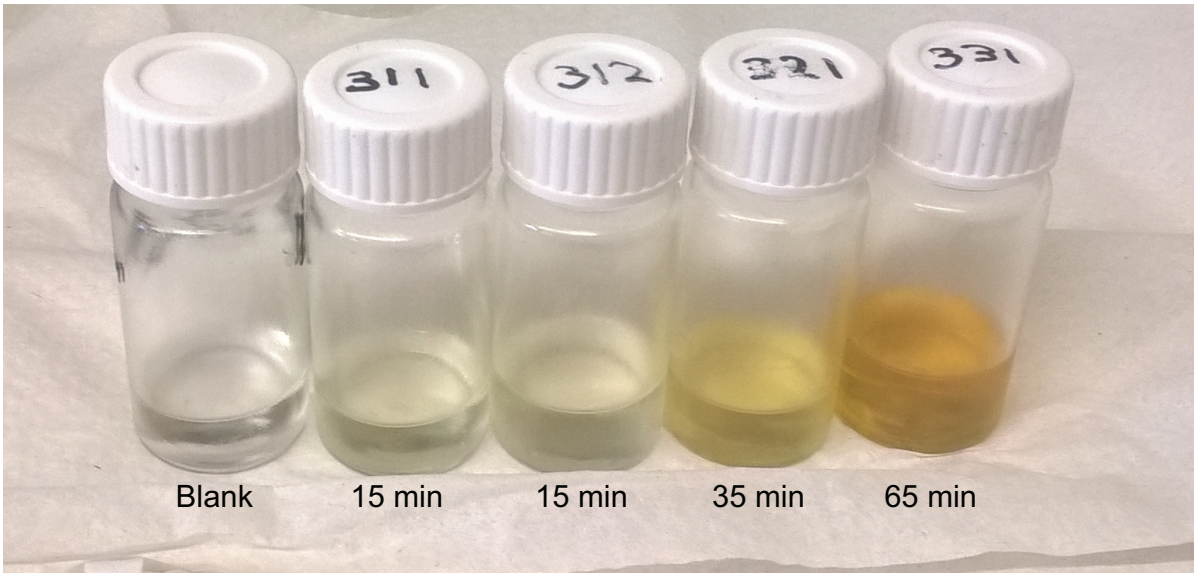

Figure 4.3: Photograph of the liquid samples acquired from experiments at T = 460°C. The most left sample is a blank colorless liquid for comparison, residence times are indicated for all 4 samples

4.2.2. Liquid product yields

The results of the 2D-GC liquid effluent analysis are presented for each reactor temperature in Figures 4.4-4.7. The alcohols & ketones and methylesthers groups are not displayed, because of the relatively low quantities they were found in. Detected oleic acid is also not displayed since its distribution over time and temperature has already been presented in Section 4.1. From the distribution of products in the liquid effluent over time and temperature decomposition pathways can be extracted, that will be discussed here.

Firstly, from the data in Figure 4.4 and 4.5 it is concluded that LFAs, VFAs and large aliphatic HCs are the first decomposition products from oleic acid in SCW. The large aliphatic HCs are probably either formed by decarboxylation/decarbonylation of a FA [43], or via the cracking of the C-C bond of a FA, creating also a new, shorter chain, FA [45]. From GC-

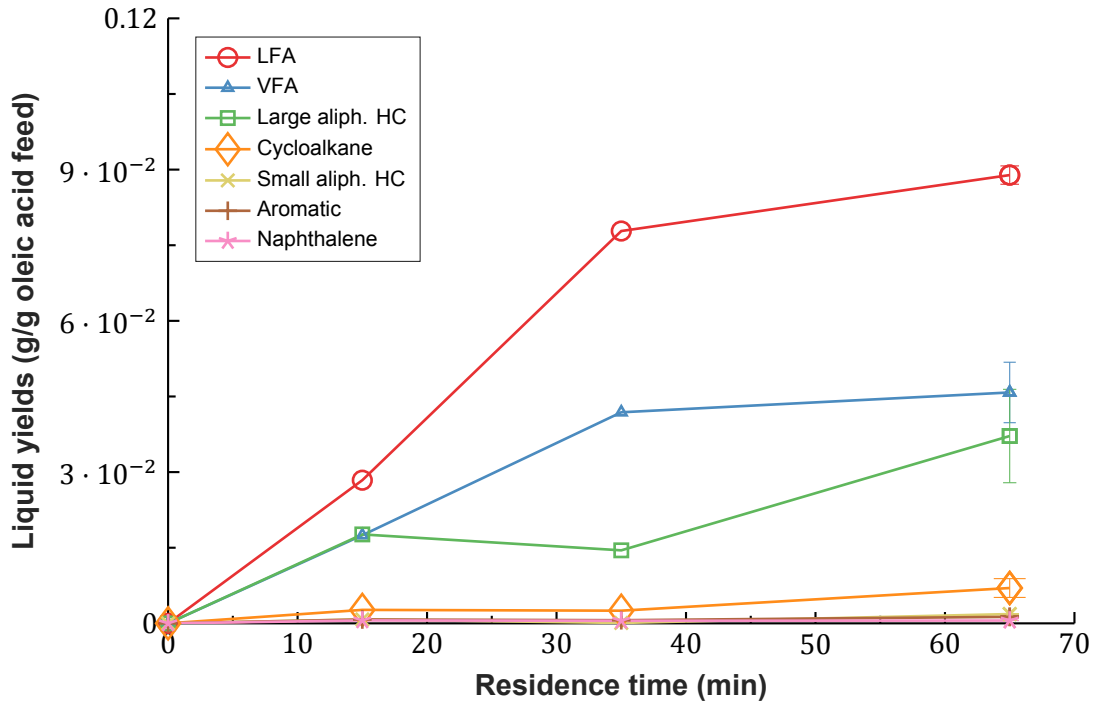

Figure 4.4: Liquid product distribution over residence time at T = 400 °C

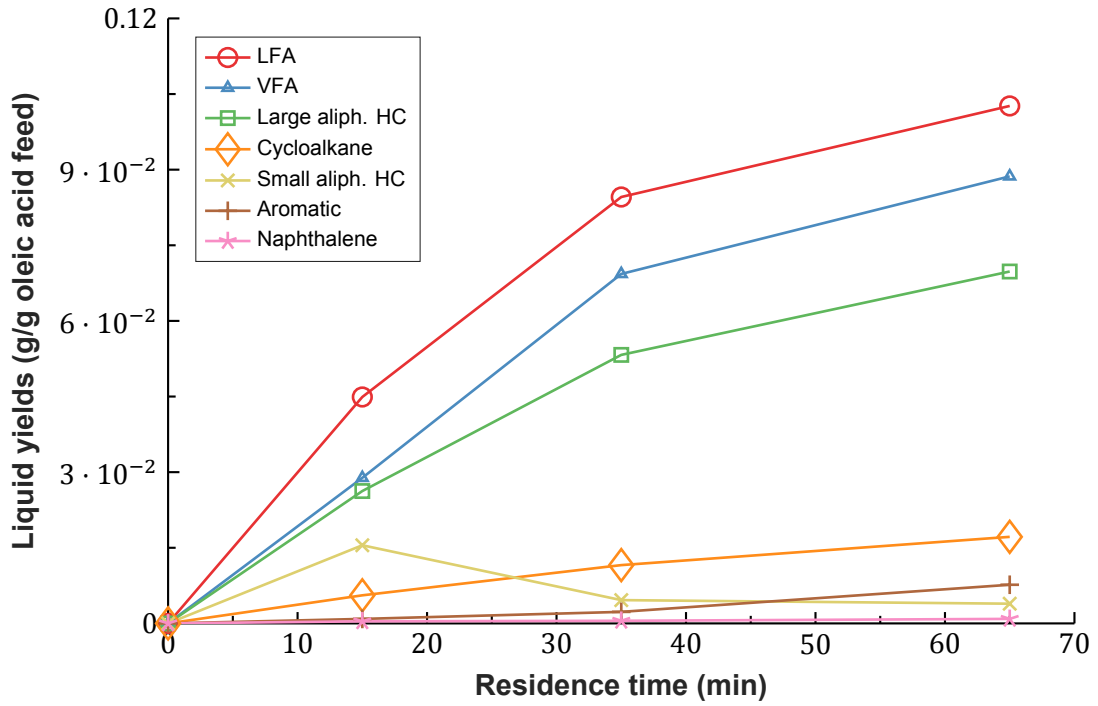

Figure 4.5: Liquid product distribution over residence time at T = 420 °C

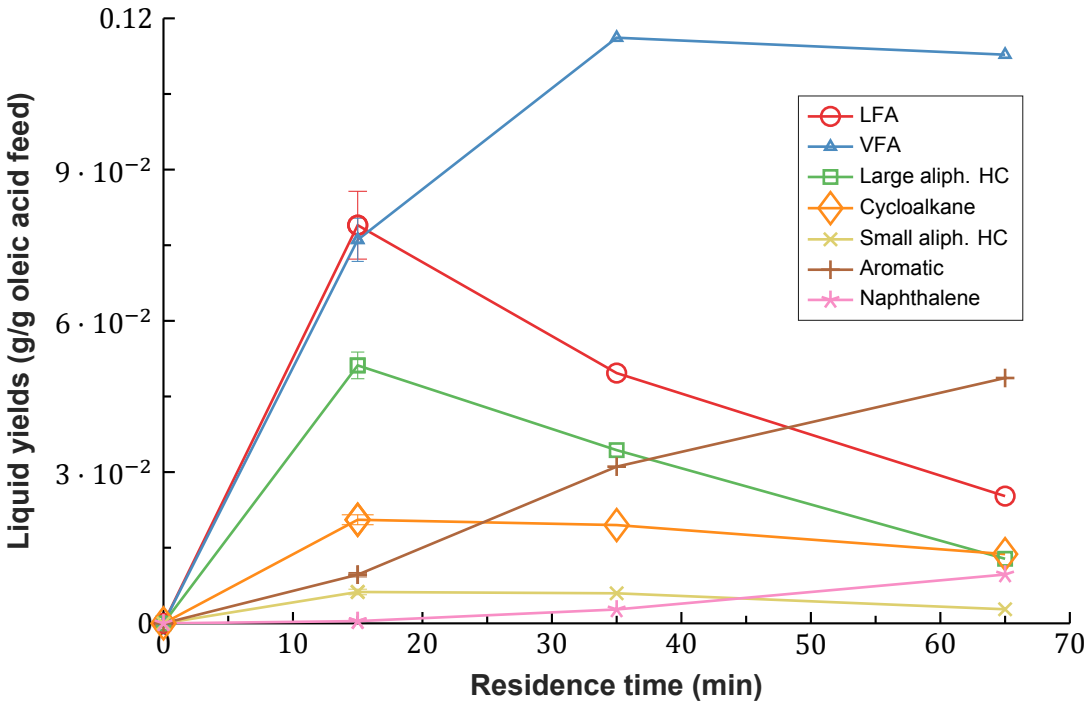

Figure 4.6: Liquid product distribution over residence time at T = 460 °C

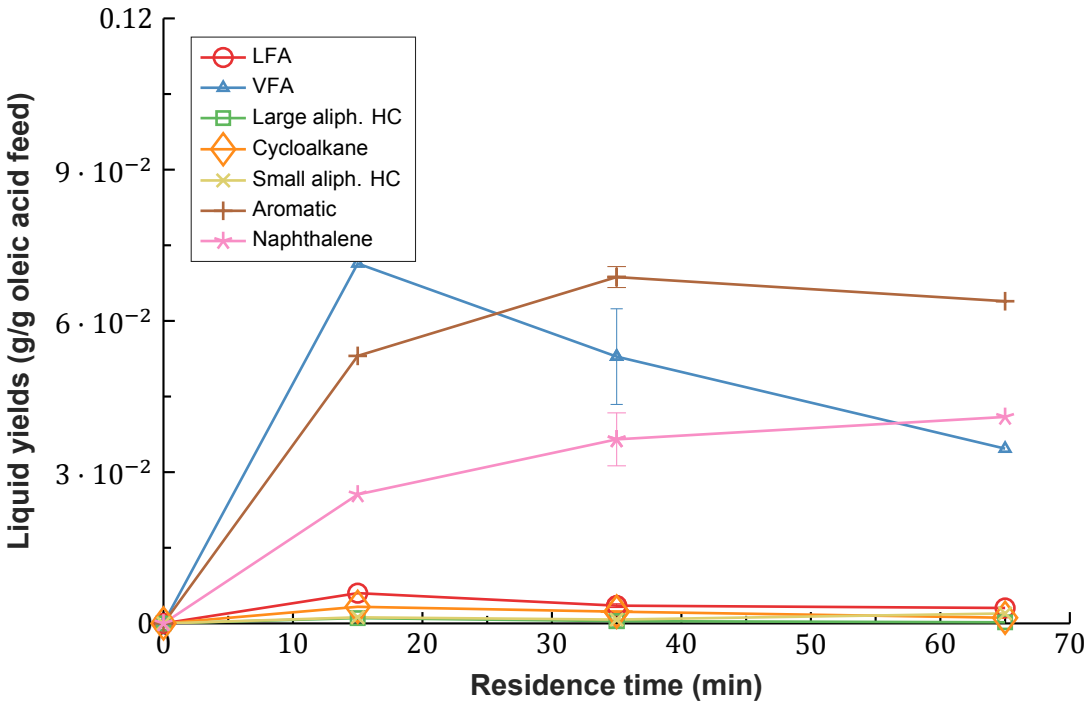

Figure 4.7: Liquid product distribution over residence time at T = 520 °C

MS analysis of the liquid samples from 400°C and 420°C heptadecene was identified, which supports the direct decarboxylation reaction of oleic acid too. At 420°C the production of small aliphatic HCs is apparent, resulting again from cracking of C-C bonds of FAs or large aliphatic HCs, or the decarboxylation/decarbonylation of VFAs.

The next decomposition products should then originate from aliphatic HCs or FAs and the first decomposition products that appear are cycloalkanes. They become apparent first at 420°C and are also detected at 460°C in significant quantities. It is known that under SCW conditions small aliphatic HCs can undergo cyclization reactions to form cycloalkanes. Cycloalkanes are then intermediates for the formation of (poly-)aromatic compounds [2]. This decomposition pathway matches the data presented here. Figure 4.6 and 4.7 show that over time the cycloalkanes concentration start to decrease, while aromatics and naphtalenes (which are poly-aromatics) are being formed and increase with time. The presence of these products does for a part explain the yellow/brown color of the liquid samples at the higher temperatures.

Finally, it is noted that although VFAs are one of the first decomposition products from oleic acid, their presence in the effluent liquid keeps increasing with time and temperature until 520°C. At 520°C the rapid increase of aromatics and naphtalenes can be seen, which are also stable liquid products containing a significant amount of carbon. This observation supports one of the conclusions made in Section 4.1, suggesting the formation of stable liquid products with time, preventing to a certain extend the increase of CGE over time.

4.3. Gas analysis results

The gaseous products found in the gas samples obtained from the experiments will be shown in this section. General trends from these results will first be discussed and compared with the study by Youssef et al. [2]. Finally possible reaction pathways that can explain the formed gases are proposed. Figures 4.8 to 4.11 show the yields of gaseous products at different temperatures over residence time.

4.3.1. General trends in gas composition

The gas that is produced most at the lower temperatures of 400°C and 420°C is CO_2, followed by light hydrocarbon gases. Youssef et al. [2] also reported CO_2 as the main gas product from oleic acid SCWG between 400°C and 450°C. They did however not report on the formation of C_2H_4, C_2H_6, C_3H_6 and C_3H_8. The order of yield of gases at 400°C was reported as follows: CO_2>H_2>CH_4>CO. Not considering the light hydrocarbon gases, this order is also found in this study.

Youssef et al. also found the relatively rapid increase with temperature of CH_4 yield. At 500°C CH_4 is the main gas product. From Figures 4.10 and 4.11 it can be seen that in this study, from 460°C at a residence time of 65 min and for 520°C at every residence time, CH_4 also becomes the main produced gas.

Lastly the selectivity towards ethane, ethylene, propane and propane is remarkable. Generally, SCWG studies only present relatively small amounts of these gases formed compared to CO_2, CH_4 and H_2 [48] [49]. A possible explanation for this is the long C-C chain in oleic acid compared to other model compounds used in SCWG studies, such as glucose and glycerol. Therefore the availability of C-C bonds, out of which these hydrocarbon gases consist, per mol of feed is bigger.

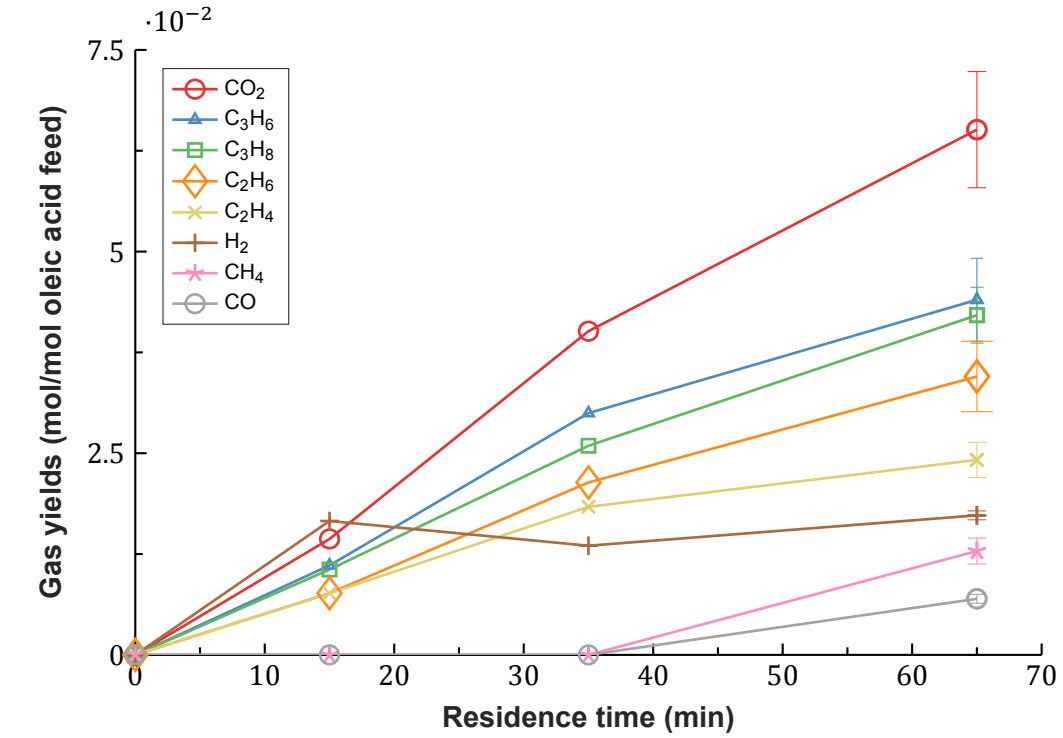

Figure 4.8: Gaseous product distribution over residence time at T = 400 °C

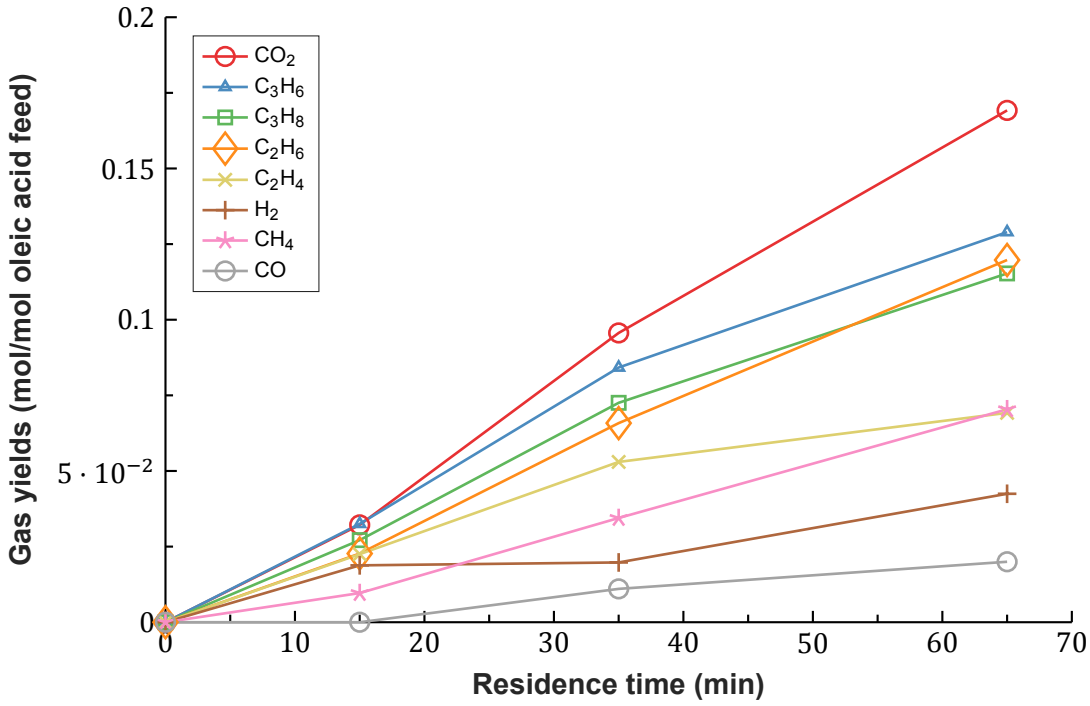

Figure 4.9: Gaseous product distribution over residence time at T = 420 °C

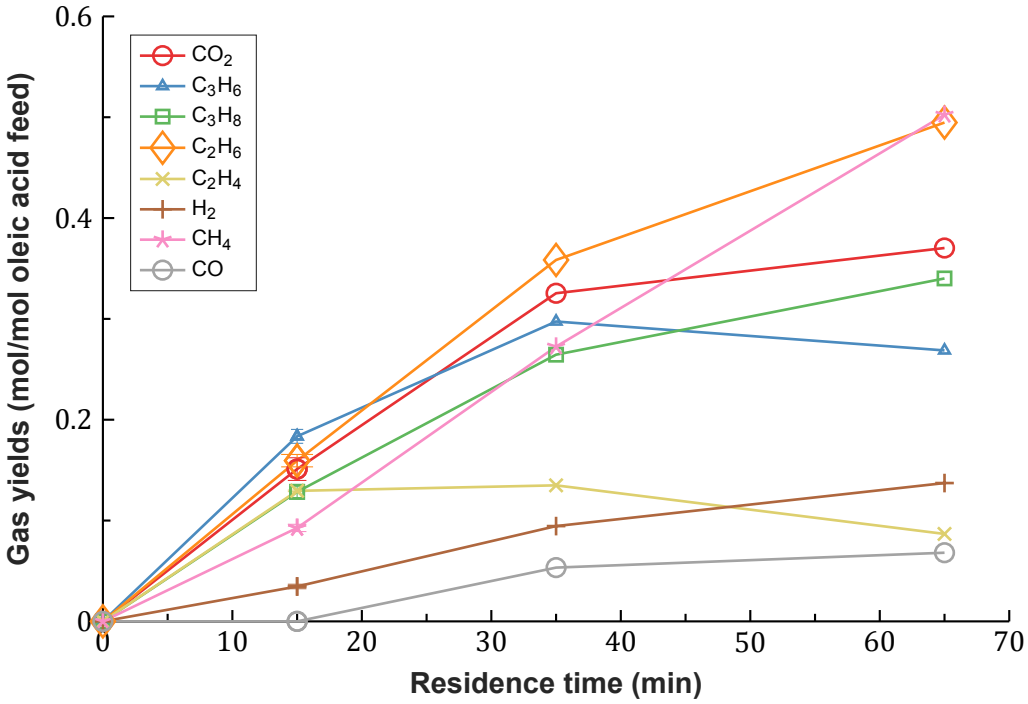

Figure 4.10: Gaseous product distribution over residence time at T = 460 °C

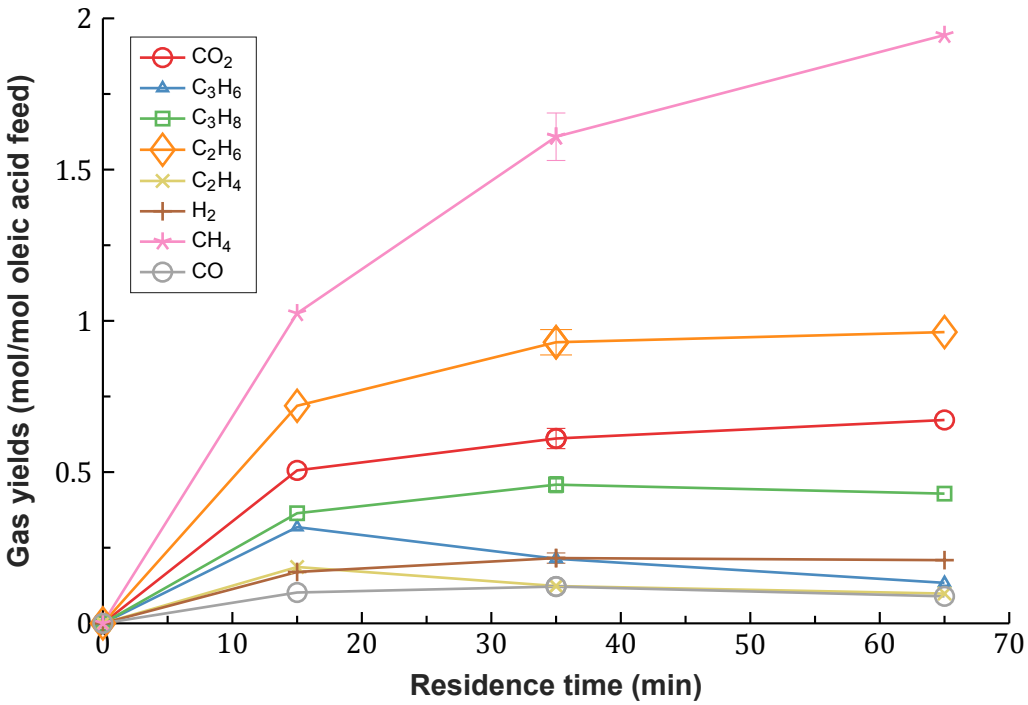

Figure 4.11: Gaseous product distribution over residence time at T = 520 °C

4.3.2. Gaseous products formation routes

The presence of CO_2 as main gas product at lower temperatures does support the earlier proposed decarboxylation reactions from FAs to aliphatic HCs, as described in Section 4.2.2. CO is produced in low quantities at higher temperatures, probably via decarbonylation reactions of FAs or other intermediate oxygenated compounds, such as methylesthers and alcohols & ketones [2]. The low quantity of CO with respect to CO_2 can also be caused by the water-gas-shift reaction [50].

The light hydrocarbon gases and methane are most likely formed by cracking of the FAs or aliphatic HCs [44]. The influence of methanation on CH_4 production is assumed to be negligible, which is further explained in Section 4.5.

The formation of H_2 can be accounted for by the formation of cycloalkanes and (poly)-aromatics from aliphatic HCs in which hydrogen is released. Furthermore hydrogen can also be formed via the water-gas-shift reaction and thermal decomposition reactions of VFAs [2]. Also, from the experiments it can be seen that the hydrogen concentration over time at the same temperature level almost stays constant. This does suggest the presence of a mechanism that consumes hydrogen. Hydrogen consumption can be explained by the saturation of unsaturated liquid compounds, as adressed before in oleic acid hydrothermal treatment experiments [44] [11].

4.4. Carbon mass balance

Figure 4.12 shows the carbon mass balance of the performed experiments. Because of the sampling of the liquid products with volatile acetone, accurate measurements of carbon in the liquid phase using a TOC or elemental analysis were not possible. The carbon mass balance shown here is thus calculated from Gas-GC, GC-MS and 2D-GC analyses results. To calculate the amount of total carbon in the liquid after the experiments, the amount of a compound group found by 2D-GC analysis was multiplied by an assumed weight percentage of carbon specific for that compound group. These weight percentages are shown in Appendix C.4.

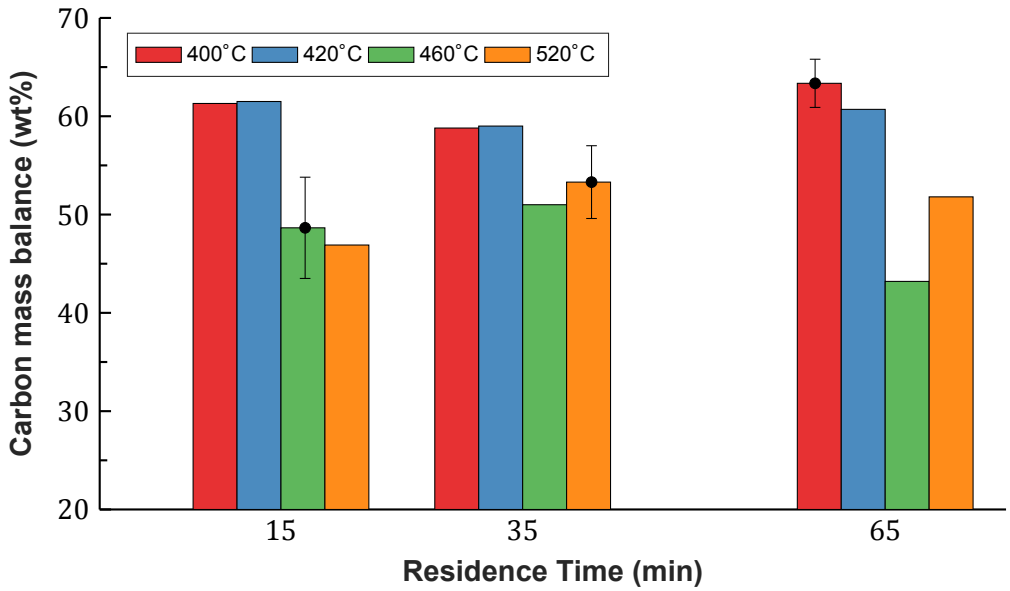

Figure 4.12: Carbon mass balance at different reaction temperatures and residence times

Carbon mass balances are between 40 and 70%, where values between 75 to 100% were expected and are usually acceptable. Since the glycerol experiments presented in Section 3.4 resulted in high carbon mass balances between 80 and 100%, the low values for oleic acid are expected to be due to liquid products that are left unidentified by the 2D-GC.

Firstly, some heavier oily products that are formed (see Section 4.2.1) can be too heavy for the 2D-GC apparatus to detect. The lower carbon mass balance for the higher temperatures supports this explanation; at higher temperatures more of these heavier oily products are formed, indicated by the darkening of the sample colors with temperature.

Secondly, some volatile compounds that have a boiling point close to acetone can be left unidentified by the 2D-GC. Their peak response on the 2D map is then covered by the broad solvent peak.

A recommendation on how the carbon in these unidentified products can be analyzed in a future study is presented in Section 6.2.

4.5. Proposed decomposition scheme

The reactions identified through experiments in Section 4.2 and 4.3 have been used to re-shape the decomposition scheme that was acquired through literature in Section 2.5.2. A schematic drawing of this decomposition scheme including a list of reactions is shown in Figure 4.13.

Liquid Decomposition Reactions

(1) Oleic Acid $\longrightarrow$ Oxygenates + Aliphatics
(2) Oxygenates $\longrightarrow$ Aliphatics + CO_2
(3) Oxygenates $\longrightarrow$ Aliphatics + CO
(4) Aliphatics $\longrightarrow$ Cyclics + H_2

Gasification Reactions

(5) Oxygenates $\longrightarrow$ H_2
(6) Oxygenates $\longrightarrow$ CH_4
(7) Oxygenates $\longrightarrow$ C_aH_b
(8) Aliphatics $\longrightarrow$ CH_4
(9) Aliphatics $\longrightarrow$ C_aH_b

Saturation- and WGS-reactions

(10) H_2 + Oxygenates $\longrightarrow$ Oxygenates
(11) H_2 + Aliphatics $\longrightarrow$ Aliphatics
(12) $CO + H_2O \longleftrightarrow CO_2 + H_2$

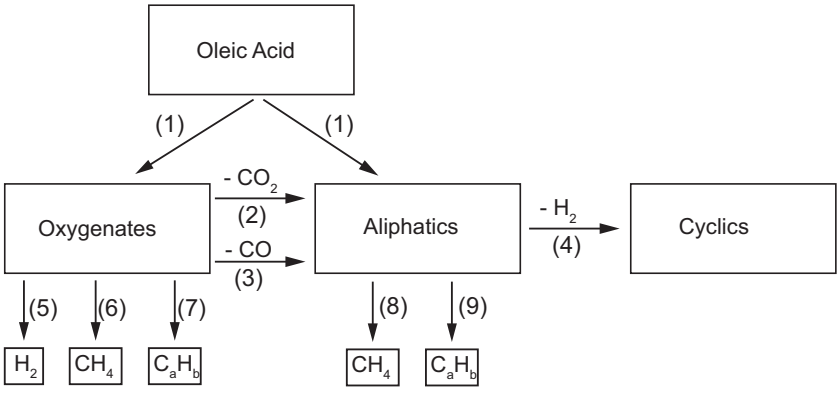

Figure 4.13: Schematic overview of proposed oleic acid SCWG decomposition scheme.

For reasons of simplicity some compound groups, that are assumed to have a similar reactive behaviour, have been lumped together. Guan et. al have previously followed a procedure like this for the kinetic modeling of algae in SCW [50]. The lumped groups in the decomposition scheme are categorized as follows:

- Oxygenates: LFAs, VFAs, ketones & alcohols and methylesthers
- Aliphatics: large aliphatic HCs and small aliphatic HCs.
- Cyclics: cycloalkanes, aromatics and naphtalenes
- C_aH_b (or light HC gases): C_2H_4, C_2H_6, C_3H_6 and C_3H_8

Some simplifications have also been made for the reactions between Oleic Acid, Aliphatics and Oxygenates. Because of the relative high amount of Oxygenates in comparison to Aliphatics and CO_2 and CO at lower temperatures and short residence times it is assumed that cracking of Oleic Acid would occur before decarboxylation and decarbonylation. Therefore in this decomposition model Oleic Acid only decomposes through cracking to Oxygenates and Aliphatics, and was not involved in any other reactions. The production of CO_2 and CO should then result from the decarboxylation and decarbonylation of FAs, and are thus implemented in the reaction scheme this way.

From the three gas-phase reactions that are likely to occur during SCWG (see Reactions 2.4 to 2.6) the only gas phase reaction that is present in this scheme is the WGS reaction. Yakaboylu et al. already assumed that methanation reactions in SCW under 650°C are insignificant with respect to CH_4 concentration for their kinetic model [10]. Bennekom et al. also found that methanation reactions hardly produce any methane in SCW conditions below 650°C [51].

4.6. Equilibrium analysis

An equilibrium analysis was realized to find out if the experimental results as presented in Sections 4.2 and 4.3 were close to or at equilibrium. If this were the case than kinetic data could not be extracted from the experimental data, since net reaction rates are zero at an equilibrium.

The RGIBBS block in Aspen Plus with the Peng-Robinson equation of state model was used to calculate equilibrium concentrations of products. This block calculates the equilibrium concentrations by minimizing the Gibbs energy. Input of the block was feed mixture as applied in the experiments. The possible decomposition products were predefined as the components shown in Figure 4.13. For the lumped liquid groups the corresponding model components as presented in Section 5.2.1 were used. Figure 4.14 shows the results of this equilibrium analysis for the examined process conditions in the experiments.

At equilibrium only four (gaseous) components are left in the system: CO, CO_2, CH_4 and H_2. On the other hand the experiments show that liquid decomposition products and also light HC gases are (still) present in significant quantities. A kinetic study is needed to model the presence of these products.

Furthermore, a comparison between the gas composition at equilibrium and after 65 min of reacting at 520°C shows that none of the gases is near or at its equilibrium composition. Table 4.2 shows this comparison. It can thus be concluded that the experimental results clearly show that at the examined process conditions the system is not near or at its chemical equilibrium. A kinetic study using the experimental data is therefore justified.

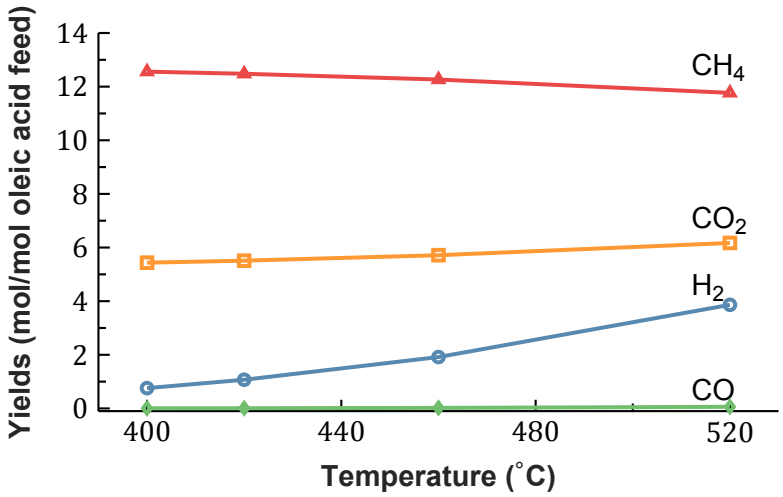

Figure 4.14: Equilibrium yields for the SCWG of oleic acid at P = 250 bar and a feed concentration of 10 wt%

Table 4.2: Gas composition at equilibrium as calculated by Aspen and found from the experiments after 65 min of residence time. T = 520°C, P = 250 bar

Concentration (mol%)	H_2	CH_4	CO_2	CO	C_aH_b
Equilibrium	19	55	27	0	0
65 min reaction	4	43	15	2	36

5 Kinetic model

In this chapter the kinetic model that is constructed from the experimental results is presented. At first the conversion of oleic acid in SCW was modeled and tested for its validity, which is presented in the first section. In the second section the equations that form the overall kinetic model are shown, and the resulting fitted parameters and predictive results from the model are presented and discussed. Finally a sensitivity analysis was performed to identify which reactions govern the kinetic model, and its results are presented and discussed in the last section.

5.1. Oleic acid conversion modeling

Since oleic acid is the component from which all other components are derived in this system, its conversion was modeled first. The resulting parameters fitted to the experimental results for the conversion of oleic acid as found in Section 4.1 are then used in the overall kinetic model. In this section the equations used and assumptions made in modeling the conversion are presented first. Lastly, the results from the fitting of model parameters are shown and the validity of the prediction will be discussed.

5.1.1. Conversion equations and assumptions

As shown in Figure 4.13 the decomposition, and therefore the conversion, of oleic acid is assumed to be (pseudo)-first order. No backward reaction forming any oleic acid is expected. The equation describing the oleic acid decomposition is:

$$\frac{d[\text{Oleic}]}{dt} = -k_1[\text{Oleic}] \tag{5.1}$$

where k_1 is the reaction rate constant in s^{-1}. In Section 4.1 it was argued from the experimental conversion results that an Arrhenius temperature dependence for the reaction is expected. Using the Arrhenius equation, the reaction constant k_1 can be described as a function of reaction temperature as follows:

$$k_1 = A_1 * \exp\left(\frac{-E_{a,1}}{RT}\right) \tag{5.2}$$

where R is the universal gas constant at a value of 8.314 J K^{-1} mol^{-1} [52] and T is the reaction temperature in K. This leaves two parameters that should be fitted to the experimental data: the pre-exponential A_1 and the activation energy $E_{a,1}$.

This fitting was performed using the MATLAB-procedure desribed by Danon et al. [53]. In this prodecure the best fit minimizes the sum of squared normalized errors (SSNE). This SSNE is a measure for the error between the model predictions and actual measurements and is formulated as follows:

$$\text{SSNE} = \sum_{i=1}^{N} \left[\left(\frac{y_i}{y_0} - \frac{y_i^{\text{mod}}}{y_0} \right)^2 \right] \tag{5.3}$$

where N is the total number of measurements, y_0 the initial concentration and y_i, and y_i^{mod} represent the experimental and modeled concentration data, respectively. This SSNE was minimized using the MATLAB toolbox *fminsearch*, which is based on the Nelder-Mead optimization method. The *fminsearch* provided estimates for A and E_a . Equations 5.1 and 5.2 were then solved for [Oleic] by the MATLAB *ode23s* stiff ODE solver using these estimates. Subsequently, the SSNE was calculated and *fminsearch* would provide new estimates until a minimum was found.

Finally the percentage output variation (FIT) was calculated. The FIT is calculated using the following equation,

$$\text{FIT} = 100 \left[1 - \frac{\text{norm}(y_i^{\text{mod}} - y_i)}{\text{norm}(y_i - \tilde{y}_i)} \right] \tag{5.4}$$

where $\tilde{y}_i$ is the mean value of y_i and the function norm(M) in MATLAB returns the largest singular value of the matrix M. A rule of thumb is that a good FIT has a minimal value of 80% [53]. Thereby the FIT provides a measure of validity for modeling the oleic acid conversion.

5.1.2. Conversion modeling results

The modeling of the conversion of oleic acid for the experiments performed at reaction temperatures from 400 to 520°C yielded a FIT of 75%. It was suspected that this low FIT was due to non-Arrhenius like behaviour at the temperature of 400°C. It is known that at temperatures near the critical point in SCWG the reaction rate shows a strong and characteristic non-Arrhenius behaviour [23]. This is probably due to the competition of ionic and free radical reaction pathways. Paksung et al. [54] found that ionic reactions generally have non-Arrhenius like behaviour in SCWG processes, when they investigated the decomposition of xylose in near-critical and supercritical water. Therefore it was concluded that at 400°C reactions were too close to the critical-point for them to be modeled using Arrhenius equation.

This then lead to the modeling of conversion, where experiments at 400°C were excluded. This model yielded a FIT of 82%. Consequently, it was decided to limit the kinetic modeling of Oleic Acid decomposition in SCW to temperatures between 420 and 520°C

Figure 5.1 shows the conversion of oleic acid as predicted by the model together with the experimental values. It must be noted that the x-axis in the graphs displaying modeling results in this chapter display the reaction time, as opposed to residence time in Chapter 4. The difference between these times was presented in Section 3.2.4

It can be seen from Figure 5.1 that the model predictions fit the experimental data quite well. However, the model over predicts the conversion at longer reaction times. Therefore a model using second-order kinetics was also tested. Reaction 5.1 was replaced with:

$$\frac{d[\text{Oleic}]}{dt} = -k_1[\text{Oleic}][\text{Oleic}] \tag{5.5}$$

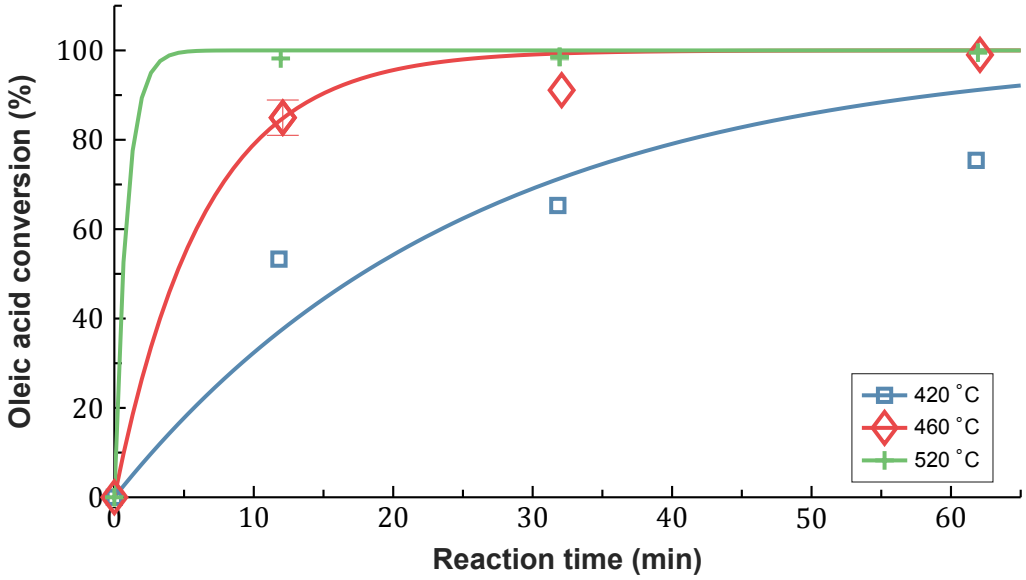

Figure 5.1: Oleic acid conversion at different reaction temperatures as a function of reaction time. The markers represent the experimental results and the lines represent the model predictions.

This model yielded a FIT of 92%. A decomposition reaction of oleic acid with itself or another decomposition product is thus suspected. The identification of alcohols and (oleic acid)-methyl esters could point to the decomposition of oleic acid via esterification, presented in the following equation:

$$C_{17}COOH + R{-}OH \longleftrightarrow C_{17}CO{-}OR + H_2O \tag{5.6}$$

However, earlier studies on the processing of oleic acid in hydrothermal water, supercritical water and using pyrolysis did not report on such a reaction taking place. Furthermore the quantities of methylesters and alcohols found are very low (see Section 4.2) and they were only detected at a few experiments. Therefore it cannot be stated with confidence that the esterification of oleic acid was taking place in the SCWG experiments. First-order kinetics will thus be used to model the decomposition of oleic acid in SCW.

The parameters fitted to the conversion model by the MATLAB optimization procedure at temperatures between 420°C and 520°C were $1.51 \bullet 10^5$ J mol^{-1} and $1.62 \bullet 10^8$ s^{-1} for $E_{a,1}$ and A_1, respectively.

This activation energy was compared to the reported activation energies of the disappearance of similar products in similar processes. Popov and Kumar reported an E_a of 120 ±5 kJ/mol for stearic acid disappearance in a HTL process between 350 and 380°C using an activated carbon catalyst in a continuous flow reactor [44]. Fu et al. reported the activation energy (125 ±3 kJ/mol) for another similar application: the hydrothermal decarboxylation of palmitic acid over an activated carbon catalyst in a batch reactor [43]. The value of 151 ±18.5 kJ/mol for the activation energy of oleic acid disappearance is comparable with these two earlier reported numbers. The slightly higher activation energy presented here compared to the ones by Popov and Kumar and Fu et al. can be explained by not using a catalyst in this study.

These fitted parameters will be implemented in the overall kinetic model.

5.2. Overall decomposition model

Using the results and conclusions of the modeling of conversion presented in Section 5.1 the further decomposition of oleic acid in SCW was modeled. The basis of this model was the decomposition scheme as shown in Section 4.5. Parameters would be fitted to experimental data from 420°C to 520°C. In this section the assumptions made and the equations used by the model will be discussed first. Finally the results of the model fitting will be presented.

5.2.1. Model equations and assumptions

For this model the kinetic reaction equations were derived from Figure 4.13. Since the kinetic equations use molar concentrations and the liquid components were quantified to mass ratio, average molar weights were prescribed for the three lumped liquid groups.

For the Oxygenates and Aliphatics groups GC-MS analysis on samples from reaction temperatures of 420°C and 460°C and 15 min residence time were used. These conditions were chosen for the relatively high presence of Aliphatics and Oxygenates (see Section 4.2). Figure 5.2 shows the distribution of FAs, the main Oxygenated components, resulting from this analysis. The C_7 FA or heptanoic acid ($C_7H_{14}O_2$) is the main FA present in both analyses and therefore its molar weight is assumed to be the average molar weight of the Oxygenates lumped group.

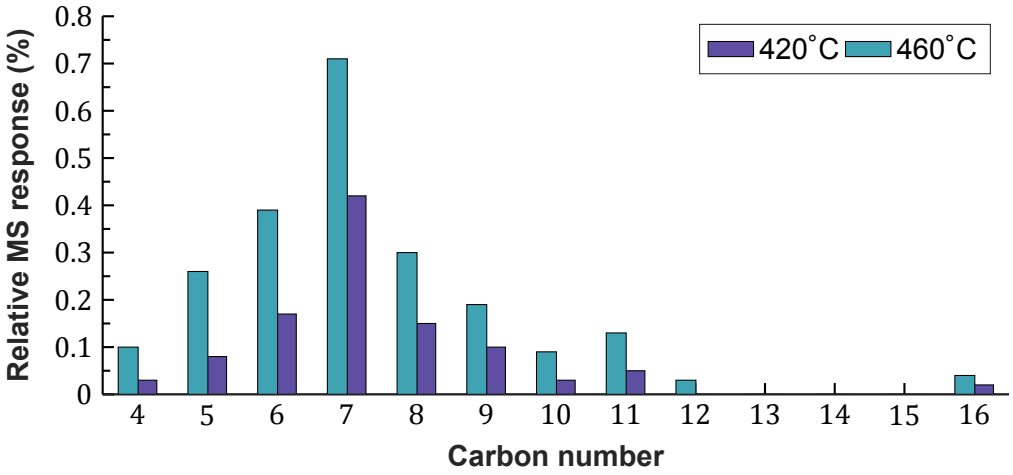

Figure 5.2: GC-MS relative response to FAs at 420°C and 460°C and residence time of 15 min

From the C-C bond cleavage of oleic acid to Oxygenates and Aliphatics as presented in Section 4.5 undecene ($C_{11}H_{22}$) was chosen to represent the Aliphatics molar weight. The relatively high presence of undecene compared to other aliphatic HCs found by the GC-MS analysis confirms this choice.

For the Cyclics it was assumed that the carbon number is equal to that of the Aliphatics group. Methyl-naphthalene ($C_{11}H_{10}$) was thus assumed to represent the Cyclics group. GC-MS analysis of a liquid sample from 520°C and residence time of 30 min was checked for the presence of methyl-naphthalene. From Section 4.2 the relatively high yield of Cyclics at these conditions was known. The GC-MS analysis indeed showed that $C_{11}H_{10}$ was present in relatively high quantities.

To handle the stoichiometry of the lumped liquid decomposition reactions, reaction (4) from Figure 4.13 was adapted to:

$$\text{Aliphatics} \longrightarrow \text{Cyclics} + 6\text{H}_2$$

Using this adapted reaction the following set of kinetic equations were implemented in the model, including Equation 5.1:

$$\frac{d[\text{Oxy}]}{dt} = k_1[\text{Oleic}] - (k_2 + k_3 + k_5 + k_6 + k_7)[\text{Oxy}] \tag{5.7}$$

$$\frac{d[\text{Aliph}]}{dt} = k_1[\text{Oleic}] + (k_2 + k_3)[\text{Ox}] - (k_7 + k_8 + k_9)[\text{Aliph}] \tag{5.8}$$

$$\frac{d[\text{Cyc}]}{dt} = k_9[\text{Aliph}] \tag{5.9}$$

$$\frac{d[\text{H}_2]}{dt} = k_5[\text{Ox}] + 6k_4[\text{Aliph}] - k_{10}[\text{Oxy}][\text{H}_2] - k_{11}[\text{Aliph}][\text{H}_2] - k_{-12}[\text{CO}_2][\text{H}_2] + k_{12}[\text{CO}][\text{H}_2\text{O}] \tag{5.10}$$

$$\frac{d[\text{CH}_4]}{dt} = k_6[\text{Oxy}] + k_8[\text{Aliph}] \tag{5.11}$$

$$\frac{d[\text{C}_\text{a}\text{H}_\text{b}]}{dt} = k_7[\text{Oxy}] + k_9[\text{Aliph}] \tag{5.12}$$

$$\frac{d[\text{CO}_2]}{dt} = k_2[\text{Oxy}] - k_{-12}[\text{CO}_2][\text{H}_2] + k_{12}[\text{CO}][\text{H}_2\text{O}] \tag{5.13}$$

$$\frac{d[\text{CO}]}{dt} = k_3[\text{Oxy}] + k_{-12}[\text{CO}_2][\text{H}_2] - k_{12}[\text{CO}][\text{H}_2\text{O}] \tag{5.14}$$

where k_i denotes the reaction rate of the according reaction number in Figure 4.13. All reaction rates were derived from the Arrhenius equation as follows:

$$k_i = A_i * \exp\left(\frac{-E_{a,i}}{RT}\right) \tag{5.15}$$

Since the water-gas-shift reaction is an equilibrium reaction either k_{12} or k_{-12} had to be fitted by the model. These reaction rates were linked to each other via the equilibrium constant K_{WGS}, which is defined as:

$$K_{WGS} = \frac{k_{12}}{k_{-12}} = \frac{[\text{CO}_2][\text{H}_2]}{[\text{CO}][\text{H}_2\text{O}]} \tag{5.16}$$

This equilibrium constant was determined using the REQUIL reactor module in Aspen Plus with the Peng-Robinson equation of state model. Peng-Robinson was chosen for its demonstrated applicability in supercritical water. Given the initial concentrations of each species and the process conditions, the REQUIL block calculates the equilibrium concentrations by the use of the chemical equilibrium constant for specified stoichiometric calculations. The initial concentrations used as input were the average concentrations of CO,CO_2,H_2 and H_2O at each experimental temperature. Finally the equilibrium constants for the WGS reaction were found

to be 4.15, 3.71 and 2.78 for 25 MPa and 420°C, 460°C and 520°C, respectively. In this study k_{-12} was chosen as the independent reaction rate.

From this analysis it was also found that water concentrations were more than two orders of magnitude higher than gas concentrations. Consequently the water-gas-shift reaction had a negligible effect on the water concentration. Therefore water concentration is assumed to be constant in this model.

The MATLAB-procedure used in Section 5.1.1 was again used in this overall decomposition model. For the fitting procedure of these kinetic parameters the SSNE equation was adapted however, since Equation 5.3 would lead to divisions by zero. This adapted equation is formulated as:

$$\text{SSNE} = \sum_{i=1}^{N} \left[\frac{y_i - y_i^{mod}}{(y_i + y_i^{mod})/2} \right]^2 \tag{5.17}$$

For all found kinetic parameters a 95% confidence interval was calculated using the approximate method described by Smith et al. [55]. A description of this method can be found in Appendix D.2

5.2.2. Model results

Figures 5.3 to 5.5 show the results of the concentrations of liquid products predicted by the fitted kinetic model together with experimental data. The results for the gas yields can be seen in Figures 5.6 to 5.8. The fitted parameters are presented in Table 5.1.

Table 5.1: Parameters fitted to the kinetic model and their 95% confidence interval. Note that the fitted parameters to reaction (12) are for the reverse rate k_{-12}

Reaction #	A_i (s^{-1})	$E_{a,i}$ (J mol^{-1})
(1)	$1.62 \cdot 10^{8} \pm 5.37 \cdot 10^{8}$	$1.51 \cdot 10^{5} \pm 1.85 \cdot 10^{4}$
(2)	$4.72 \cdot 10^{0} \pm 2.95 \cdot 10^{2}$	$5.95 \cdot 10^{4} \pm 3.78 \cdot 10^{5}$
(3)	$3.18 \cdot 10^{1} \pm 8.48 \cdot 10^{3}$	$7.93 \cdot 10^{4} \pm 1.76 \cdot 10^{4}$
(4)	$1.41 \cdot 10^{9} \pm 2.42 \cdot 10^{11}$	$1.75 \cdot 10^{5} \pm 1.16 \cdot 10^{6}$
(6)	$6.66 \cdot 10^{0} \pm 4.12 \cdot 10^{3}$	$8.09 \cdot 10^{4} \pm 3.91 \cdot 10^{6}$
(8)	$1.44 \cdot 10^{14} \pm 3.46 \cdot 10^{16}$	$2.41 \cdot 10^{5} \pm 1.67 \cdot 10^{6}$
(9)	$8.79 \cdot 10^{5} \pm 2.74 \cdot 10^{7}$	$1.16 \cdot 10^{5} \pm 1.70 \cdot 10^{5}$
(11)	$1.35 \cdot 10^{8} \pm 8.17 \cdot 10^{9}$	$1.12 \cdot 10^{5} \pm 3.34 \cdot 10^{5}$
(12)	$3.51 \cdot 10^{-5} \pm 6.90 \cdot 10^{-3}$	$9.83 \cdot 10^{2} \pm 1.31 \cdot 10^{6}$

It was found that for reactions (5), (7) and (10) physically unrealistic activation energies of higher than 10^{10} were fitted. These reactions are the gasification of Oxygenates to H_2, the cracking of Oxygenates to C_aH_b and the saturation of Oxygenates with H_2. The influence of these reactions on the concentrations predicted by the model is negligible. Therefore these reactions were removed from the model and were not considered in any further analysis on the model.

From Figures 5.3 to 5.5 it is observed that the model is able to give a good qualitative prediction on formed liquid products. The behavior of the Oxygenates as the slower reacting liquid and Aliphatics as the faster reacting liquid, described earlier in Section 4.1, can also be seen from the model predictions. Quantitatively however, the model fails to give good predictions on the presence of Oxygenates. Especially for higher temperatures and short

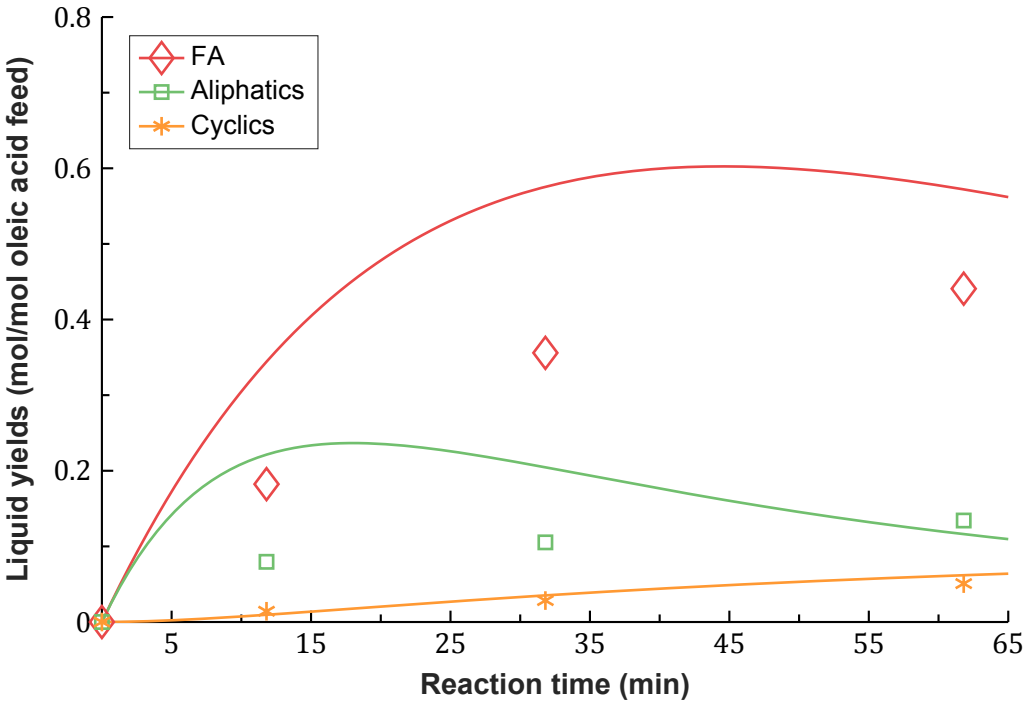

Figure 5.3: Liquid yields at 420°C as a function of reaction time. The markers represent the experimental results and the lines represent the model predictions.

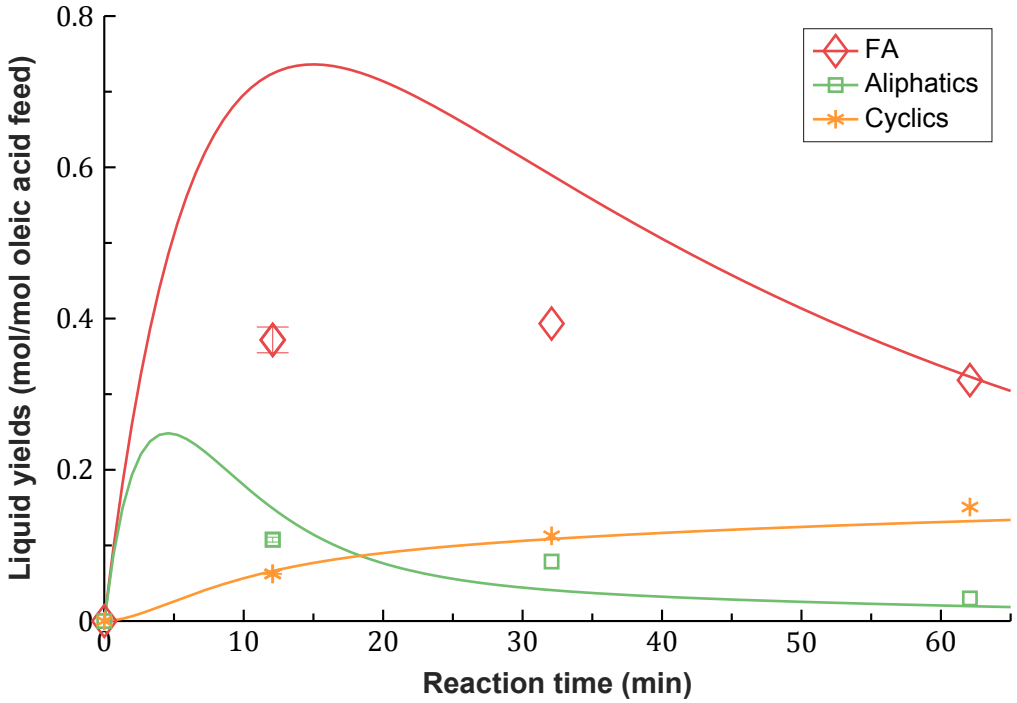

Figure 5.4: Liquid yields at 460°C as a function of reaction time. The markers represent the experimental results and the lines represent the model predictions.

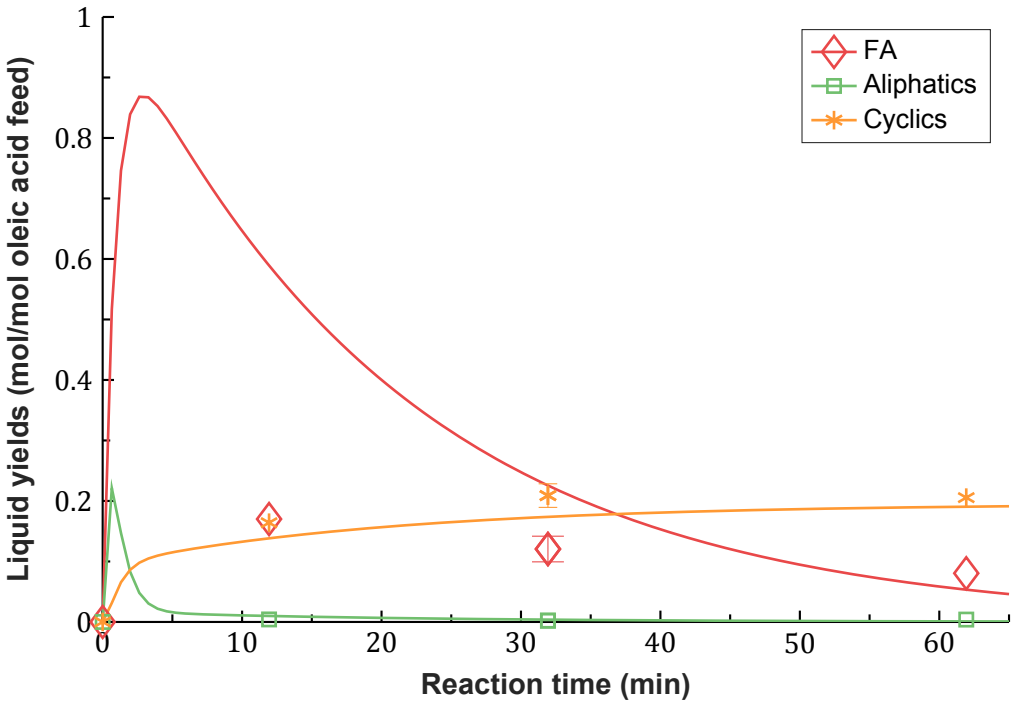

Figure 5.5: Liquid yields at 520°C as a function of reaction time. The markers represent the experimental results and the lines represent the model predictions.

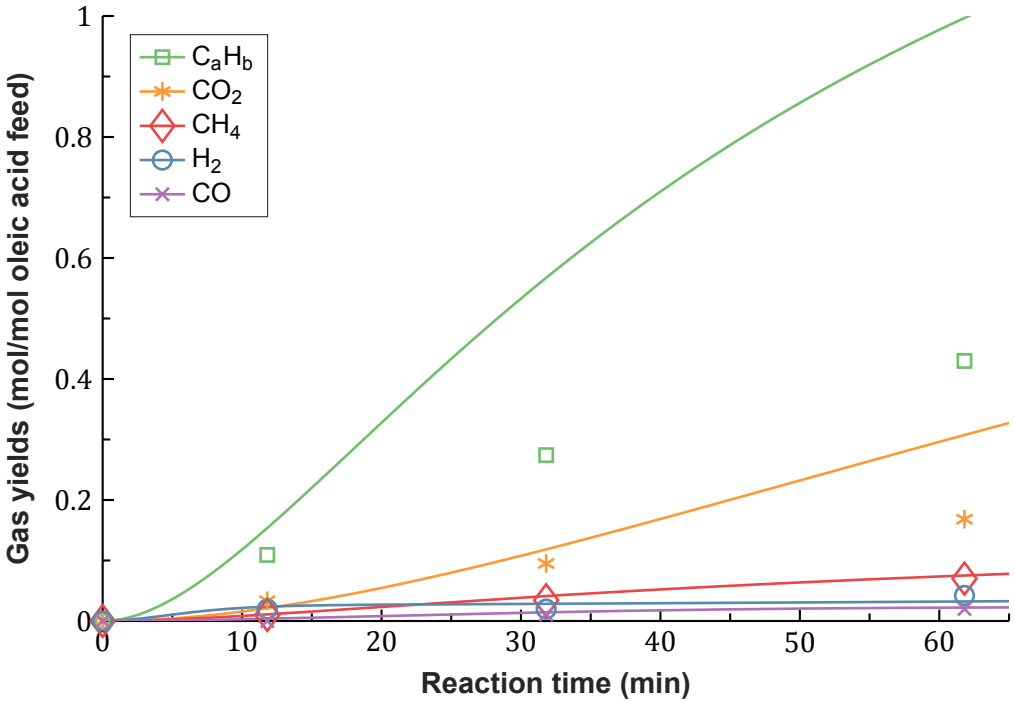

Figure 5.6: Gas yields at 420°C as a function of reaction time. The markers represent the experimental results and the lines represent the model predictions.

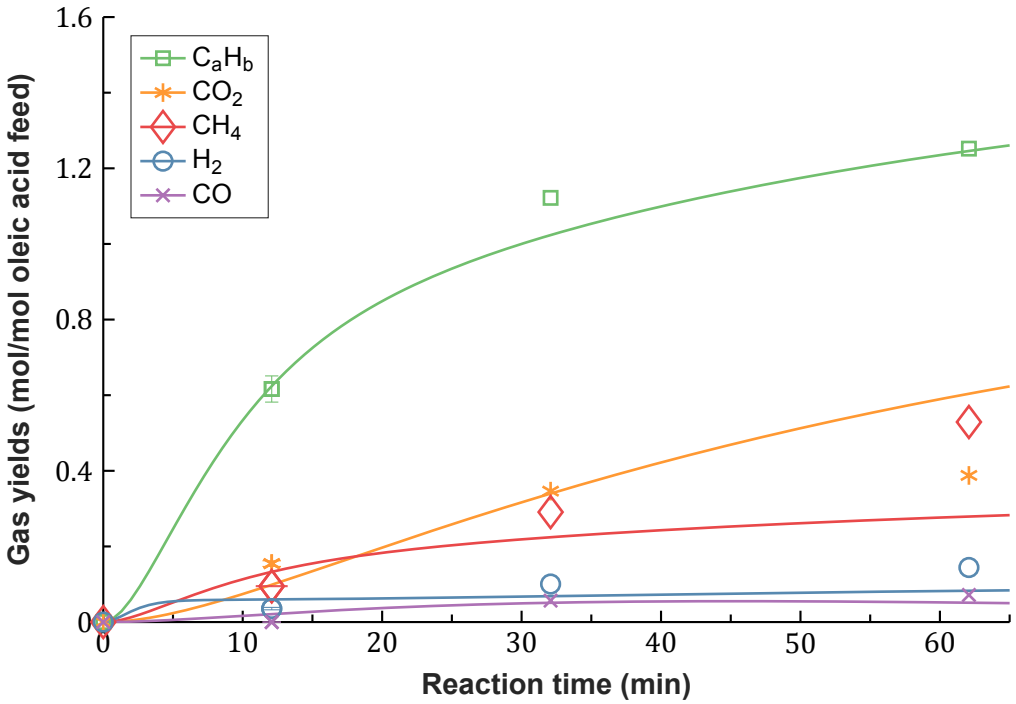

Figure 5.7: Gas yields at 460°C as a function of reaction time. The markers represent the experimental results and the lines represent the model predictions.

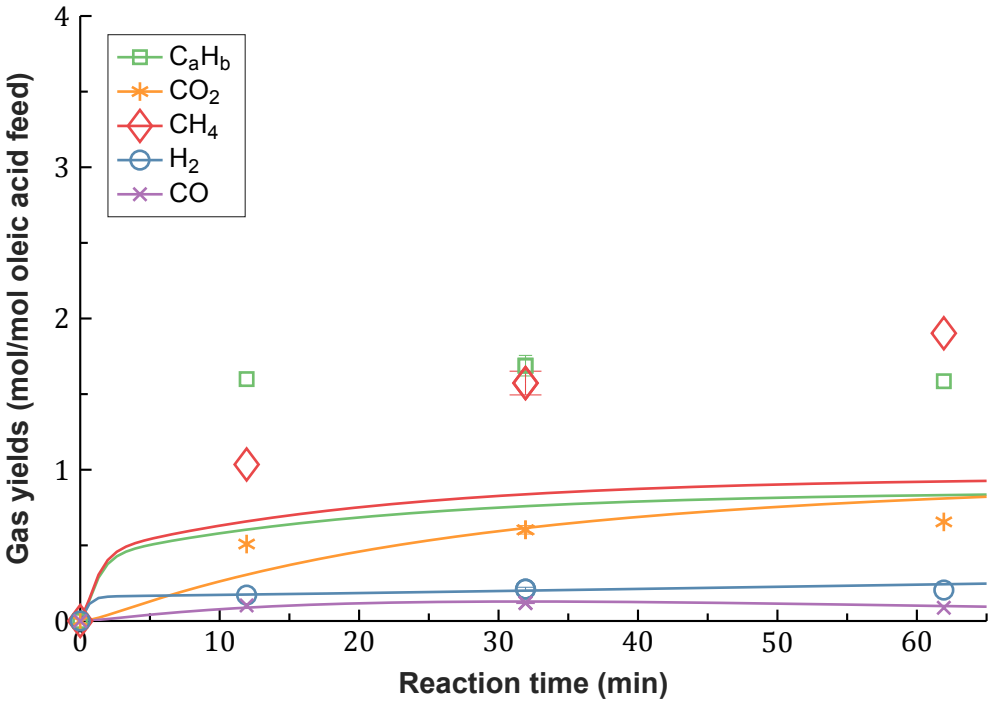

Figure 5.8: Gas yields at 520°C as a function of reaction time. The markers represent the experimental results and the lines represent the model predictions.

reaction times the model significantly over predicts the amount of Oxygenates present in the system. On the other hand the Aliphatics and Cyclics concentrations are predicted well by the system.

For the gas yields the model does also predict the qualitative trends well. The dominance of C_aH_b and CO_2 in the gas product distribution at the lower temperatures and the rapid increase of CH_4 production at higher temperatures are also presented by the model. Quantitatively the produced amount of CO_2, CO and H_2 are predicted quite well over the whole range of temperatures and reaction times. However, the significant over prediction of C_aH_b at 420°C and under prediction of C_aH_b and CH_4 at 520°C leads to the conclusion that this kinetic model cannot adequately give a good quantitative prediction of the gas yields. Because of this also, a good prediction on an important process value as the CGE cannot be given by the model.

Taking all this in account, it is concluded that this kinetic model is able to give good qualitative predictions on the SCWG of oleic acid between 420°C and 520°C. Quantitatively however, the model predictions have shown to be inaccurate for both liquid and gas yields. Two possible reasons for the inaccurate model predictions and possible solutions for them have been identified.

Firstly, the model suffers from a shortage of data points, especially in the shorter time ranges. As can be seen from the predicted liquid yield at 520°C (Figure 5.5), the system is the most reactive in the first 15 min of reaction time. There are only two data points in this range however, at 0 and 11-13 min. An accurate fit of kinetic parameters that govern these short timescale reactions could therefore not be realized. This shortage of data points can also be drawn from the broad 95% confidence intervals for the activation energies $E_{a,i}$ as presented in Table 5.1. These intervals, not including the Oleic Acid decomposition and Oxygenate decarboxylation, are between a factor of 1 to 10 broader than the value of the activation energy itself. The fitting of the parameters is thus highly uncertain. More experimental data should be acquired for reaction times between 0 and 15 min.

Secondly, Some reaction pathways that play an important role might not have been identified and added to the model or are oversimplified. The current model reactions and lumped groups are a simplification of the more complex decomposition reactions that govern the SCWG of oleic acid. An experimental study into the decomposition of certain isolated reaction products might discover these more detailed reaction pathways. The next section will highlight which decomposition products are most valuable for further study.

5.3. Sensitivity analysis

A sensitivity analysis provides insight in the relative importance of reaction rates on the yields of different products. Reactions that have the biggest impact on the model predictions and are therefore the most valuable for further research can be recognized. The governing equations and used procedure for this analysis are presented first. Subsequently the analysis results are shown and will be discussed.

5.3.1. Equations and procedure

The governing equations and procedure used for this sensitivity analysis are reported earlier by Guan et al. [50]. The sensitivity coefficient, S_{ij}, can be defined as:

$$S_{ij} = \frac{\partial \ln C_i}{\partial \ln k_j} = \frac{\Delta C_i / C_i}{\Delta k_j / k_j} \tag{5.18}$$

The larger the absolute value of the sensitivity coefficient, the more sensitive that concentration is to the value of the particular reaction rate.

The sensitivity coefficient was calculated by changing each reaction rate k_j with 5%, one at a time, and then using the kinetic model to calculate the change in each species concentration. This was repeated for reaction temperatures of 420, 460 and 520°C and a short reaction time of 5 min and long reaction time of 60 min.

For a general view on the influence of each reaction rate on the model results as a whole, the absolute value of the sensitivity coefficient was summed over all species concentrations i for each j as follows:

$$S_{sum,j} = \sum_i \text{abs}(S_{ij}) \tag{5.19}$$

5.3.2. Analysis results

Table 5.2 shows the summed sensitivity coefficient resulting from the sensitivity analysis for different temperatures and reaction times. Values of 2 and above are highlighted in ***bold and italics***. This value corresponds to a summed change of 10% in product yields for a 5% perturbation in reaction rate.

Table 5.2: Summed sensitivity coefficients for different temperatures and reaction times. Values of 2 and above are in ***bold and italics***.

	T = 420 C		T = 460 C		T = 520 C	
Rate	**5 min**	**60 min**	**5 min**	**60 min**	**5 min**	**60 min**
k_1	***7.35***	***4.48***	***5.82***	***8.21***	***6.07***	***10.51***
k_2	1.09	***2.04***	1.17	***2.41***	1.93	19.68
k_3	1.04	1.41	1.05	1.51	1.31	***2.37***
k_4	***2.01***	1.94	***2.08***	***2.18***	***2.19***	***2.45***
k_6	0.06	0.16	0.02	0.18	0.04	0.37
k_8	0.97	1.01	1.18	1.56	1.96	***9.76***
k_9	1.45	***2.80***	1.92	***2.59***	1.90	***4.72***
k_{11}	0.23	0.93	0.78	0.98	0.89	0.79
k_{-12}	0.10	0.82	0.08	0.93	0.07	1.40

Reactions rates that show to have a major influence on the product yields are k_1, k_2, k_4 and k_9. For higher temperatures and longer reaction times product yields are also sensitive to k_3 and k_8. This suggests that the decomposition of oleic acid in SCWG is governed by the reactions that belong to these reaction rates, which are:

- Oleic Acid C-C bond cleavage into Aliphatics and Oxygenates
- Decarboxylation of Oxygenates to CO_2 and Aliphatics
- Decarbonylation of Oxygenates to CO and Aliphatics
- Dehydrogenation of Aliphatics to H_2 and Cyclics
- Cracking of Aliphatics to CH_4 and C_aH_b.

Kinetic models in SCWG will be mainly used for predictions on gas yields. As concluded in Section 5.2 the yields of mainly CH_4 and C_aH_b should be improved for the presented kinetic model to give reliable predictions on absolute gas yields and CGE values. Therefore the sensitivity coefficient for these two gas products was analyzed. Table 5.3 shows the absolute sensitivity coefficient for CH_4 and C_aH_b. A value of 1 means that a 5% perturbation in the reaction rate results in a 5% change in product concentration.

Table 5.3: Absolute sensitivity coefficient for CH_4 and C_aH_b concentrations. Values above 0.1 are shown in ***bold and italics***.

		T=420°C		**T=460°C**		**T=520°C**	
Time	**Rate**	**CH_4**	**C_aH_b**	**CH_4**	**C_aH_b**	**CH_4**	**C_aH_b**
5 min	k_1	***0.932***	***0.932***	***0.736***	***0.735***	0.052	0.050
60 min	k_1	***0.355***	***0.344***	***0.034***	***0.031***	0.001	0.001
5 min	k_2	0.014	0.015	0.028	0.029	0.091	0.093
60 min	k_2	***0.109***	***0.150***	***0.133***	***0.173***	0.045	0.072
5 min	k_3	0.003	0.003	0.007	0.008	0.031	0.032
60 min	k_3	0.024	0.033	0.035	0.046	0.016	0.025
5 min	k_4	0.008	0.009	0.036	0.037	0.097	0.098
60 min	k_4	0.042	0.048	0.073	0.079	0.095	0.099
5 min	k_6	0.056	0.000	0.019	0.000	0.013	0.001
60 min	k_6	***0.120***	0.001	0.071	0.005	0.024	0.015
5 min	k_8	***0.935***	0.009	***0.908***	0.071	***0.524***	***0.447***
60 min	k_8	***0.831***	0.051	***0.774***	***0.154***	***0.503***	***0.453***
5 min	k_9	***0.133***	***0.853***	***0.335***	***0.642***	***0.415***	***0.558***
60 min	k_9	***0.652***	***0.221***	***0.669***	***0.239***	***0.409***	***0.552***
5 min	k_{11}	0	0	0	0	0	0
60 min	k_{11}	0	0	0	0	0	0
5 min	k_{-12}	0	0	0	0	0	0
60 min	k_{-12}	0	0	0	0	0	0

It is noticed at first from this sensitivity analysis that reaction (6), the formation of CH_4 from Oxygenates, has relatively little to no influence on the yields of these gases. Almost all of the production of methane and the light hydrocarbon gases should then proceed via cracking of Aliphatics. This leads to the high sensitivity coefficients for the cracking reactions (8) and (9) from Aliphatics.

Furthermore, the Oleic Acid C-C bond cleavage (k_1) and Oxygenate decarboxylation (k_2) rates show to have a significant impact on CH_4 and C_aH_b production at 420 and 460°C. These are the main formation routes to Aliphatics, out of which as argued the vast majority of hydrocarbon gases are produced.

Conclusively, from the sensitivity analysis presented in this section three reactions show to be dominant in both overall products yields as well as CH_4 and C_aH_b gases yields. These three reactions are the C-C bond cleavage of Oleic Acid, the decarboxylation of Oxygenates and the cracking of Aliphatics. This study already looked at the isolated decomposition of Oleic Acid. Further studies could look into the decomposition of Oxygenates in SCW and the influence of the decarboxylation reaction on it. Also, studying the isolated decomposition of Aliphatics and dominance of the cracking reaction in a SCWG process could be valuable. Results from these studies can improve the model predictions in general as well as improve the predictions on

yields of methane and the light HC gases. The absolute sensitivity coefficients for all 9 model components can be found in Appendix D.1

6

Conclusions and Recommendations

In this thesis the results of a study into the supercritical water gasification of lipids forming a substantial part of sewage sludge were presented. This chapter presents the conclusions and recommendations of this work.

In the first section the conclusions of the study and answers to the research questions will be given. From these conclusions recommendations for further research were made and they are shown in the final section.

6.1. Conclusions

- *Which compound can act as a representative model compound for the SCWG of lipids from sewage sludge?*

In hydrothermal media lipids quickly hydrolyze to individual FAs and glycerol. Glycerol is a well defined compound and its decomposition in SCW has been covered by literature well. A decomposition model of FAs in SCW has however not yet been proposed. Therefore it was decided to study and model the decomposition of a fatty acid in SCW, thereby improving the gasification modeling of a sewage sludge SCWG process. Oleic acid was found to be the most representative FA for the SCWG of lipids from sewage sludge.

- *What experiments and analyses are needed to build-up a kinetic model consisting of the main reactions of the SCWG of the model compound?*

An experimental set-up from the University of Groningen was used to conduct the experiments. A mixture of oleic acid and water was loaded into a stainless steel batch reactor, which was heated by placing it into a heated fluidized sand bath and cooled down in another fluidized sand bath at room temperature. When the reactor was cooled down liquid and gas samples would be taken and analyzed. A feed concentration of 10 wt% and pressure of 25 MPa were applied at each experiment. Experiments at temperatures of 400, 420, 460 and 520°C and residence times of 15, 35 and 65 min were performed.

Gas samples were analyzed with a Gas-GC for the presence of H_2, CH_4, CO, CO_2, C_2H_4, C_2H_6, C_3H_6 and C_3H_8 gases. Liquid samples were analyzed on the presence of oleic acid using a GC-MS and a 2D-GC analysis was used to identify and quantify the decomposition product groups in the liquid.

- *Which reaction products are found from the experiments and what main reaction pathways can explain their presence?*

Results for the yields of liquid products revealed that the first decomposition products from oleic acid in SCW are LFAs, VFAs and aliphatic HCs. The proposed mechanism for this decomposition is the C-C bond cleavage of oleic acid to shorter chain FAs and aliphatic HCs. These FAs themselves also decompose to aliphatic HCs via decarboxylation and decarbonylation. The next liquid decomposition components that were identified were the cycloalkanes. Components in this group are formed via the cyclization of aliphatic HCs and are precursors for the aromatics and napthalenes, that form through dehydrogenation of the cycloalkanes at higher temperatures and longer residence times.

The main gas produced at lower temperatures was CO_2. Also a remarkably high selectivity of the light HC gases compared to an earlier oleic acid SCWG study was observed. Production of CO_2 at lower temperatures confirms the presence of the decarboxylation reaction. Through decarbonylation the relatively small amounts of CO were produced, which could also be consumed through the water-gas-shift reaction. Methane, which was the main product gas at higher temperatures, and light HC gases are most likely formed trough cracking of the FAs and aliphatic HCs. Hydrogen was also found in small quantities and could be formed via gasification of FAs, the WGS reaction and the dehydrogenation of aliphatic HCs to aromatics via cycloalkanes. Saturation reactions with unsaturated aliphatic HCs and fatty acids consume H_2.

A decomposition model was constructed from the identified decomposition products and reactions. A simplification on the decomposition of the liquid products was made by creating lumped groups, in which compound groups are lumped together that are assumed to have a similar reactive behaviour. These lumped groups are:

- Oxygenates: LFAs, VFAs, ketones & alcohols and methylesthers
- Aliphatics: large and small aliphatic hydrocarbons.
- Cyclics: cycloalkanes, aromatics and naphtalenes
- C_aH_b (or light HC gases): C_2H_4, C_2H_6, C_3H_6 and C_3H_8

- *Which kinetic parameters can be fitted to these reaction pathways?*

Before kinetic parameters were fitted to the decomposition model, the conversion of oleic acid was modeled. A (pseudo)first-order kinetic and Arrhenius behaviour were assumed for this conversion reaction. Using a MATLAB routine that minimized the error between the experimental results and model predictions on species concentration, an activation energy E_a and pre-exponential A were fitted. The percentage output variation (FIT) was used as a measure for validity of predictions by the model: a FIT of 80% or higher is regarded a good prediction.

It was decided to exclude the data at 400°C from the kinetic modeling since this resulted in a low FIT. This temperature is near the critical point and reactions at near-critical conditions show non-Arrhenius like behaviour. The fitting of the conversion model to data at 420, 460 and 520°C yielded a FIT of 82%. The A and E_a of oleic acid decomposition in SCW were found to be $1.62 \bullet 10^8$ s^{-1} and $1.51 \bullet 10^5$ J mol^{-1}, respectively. These fitted parameters were implemented in the kinetic model.

The kinetic model that was finally constructed from the proposed decomposition scheme and conversion model results consisted out of nine components and their concentrations were determined by nine reactions. For each reaction the E_a and A were fitted to the experimental data using the same Matlab routine as for the conversion modeling.

- *Under which conditions and for what purposes can this kinetic model be used?*

From the comparison of the model predictions and the experimental results on liquid and gas yields it was concluded that the model was able to correctly predict the qualitative trends. The distinction between Aliphatics as a fast reacting intermediate versus Oxygenates and Cyclics as more stable liquid components, as concluded from the experiments, was also displayed by the model. The model also showed the production of CO_2 and C_aH_b as main gases at lower temperatures, which shifts to CH_4 and light hydrocarbon gases as main gas products at the highest temperatures. This trend was shown by the experimental results likewise.

However, quantitative predictions are inaccurate. Especially the yields of methane and light hydrocarbon gases are not accurately predicted. This leads to wrong predictions on important quantitative process values such as the CGE. The model in its current state can therefore not be implemented into a kinetic model on the SCWG of sewage sludge for operational purposes.

6.2. Recommendations

It has been concluded that the presented kinetic model cannot give accurate quantitative predictions. Recommendations on how this model can be improved as as a result of future studies are listed below.

- From a sensitivity analysis three reactions were identified as the governing reactions in the model: The C-C bond cleavage of Oleic Acid, the Oxygenates decarboxylation and the cracking reaction of Aliphatics to methane and light HC gases. Isolated Oleic Acid decomposition has been studied in this thesis. Studying the isolated decomposition of Oxygenates and Aliphatics can give insight into more detailed reaction mechanisms that possibly describe the decomposition of Oleic Acid in SCWG better than decarboxylation and cracking. Extending the model with more detailed reactions can improve its predictions. These more detailed reactions should follow from a more detailed analysis of reactions products, identifying individual components. One can think of analyzing the distribution of aliphatic HCs by carbon chain length from decomposition of a Aliphatic model compound in SCW.

- More experimental data should be acquired for reaction times between 0 and 15 min. While the studied SCWG process is the most reactive in this time scale, only two data points are available for each component and temperature in this range. This is the main reason for the broad 95% confidence intervals of the kinetic parameters, which indicates that the fitted value for them is highly uncertain. To find accurate data in this time range the heat-up times should be reduced however. This can be done by equipping the reactor with a special valve that allows the addition of oleic acid when the reactor with water is at the desired temperature and pressure.

- When the conversion of oleic acid was modeled with a second-order reaction a FIT of 92% was found. A possible second-order reaction of oleic acid is the esterification

with an alcohol to a fatty acid methyl ester (FAME). However, the amounts of these products found were too low to implement this reaction in the kinetic model. The study and possible identification of a second-order decomposition reaction of oleic acid in SCW could significantly improve the model predictions.

Finally some general recommendations on the SCWG of lipids from sewage sludge are presented.

- To validate the choice for a fatty acid as model compound for lipids, similar experiments as in this thesis should be performed with an adapted feed. One should replace the pure oleic acid used here with a mixture of glycerol:oleic acid 1:3 on a molar basis, since that represents the natural ratio of the glycerol backbone and FAs in lipids. The feed concentration of this mixture in water should be equal to the 10 wt% feed concentration used here. Results between both studies can then be compared.
- The low carbon mass balance from the oleic acid experiments indicates that a significant amount of products was left unidentified. To account for the carbon in these products the liquid effluent should be sampled differently. A separate aqueous phase sample and non-aqueous phase sample should be acquired. The carbon in this aqueous phase sample can be found through TOC analysis. The carbon in the non-aqueous phase can be detected by using a thermogravimetric analyzer that can measure the amount of formed CO_2.
- From earlier studies on the hydrothermal liquefaction (HTL) and pyrolysis of FAs the rate of olefinicity showed to have a large influence on the formed decomposition products. Stearic acid as saturated FA and linoleic acid as poly-unsaturated FA have the same carbon number as oleic acid. With an experimental study similar to the one carried out in this thesis using these FAs, the influence of olefinicity on the decomposition product yields in SCW can be determined.

Bibliography

[1] Dmitri Ma. Modern urban wastewater treatment plant. URL https://www.shutterstock.com/image-photo/modern-urban-wastewater-treatment-plant-576627958?src=qouSyXhuCyaw3CmWEVU8iA-1-1. [Online; accessed October 17, 2017].

[2] Emhemmed A Youssef, George Nakhla, and Paul A Charpentier. Oleic acid gasification over supported metal catalysts in supercritical water: hydrogen production and product distribution. *international journal of hydrogen energy*, 36(8):4830–4842, 2011.

[3] U.S. Energy Information Agency. International energy outlook 2016, 2016.

[4] Ministerie van Economische Zaken. Energieagenda, naar een co2-arme energievoorziening, 2016. URL "https://www.rijksoverheid.nl/documenten/rapporten/2016/12/07/ea".

[5] Isabel Fonts, Gloria Gea, Manuel Azuara, Javier Ábrego, and Jesús Arauzo. Sewage sludge pyrolysis for liquid production: a review. *Renewable and sustainable energy reviews*, 16(5):2781–2805, 2012.

[6] Alexandros Kelessidis and Athanasios S Stasinakis. Comparative study of the methods used for treatment and final disposal of sewage sludge in european countries. *Waste management*, 32(6):1186–1195, 2012.

[7] Chao He, Chia-Lung Chen, Apostolos Giannis, Yanhui Yang, and Jing-Yuan Wang. Hydrothermal gasification of sewage sludge and model compounds for renewable hydrogen production: a review. *Renewable and Sustainable Energy Reviews*, 39:1127–1142, 2014.

[8] Miao Gong, Wei Zhu, Huiwen Zhang, Ying Su, and Yujie Fan. Polycyclic aromatic hydrocarbon formation from gasification of sewage sludge in supercritical water: The concentration distribution and effect of sludge properties. *The Journal of Supercritical Fluids*, 113:112–118, 2016.

[9] Yoshikuni Yoshida, Kiyoshi Dowaki, Yukihiko Matsumura, Ryuji Matsuhashi, Dayin Li, Hisashi Ishitani, and Hiroshi Komiyama. Comprehensive comparison of efficiency and co2 emissions between biomass energy conversion technologies - position of supercritical water gasification in biomass technologies. *Biomass and Bioenergy*, 25(3):257–272, 2003.

[10] Onursal Yakaboylu, Guchan Yapar, Mayra Recalde, John Harinck, KG Smit, Emanuele Martelli, and Wiebren de Jong. Supercritical water gasification of biomass: An integrated kinetic model for the prediction of product compounds. *Industrial & Engineering Chemistry Research*, 54(33):8100–8112, 2015.

[11] Derek R Vardon, Brajendra K Sharma, Humberto Jaramillo, Dongwook Kim, Jong Kwon Choe, Peter N Ciesielski, and Timothy J Strathmann. Hydrothermal catalytic processing of saturated and unsaturated fatty acids to hydrocarbons with glycerol for in situ hydrogen production. *Green Chemistry*, 16(3):1507–1520, 2014.

[12] Thomas Robin, Jenny M Jones, and Andrew B Ross. Catalytic hydrothermal processing of lipids using metal doped zeolites. *Biomass and Bioenergy*, 98:26–36, 2017.

[13] Michael C Johnson and Jefferson W Tester. Lipid transformation in hydrothermal processing of whole algal cells. *Industrial & Engineering Chemistry Research*, 52(32): 10988–10995, 2013.

[14] Xander Dupain, Daniel J Costa, Colin J Schaverien, Michiel Makkee, and Jacob A Moulijn. Cracking of a rapeseed vegetable oil under realistic fcc conditions. *Applied Catalysis B: Environmental*, 72(1):44–61, 2007.

[15] David GB Boocock, Samir K Konar, Anna Leung, and Lang D Ly. Fuels and chemicals from sewage sludge: 1. the solvent extraction and composition of a lipid from a raw sewage sludge. *Fuel*, 71(11):1283–1289, 1992.

[16] Véronique Réveillé, Laurence Mansuy, Émilie Jardé, and Évelyne Garnier-Sillam. Characterisation of sewage sludge-derived organic matter: lipids and humic acids. *Organic Geochemistry*, 34(4):615–627, 2003.

[17] Wolfgang Wagner and Hans-Joachim Kretzschmar. Iapws industrial formulation 1997 for the thermodynamic properties of water and steam. *International Steam Tables: Properties of Water and Steam Based on the Industrial Formulation IAPWS-IF97*, pages 7–150, 2008.

[18] Andrea Kruse and Nicolaus Dahmen. Water–a magic solvent for biomass conversion. *The Journal of Supercritical Fluids*, 96:36–45, 2015.

[19] M Uematsu and EU Frank. Static dielectric constant of water and steam. *Journal of Physical and Chemical Reference Data*, 9(4):1291–1306, 1980.

[20] William L Marshall and EU Franck. Ion product of water substance, 0–1000 c, 1–10,000 bars new international formulation and its background. *Journal of Physical and Chemical Reference Data*, 10(2):295–304, 1981.

[21] Prabir Basu and Vichuda Mettanant. Biomass gasification in supercritical water–a review. *International Journal of Chemical Reactor Engineering*, 7(1), 2009.

[22] A Kruse and E Dinjus. Hot compressed water as reaction medium and reactant: properties and synthesis reactions. *The Journal of supercritical fluids*, 39(3):362–380, 2007.

[23] Onursal Yakaboylu, John Harinck, KG Smit, and Wiebren de Jong. Supercritical water gasification of biomass: A literature and technology overview. *Energies*, 8(2):859–894, 2015.

[24] JerryáW King, RussellálL Holliday, and GaryáR List. Hydrolysis of soybean oil. in a subcritical water flow reactor. *Green Chemistry*, 1(6):261–264, 1999.

[25] Andrew A Peterson, Frédéric Vogel, Russell P Lachance, Morgan Fröling, Michael J Antal Jr, and Jefferson W Tester. Thermochemical biofuel production in hydrothermal media: a review of sub-and supercritical water technologies. *Energy & Environmental Science*, 1(1):32–65, 2008.

[26] Sivamohan N Reddy, Sonil Nanda, Ajay K Dalai, and Janusz A Kozinski. Supercritical water gasification of biomass for hydrogen production. *International Journal of Hydrogen Energy*, 39(13):6912–6926, 2014.

[27] O Yakaboylu, J Harinck, KG Smit, and W de Jong. Testing the constrained equilibrium method for the modeling of supercritical water gasification of biomass. *Fuel Processing Technology*, 138:74–85, 2015.

[28] Michael Modell. Gasification and liquefaction of forest products in supercritical water. In *Fundamentals of thermochemical biomass conversion*, pages 95–119. Springer, 1985.

[29] Michael Jerry Antal Jr, Stephen Glen Allen, Deborah Schulman, Xiaodong Xu, and Robert J Divilio. Biomass gasification in supercritical water. *Industrial & Engineering Chemistry Research*, 39(11):4040–4053, 2000.

[30] Xiadong Xu and Michael Jerry Antal. Gasification of sewage sludge and other biomass for hydrogen production in supercritical water. *Environmental progress*, 17(4):215–220, 1998.

[31] Yunan Chen, Liejin Guo, Wen Cao, Hui Jin, Simao Guo, and Ximin Zhang. Hydrogen production by sewage sludge gasification in supercritical water with a fluidized bed reactor. *International Journal of Hydrogen Energy*, 38(29):12991–12999, 2013.

[32] ZR Xu, W Zhu, M Li, HW Zhang, and M Gong. Quantitative analysis of polycyclic aromatic hydrocarbons in solid residues from supercritical water gasification of wet sewage sludge. *Applied energy*, 102:476–483, 2013.

[33] L. Korving. Experimenteel onderzoek superkritisch vergassen van zuiveringsslib, 2015.

[34] Motonobu Goto, Takatsugu Nada, Akio Kodama, and Tsutomu Hirose. Kinetic analysis for destruction of municipal sewage sludge and alcohol distillery wastewater by supercritical water oxidation. *Industrial & engineering chemistry research*, 38(5):1863–1865, 1999.

[35] D Klingler, J Berg, and H Vogel. Hydrothermal reactions of alanine and glycine in sub-and supercritical water. *The Journal of Supercritical Fluids*, 43(1):112–119, 2007.

[36] Lailatul Qadariyah, Siti Machmudah, Mitsuru Sasaki, Motonobu Goto, et al. Degradation of glycerol using hydrothermal process. *Bioresource technology*, 102(19):9267–9271, 2011.

[37] Bernard M Kabyemela, Tadafumi Adschiri, Roberto M Malaluan, and Kunio Arai. Glucose and fructose decomposition in subcritical and supercritical water: detailed reaction pathway, mechanisms, and kinetics. *Industrial & Engineering Chemistry Research*, 38 (8):2888–2895, 1999.

[38] Tau Len-Kelly Yong and Matsumura Yukihiko. Kinetic analysis of guaiacol conversion in sub-and supercritical water. *Industrial & Engineering Chemistry Research*, 52(26): 9048–9059, 2013.

[39] Pooya Azadi, Elie Afif, Hooman Foroughi, Tingsong Dai, Faraz Azadi, and Ramin Farnood. Catalytic reforming of activated sludge model compounds in supercritical water using nickel and ruthenium catalysts. *Applied Catalysis B: Environmental*, 134:265–273, 2013.

[40] Elena Markočič, Boris Kramberger, Joost G van Bennekom, Hero Jan Heeres, John Vos, and Željko Knez. Glycerol reforming in supercritical water; a short review. *Renewable and Sustainable Energy Reviews*, 23:40–48, 2013.

[41] W Bühler, E Dinjus, HJ Ederer, A Kruse, and C Mas. Ionic reactions and pyrolysis of glycerol as competing reaction pathways in near-and supercritical water. *The Journal of Supercritical Fluids*, 22(1):37–53, 2002.

[42] Russell L Holliday, Jerry W King, and Gary R List. Hydrolysis of vegetable oils in sub-and supercritical water. *Industrial & Engineering Chemistry Research*, 36(3):932–935, 1997.

[43] Jie Fu, Xiuyang Lu, and Phillip E Savage. Hydrothermal decarboxylation and hydrogenation of fatty acids over pt/c. *ChemSusChem*, 4(4):481–486, 2011.

[44] Sergiy Popov and Sandeep Kumar. Rapid hydrothermal deoxygenation of oleic acid over activated carbon in a continuous flow process. *Energy & Fuels*, 29(5):3377–3384, 2015.

[45] Justice Asomaning, Paolo Mussone, and David C Bressler. Thermal deoxygenation and pyrolysis of oleic acid. *Journal of Analytical and Applied Pyrolysis*, 105:1–7, 2014.

[46] C M Schonlein. System modeling of supercritical water gasification processes: Thermo-fluid one-dimensional modeling in modelica language. Master's thesis, Delft University of Technology, 2016.

[47] Johannes B Müller and Frédéric Vogel. Tar and coke formation during hydrothermal processing of glycerol and glucose. influence of temperature, residence time and feed concentration. *The Journal of Supercritical Fluids*, 70:126–136, 2012.

[48] Qingqing Guan, Phillip E Savage, and Chaohai Wei. Gasification of alga nannochloropsis sp. in supercritical water. *The Journal of Supercritical Fluids*, 61:139–145, 2012.

[49] JG Van Bennekom, VA Kirillov, YI Amosov, T Krieger, RH Venderbosch, D Assink, KPJ Lemmens, and HJ Heeres. Explorative catalyst screening studies on reforming of glycerol in supercritical water. *The Journal of Supercritical Fluids*, 70:171–181, 2012.

[50] Qingqing Guan, Chaohai Wei, and Phillip E Savage. Kinetic model for supercritical water gasification of algae. *Physical Chemistry Chemical Physics*, 14(9):3140–3147, 2012.

[51] JG Van Bennekom, RH Venderbosch, D Assink, and HJ Heeres. Reforming of methanol and glycerol in supercritical water. *The Journal of Supercritical Fluids*, 58(1):99–113, 2011.

[52] National Institute of Standards and Technology. Nist chemistry webbook, 2016. URL "http://webbook.nist.gov/chemistry/".

[53] B Danon, L Van der Aa, and W De Jong. Furfural degradation in a dilute acidic and saline solution in the presence of glucose. *Carbohydrate research*, 375:145–152, 2013.

[54] Nattacha Paksung, Ren Nagano, and Yukihiko Matsumura. Detailed mechanism of xylose decomposition in near-critical and supercritical water. *Energy & Fuels*, 30(10):7930–7936, 2016.

[55] Laurence H Smith, Peter K Kitanidis, and Perry L McCarty. Numerical modeling and uncertainties in rate coefficients for methane utilization and tce cometabolism by a methane-oxidizing mixed culture. *Biotechnology and Bioengineering*, 53(3):320–331, 1997.

A Pre-experimental data and calculations

A.1. Decomposition described by Youssef et al. [2]

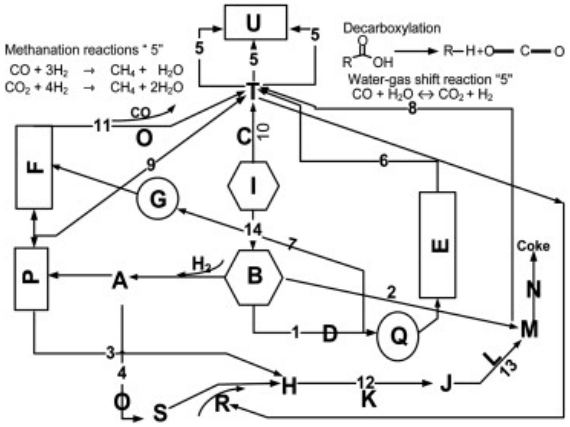

Figure A.1: Reaction pathway of oleic acid in SCW as proposed by [2].

A	Fatty acid esters (e.g. Hexadecanoic acid (ethyl, methyl, tetradecyl, and octadecyl esters))
B	LCFA's, saturated FA, and VFA's
C	Thermal decomposition
D	Decarboxylation and decarbonylation
E	Ether dehydration and alcohol dehydration
F	Ketones, fatty acids and fatty acid esters
G	C-C cleavage
H	Olefins (e.g. Nonene)
I	Oleic acid
J	Cyclo-compounds
K	Diels-Alder Cyclization
L	Aromatization
M	Aromatics (e.g. toluene, ethylbenzene)
N	Polymerization and condensation
O	Decarbonylation
P	Unknown intermediates
Q	R-H, R-OH, CO2, CO
R	Ethylene
S	'R"-CO2
T	H2, CO, CO2, CH4, and C2-C3
U	H2, CH4, CO2, and H2O

Table A.1: Product formation main routes

Detected products	Process No. in Fig. A.1	Possible formation route
H2	5, 8 and 10	Dehydrogenation of the saturated compounds forming olefins, splitting of hydrocarbon molecules into its elements, formation of aromatics, and the water-gas shift reaction
CO2	1, 4, and 5	Decarboxylation of unsaturated and saturated carboxylic acids
CH4	9 and 5	Decomposition of formed intermediate compounds such as acetic acid), other possible gasification routes, methanation reactions (Eqs. (3) and (4))
CO	1, 9, and 11	Decarbonylation of fatty acids, fatty acid esters, and other intermediate oxygenated hydrocarbons
LCFAs and VFAs and hydrocarbon radicals	14	Hydrolysis of oleic acid followed by thermal cracking and C-C bond cleavage.
Cyclo-compounds (indene, naphthalene, cyclobutene, 2-propenylidene-, etc)	12	Diels-Alder addition of ethylene to a conjugated diene
Conjugated dienes	7	β-scission of unsaturated free fatty acids and hydrocarbons
Aromatics (toluene, ethylbenzene, p-xylene, etc)	2 and 13	Elimination of hydrogen from cyclo-compounds

A.2. Initial loading calculations and experiments

The calculations used to determine the initial feed and nitrogen loading in the reactor for different temperatures are presented here. This analysis was performed prior to the preliminary experiments, were only water and nitrogen were initially loaded. From results of the preliminary experiments it was decided to apply some changes in reaction temperatures. Therefore calculations here are performed for different temperatures than the eventually applied temperatures in experiments. In practice, calculated initial loading values of evaluated temperatures near the experimental temperatures were used as a first trial in preliminary experiments. Using trial and error the nitrogen pressure and water loading were changed to obtain the desired pressure at the experimental temperatures.

Since the pressure in the reactor could not be actively controlled during the experiments, the initial fraction of reaction mixture to inert gas had to be adapted to reach the specific pressure at the desired temperature level. It was assumed that the influence of oleic acid and formed gas- and liquid products during the experiments, did not have a significant influence on the pressure. A concentration of 10 wt% oleic acid in water only represents $6*10^{-3}$ moles of oleic acid per mole water. This simplified the reaction mixture calculations to a binary nitrogen-water system. The validity of this simplification was tested for a system with initially 10 wt% oleic acid to water, where 2 moles of CH_4, 2 moles of H_2 and 1 mole of CH_4 per mole of oleic acid were formed. These gas formation rates were based on the results of non-catalytic oleic acid SCWG at 500 °C, 280 bar and 30 min residence time by Youssef et al. [2]. At a reaction temperature and pressure of 550 °C and 250 bar respectively, the system including oleic acid and formed gases only deviated 0.5% in specific volume from the binary system with the same initial water molar fraction.

The reactor is a closed, fixed volume system. This means that the volume in the system is constant throughout the whole heating process. Specific volume is a function of temperature, pressure and molar composition. The following equation thus had to be solved for the molar water fraction:

$$v_{mix}(P_0, T_0, x_{\mathrm{H_2O}}) = v_{mix}(P_1, T_1, x_{\mathrm{H_2O}}) \tag{A.1}$$

where v_{mol} is the specific molar volume of the mixture in l/mol and $x_{\mathrm{H_2O}}$ is the molar fraction of H_2O in the mixture. T_0 and P_0 denote the temperature and pressure of the reactor before entering the sand bath. T_1 and P_1 are the desired reaction temperature and pressure. Assuming an ideal mixture between water and nitrogen at T_0 = 20°C and P_0 = 20 bar, the specific volume can be defined as:

$$v_{mix}(P_0, T_0, x_{\mathrm{H_2O}}) = v_{\mathrm{H_2O}}(P_0, T_0) \cdot x_{\mathrm{H_2O}} + v_{\mathrm{N_2}}(P_0, T_0) \cdot (1 - x_{\mathrm{H_2O}}) \tag{A.2}$$

Specific volumes for pure water and nitrogen at 20 bar and 20°C were obtained from the NIST Chemistry Webbook [52] as 0.018 l/mol and 1.2 l/mol respectively.

At the desired reaction temperatures and pressures the ideal mixture assumption is not valid anymore, since the water and nitrogen will together form a supercritical vapor phase. The Aspen Plus software package was then used, with the Peng-Robinson EOS, to calculate the v_{mix} at P_1 and T_1. Equation A.1 was then solved for the molar fraction of water, and translated to the initial vol% of the reactor filled with water. Figure A.2 shows the inverse of the specific volume, the density, as a function of water volume fraction at 20 bar, 20°C and 250 bar, 550°C.

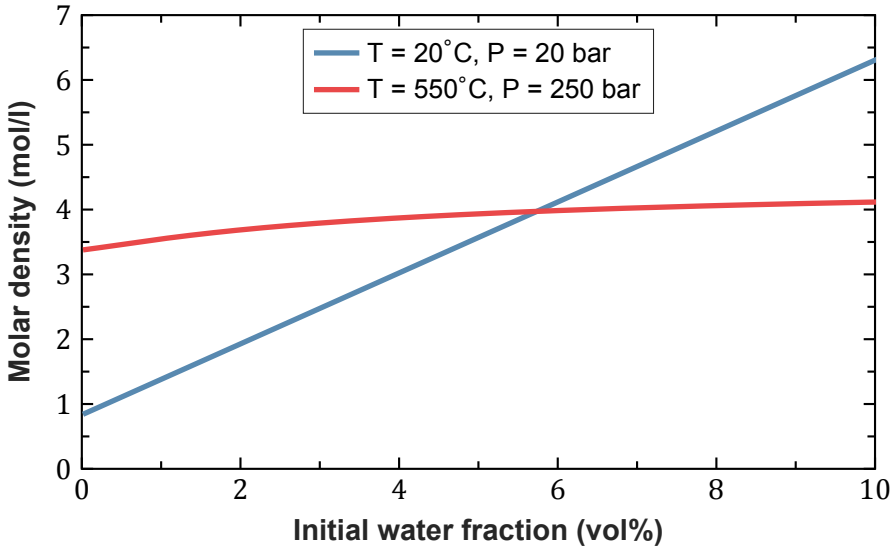

Figure A.2: Molar density of the binary water/nitrogen system as a function of initial water volume fraction at 20 bar, 20°C and 250 bar, 550°C

The initial water volume fraction needed can be found where the two graphs intersect. For reaction conditions of 250 bar, 550°C this is 5.7 vol%. The water fractions for the other reaction conditions are listed in Table A.2.

Table A.2: Initial volume fraction of water loaded in the reactor for the desired reaction temperatures and pressures T_1, P_1

P_1 (bar)	T_1 (°C)	Water (vol%)
250	550	5.7
250	450	7.8
250	380	11.9
250	340	48.8

B

Pressure and temperature data

B.1. Pressure measurements during experiments

Table B.1: Pressure measurements of the experiments performed at T = 400°C

T = 400°C	Experiment duration:	15 min	35 min	65 min	65 min
		P (bar)	P (bar)	P (bar)	P (bar)
Time	0 min	45	45	45	45
	1 min	-	-	-	-
	2 min	170	170	165	170
	3 min	-	-	-	-
	4 min	239	231	233	238
	5 min	-	-	-	-
	6 min	250	240	246	250
	7 min	-	-	-	-
	8 min	251	242	246	-
	9 min	-	-	-	-
	10 min	254	244	254	257
	14 min	258	-	-	-
	20 min	-	249	255	260
	35 min	-	251	259	262
	65 min	-		260	265

Table B.2: Pressure measurements of the experiments performed at T = 420°C

T = 420°C	Experiment duration:	15 min	35 min	65 min
		P (bar)	P (bar)	P (bar)
Time	**0 min**	45	46	42
	1 min	96	-	-
	2 min	170	170	162
	3 min	218	-	-
	4 min	230	229	230
	5 min	238	-	-
	6 min	241	241	240
	7 min	242	-	-
	8 min	245	249	245
	9 min	247	-	-
	10 min	249	250	249
	15 min	250	-	-
	20 min	-	258	254
	35 min	-	261	260
	65 min	-	-	265

Table B.3: Pressure measurements of the experiments performed at T = 460°C

T = 460°C	Experiment duration:	15 min	15 min	35 min	65 min
		P (bar)	P (bar)	P (bar)	P (bar)
Time	**0 min**	60	57	55	60
	1 min	-	-	-	-
	2 min	219	210	228	221
	3 min	-	-	-	-
	4 min	235	240	255	238
	5 min	-	-	-	-
	6 min	240	249	262	242
	7 min	-	-	-	-
	8 min	241	253	265	245
	9 min	-	-	-	-
	10 min	243	258	267	249
	15 min	247	262	-	-
	20 min	-	-	276	252
	35 min	-	-	287	256
	65 min	-	-	-	261

Table B.4: Pressure measurements of the experiments performed at T = 520°C

T = 520°C	**Experiment duration:**	**15 min**	**35 min**	**35 min**	**65 min**
		P (bar)	**P (bar)**	**P (bar)**	**P (bar)**
Time	**0 min**	60	60	65	60
	1 min	-	-	-	-
	2 min	215	210	221	212
	3 min	-	-	-	-
	4 min	228	230	240	230
	5 min	-	-	-	-
	6 min	232	239	248	239
	7 min	-	-	-	-
	8 min	235	241	250	241
	9 min	-	-	-	-
	10 min	237	242	252	242
	15 min	239	-	-	-
	20 min	-	250	260	249
	35 min	-	255	266	250
	65 min	-	-	-	251

B.2. Temperature measurements from thermocouple reactor

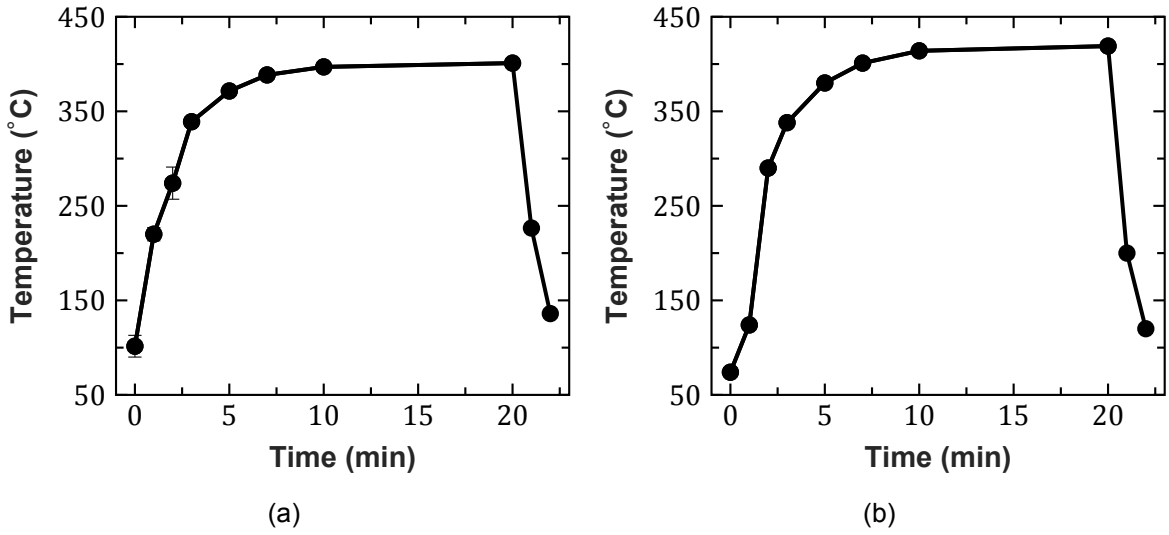

Figure B.1: Temperature measurements of thermocouple reactor at sand bath temperature T = 400°C (a) and T = 420°C (b)

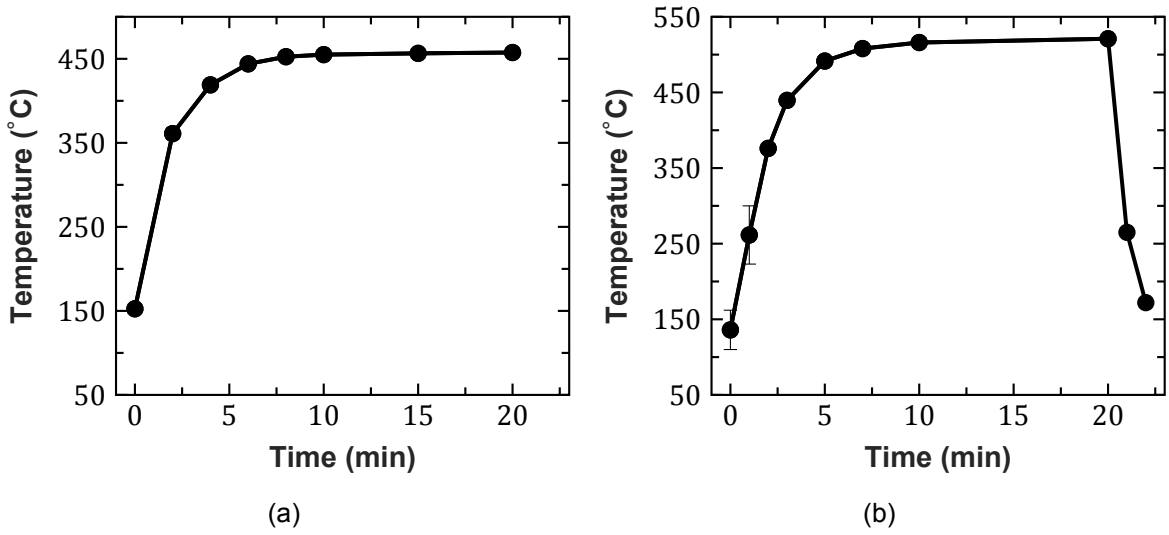

Figure B.2: Temperature measurements of thermocouple reactor at sand bath temperature T = 460°C (a) and T = 520°C (b)

C

Chemical analysis results

C.1. Gas GC calibration

The concentrations of gases in the standard calibration gas mixture were much higher then the concentrations of product gases in the gas samples from the experiments. Generally, the sample gas contained 90-99 mol% N_2. Product gases concentrations in the gas samples were therefore in the order of 0.1-5 mol%, while concentrations of gases in the calibration gas mixture were ranging from 0.5-55 mol%. To validate if the linear relationship between the standard calibration gas mixture and peak area would still hold for the lower gas concentration in the experimental gas samples, a calibration test was performed.

An empty gas bag was filled with 50 mL of standard calibration gas and subsequently diluted 9 times with nitrogen using a gas syringe. A 50 mL sample from this 1:10 calibration mixture was transferred to a second gas bag and was again diluted 9 times with nitrogen, obtaining a 1:100 calibration mixture . Three different calibration gas mixtures were then analyzed using the Gas GC. Table C.1 shows the results of the analysis of the standard gas calibration mixture and pure nitrogen gas, Table C.2 shows the results for the 1:10 calibration mixture and Table C.3 for the 1:100 calibration mixture. All GC measurements were performed twice for consistency. The concentrations of ethene and propene in the 1:100 calibration mixture were too low for GC detection.

Table C.1: Gas GC calibration results for the standard calibration mixture and pure nitrogen

Reference gas	Area meas. 1	Area meas. 2	Average	Concentration (mol%)
N_2	9.33E+05	9.31E+05	9.32E+05	100
CO_2	1.90E+05	2.10E+05	2.00E+05	18.1
Ethene	5.64E+03	5.60E+03	5.62E+03	0.514
Ethane	1.82E+04	1.79E+04	1.81E+04	1.49
Propene	7.80E+03	7.78E+03	7.79E+03	0.514
Propane	2.41E+04	2.38E+04	2.40E+04	1.50
Hydrogen	3.91E+05	3.84E+05	3.87E+05	55.2
Methane	1.67E+05	1.65E+05	1.66E+05	19.7
CO	3.17E+04	3.15E+04	3.16E+04	3

Linear relationships were then fitted between the average areas and the concentrations as shown in Tables C.1 to C.3 using Microsoft Excel 2016. Table C.4 shows the equations and

Table C.2: Gas GC calibration results for a 1:10 diluted calibration mixture with nitrogen

1:10 mix	Area meas. 1	Area meas. 2	Average	Concentration (mol%)
N_2	8.89E+05	8.84E+05	8.87E+05	90
CO_2	2.02E+04	2.00E+04	2.01E+04	1.81
Ethene	5.49E+02	5.45E+02	5.47E+02	0.0514
Ethane	1.73E+03	1.72E+03	1.72E+03	0.149
Propene	7.47E+02	7.60E+02	7.53E+02	0.0514
Propane	2.29E+03	2.20E+03	2.25E+03	0.150
Hydrogen	3.65E+04	3.94E+04	3.80E+04	5.52
Methane	1.60E+04	1.59E+04	1.60E+04	1.97
CO	3.00E+03	2.96E+03	2.98E+03	0.3

Table C.3: Gas GC calibration results for a 1:100 diluted calibration mixture with nitrogen

1:100 mix	Area meas. 1	Area meas. 2	Average	Concentration (mol%)
N_2	9.32E+05	9.30E+05	9.31E+05	99
CO_2	2.00E+03	1.96E+03	1.98E+03	0.181
Ethene	-	-	-	0.00514
Ethane	1.58E+02	1.84E+02	1.71E+02	0.0149
Propene	-	-	-	0.00514
Propane	2.36E+02	2.73E+02	2.55E+02	0.0150
Hydrogen	3.59E+03	3.60E+03	3.60E+03	0.552
Methane	1.48E+03	1.54E+03	1.51E+03	0.197
CO	3.49E+02	2.87E+02	3.18E+02	0.03

R^2 values for this linear fitting. The R^2 can be interpreted as the proportion of the variance in y, the measured peak area, attributable to the variance in z, the peak area calculated by the fit. The value of R^2 lies between 0 and 1, where 1 denotes the best fit possible. The equation for R^2 used by Excel is:

$$R^2 = \left[\frac{\sum(z - \tilde{z})(y - \tilde{y})}{\sqrt{\sum(z - \tilde{z})^2 \sum(y - \tilde{y})^2}} \right]^2 \tag{C.1}$$

where the ˜ sign denotes the average.

Table C.4: Linear fitting results of calibration data from the Gas GC

	Equation fit	**R^2**
N_2	-394.44x^2 + 79494x - 3E+06	1.000
CO_2	11050x	1.000
Ethene	10926x	1.000
Ethane	12109x	1.000
Propene	15154x	1.000
Propane	15957x	1.000
Hydrogen	7017.1x	1.000
Methane	8423.1x	1.000
CO	10534x	1.000

From the high R^2 values it can be concluded that all product gases show a good linear relationship between molar concentration and GC peak area. Nitrogen calibration data could not be fitted well using a linear equation. Reason for this is probably the saturation of the TCD at the high gas concentration of more then 90 mol%. It was chosen to fit the three calibration data points of nitrogen at 90, 99 and 100 mol% with a second order polynomial. This equation showed a high R^2 value and was therefore used for the quantification of nitrogen in the gas samples.

C.2. GC-MS calibration

The GC-MS was calibrated using mixtures of 5000, 500 and 50 ppm-by-mass of oleic acid. It was assumed that the linear relation between concentration and peak area found for these three mixtures would be applicable to the liquid sample concentrations between 30 and 8000 ppm by mass measured by GC-MS analysis. The internal standard hexadecane concentration in the calibration mixtures was 500 ppm-by-mass. For both oleic acid and hexadecane a response factor (RF) was calculated. From these response factors a relative response factor (RRF) between oleic acid and hexadecane was found. The RRF could be used to quantify oleic acid in a liquid sample using a known amount of internal standard in the sample. The RF and RRF are defined as:

$$\mathrm{RF} = \frac{\text{Peak Area}}{\text{Concentration}} \tag{C.2}$$

$$\mathrm{RRF} = \frac{\mathrm{RF}_{\text{oleic acid}}}{\mathrm{RF}_{\text{int std}}} \tag{C.3}$$

Table C.5 shows the measurement results of the calibration mixtures and calculated RF and RRF. The R^2 values are related to the linear relationship between concentration and peak area of both oleic acid and hexadecane.

Table C.5: Calibration results for GC-MS analysis of oleic acid

Oleic acid	**Concentration (g/g)**	**Peak area**	**RF**	**RRF**
	4.342E-03	2.222E+08	5.118E+10	8.417E-01
	4.970E-04	2.266E+07	4.559E+10	7.416E-01
	5.657E-05	3.126E+06	5.526E+10	8.924E-01
Average			5.068E+10	8.253E-01
R^2			0.9998	

Hexadecane	**Concentration (g/g)**	**Peak area**	**RF**
	2.159E-04	1.313E+07	6.080E+10
	4.748E-04	2.919E+07	6.147E+10
	5.009E-04	3.102E+07	6.192E+10
Average			6.140E+10
R^2			0.9999

C.3. 2D-GC calibration

A similar procedure as presented in C.2 was executed for the 2D-GC. The 2D-GC used an FID for which it was known that the response was strictly linear for all components between 0 and 1000 ppm. All found concentrations of individual liquid components from experimental samples by 2D-GC analyses were in this range. For consistency two calibration mixtures were analyzed with chemical concentrations of 500 and 250 ppm-by-mass, as shown in Table C.6 and Table C.7, respectively. Averages of the RRFs of these two measurments used for experimental analyses are shown in Table C.8.

Table C.6: 2D-GC calibration results for the 500 ppm mixture

500 ppm	Compound	Intensity	Concentration (g/g)	RF	RRF
	Acetic Acid	2.632E+06	5.345E-04	4.924E+09	3.152E-01
	Propiophenone	9.315E+06	5.028E-04	1.853E+10	1.186E+00
	Hexadecane	9.570E+06	4.679E-04	2.045E+10	1.309E+00
	DBE	8.255E+06	5.284E-04	1.562E+10	1.000E+00
	Cyclo-octane	1.245E+07	5.490E-04	2.268E+10	1.452E+00
	n-Heptane	1.079E+07	4.867E-04	2.216E+10	1.419E+00
	o-Xylene	1.374E+07	5.284E-04	2.600E+10	1.664E+00

Table C.7: 2D-GC calibration results for the 250 ppm mixture

250 ppm	Compound	Intensity	Concentration (g/g)	RF	RRF
	Acetic Acid	1.345E+06	2.713E-04	4.959E+09	3.051E-01
	Propiophenone	4.736E+06	2.552E-04	1.856E+10	1.142E+00
	Hexadecane	5.161E+06	2.375E-04	2.173E+10	1.337E+00
	DBE	4.359E+06	2.682E-04	1.626E+10	1.000E+00
	Cyclo-octane	6.589E+06	2.786E-04	2.365E+10	1.454E+00
	n-Heptane	5.788E+06	2.470E-04	2.343E+10	1.441E+00
	o-Xylene	7.270E+06	2.682E-04	2.711E+10	1.668E+00

Table C.8: Average relative response factors for the 2D-GC calibration as used for experimental analysis

Compound	Average RRF
Acetic Acid	3.101E-01
Propiophenone	1.164E+00
Hexadecane	1.323E+00
DBE	1.000E+00
Cyclo-octane	1.453E+00
n-Heptane	1.430E+00
o-Xylene	1.666E+00

C.4. Used chemicals

Table C.9: List of chemicals used for analysis

Chemical	Purity	Supplier
Acetic acid (glacial)	100%	Merck KGaA
Acetone	≥99.5%	Boom Chemicals
Cyclo-Octane	≥99%	Aldrich
Di-n-Buthylether	≥99%	-
Hexadecane	≥99%	Janssen Chimica
n-Heptane	≥99%	Acros Organics
Nitrogen	≥99.9%	Hoekloos
O-Xylene	≥98%	JT Baker
Propiophenone	≥99%	Acros Organics
Trimethylsulfonium hydroxide	0.25 M in MeOH	Sigma Aldrich

C.5. 2D-GC 2D plots

C.5.1. T = 400

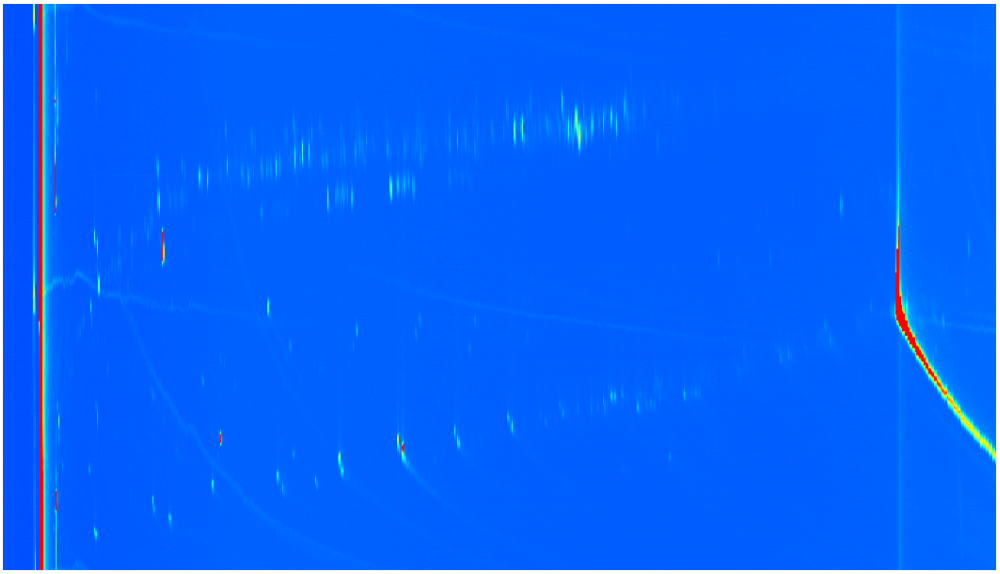

Figure C.1: 2D-plot of 2D-GC analysis performed on sample liquid from an experiment at T = 400°C and residence time of 15 min.

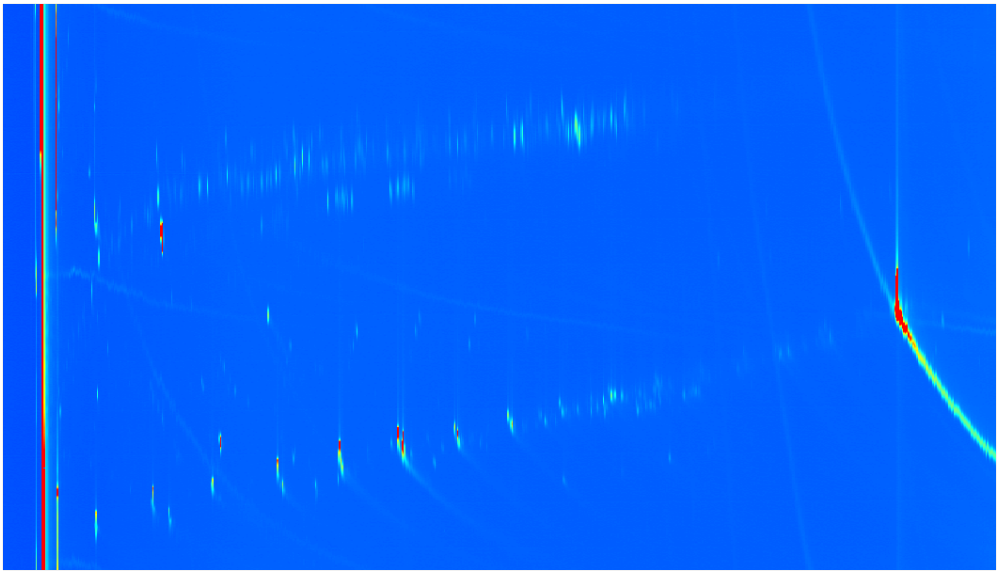

Figure C.2: 2D-plot of 2D-GC analysis performed on sample liquid from an experiment at T = 400°C and residence time of 35 min.

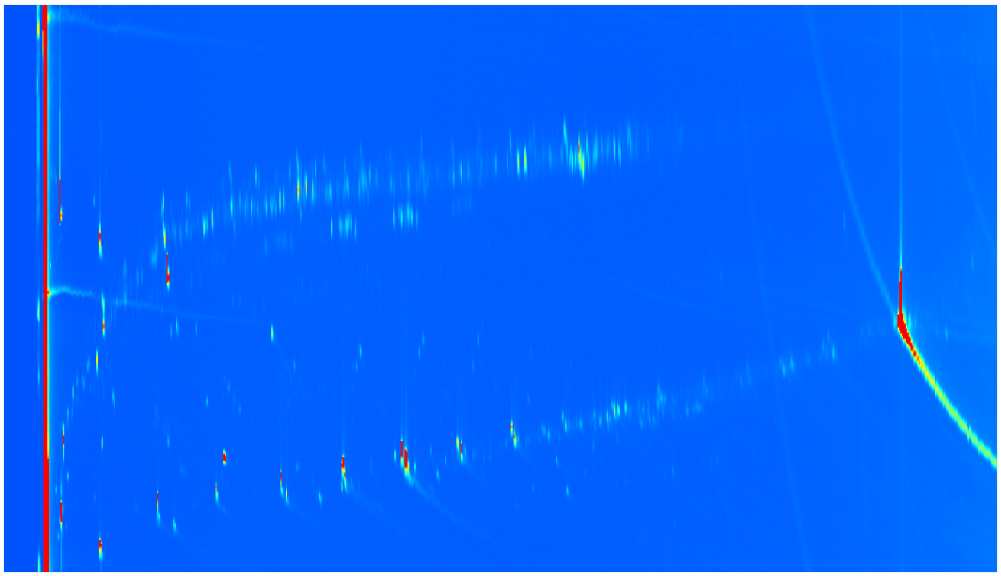

Figure C.3: 2D-plot of 2D-GC analysis performed on sample liquid from an experiment at T = 400°C and residence time of 65 min.

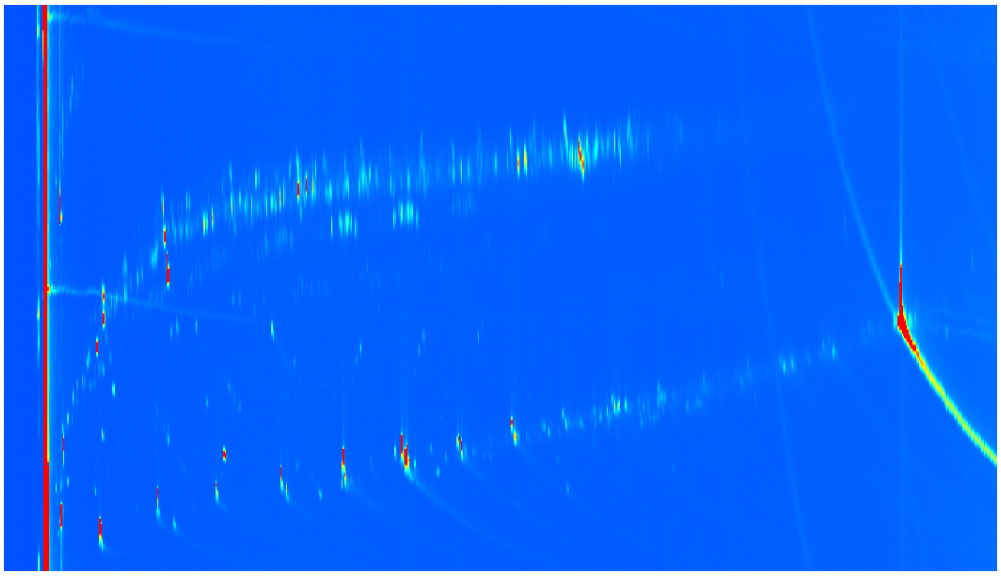

Figure C.4: 2D-plot of 2D-GC analysis performed on sample liquid from an experiment at T = 400°C and residence time of 65 min.

C.5.2. T = 420

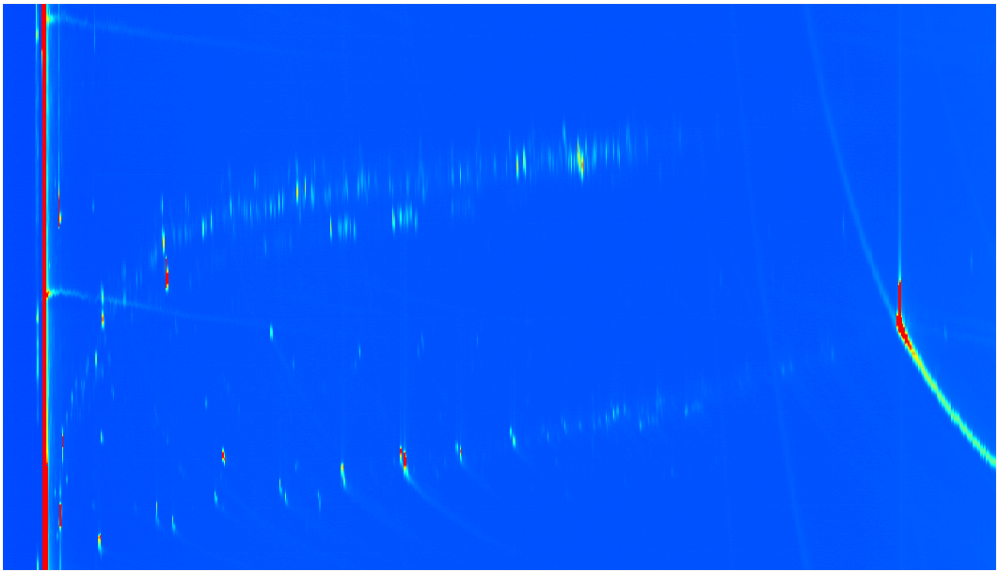

Figure C.5: 2D-plot of 2D-GC analysis performed on sample liquid from an experiment at T = 420°C and residence time of 15 min.

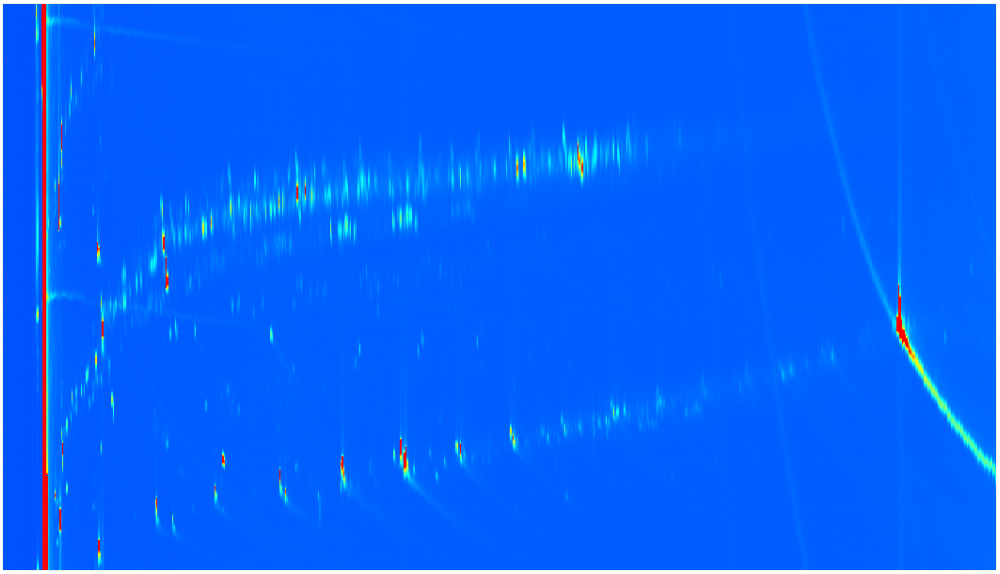

Figure C.6: 2D-plot of 2D-GC analysis performed on sample liquid from an experiment at T = 420°C and residence time of 35 min.

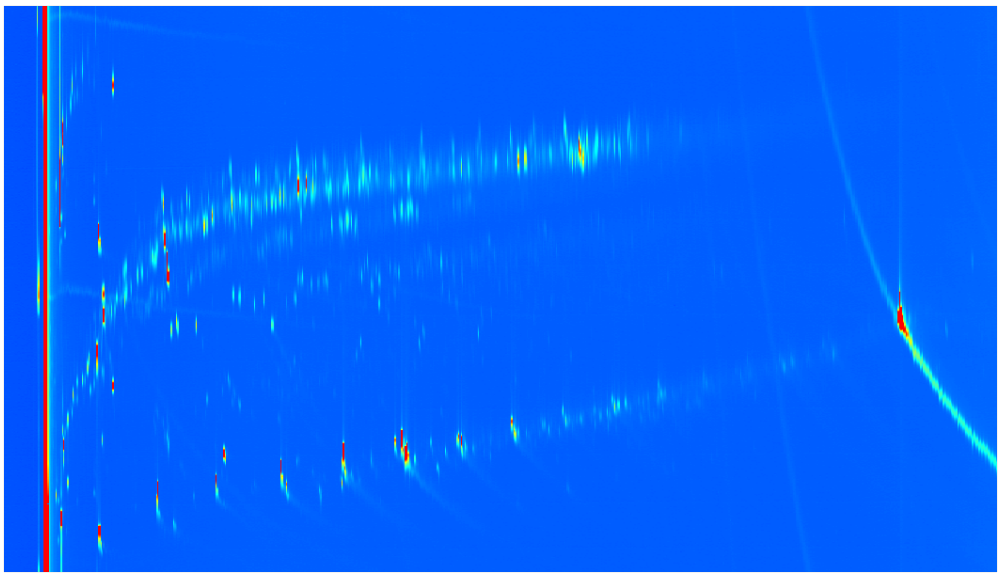

Figure C.7: 2D-plot of 2D-GC analysis performed on sample liquid from an experiment at T = 420°C and residence time of 65 min.

C.5.3. T = 460

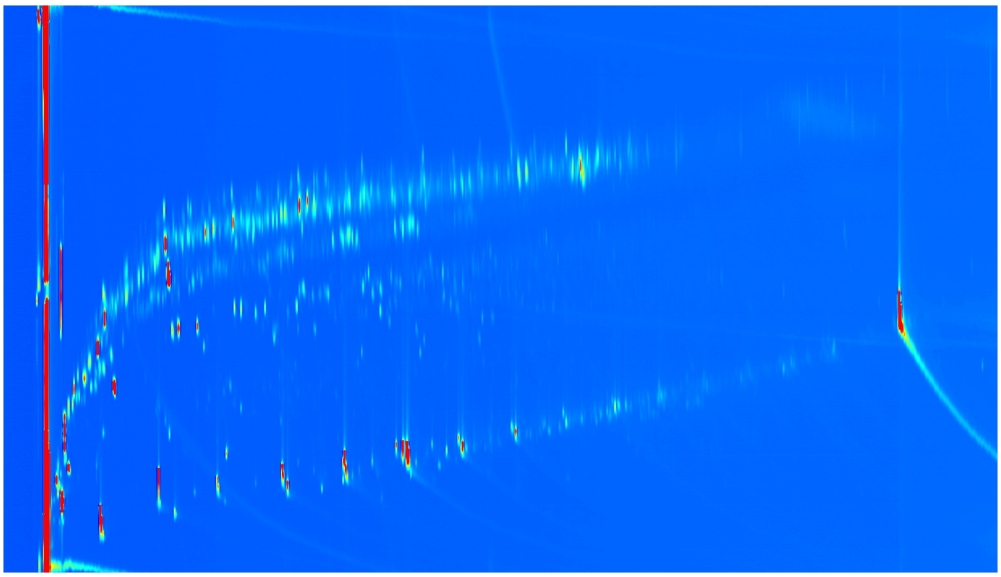

Figure C.8: 2D-plot of 2D-GC analysis performed on sample liquid from an experiment at T = 460°C and residence time of 15 min.

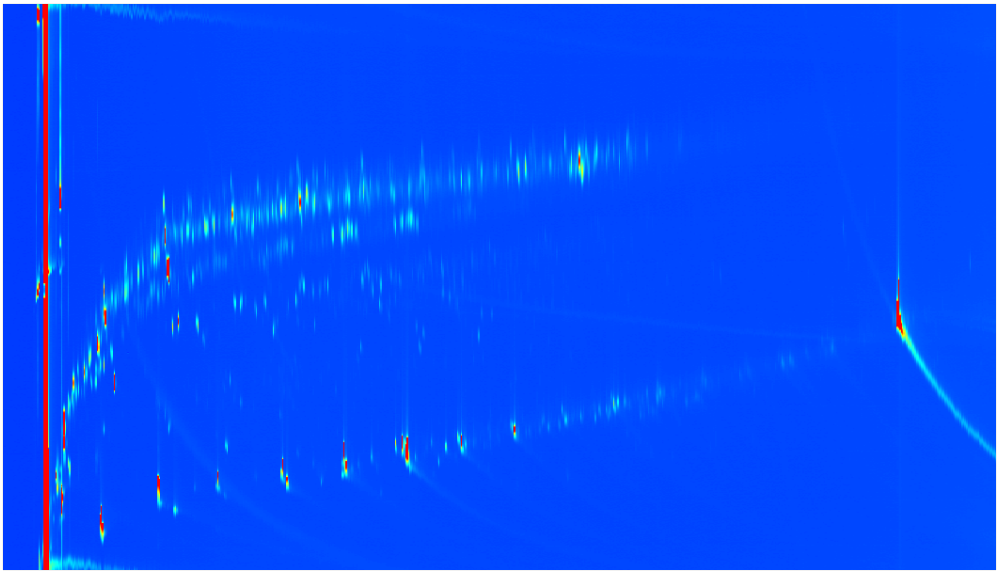

Figure C.9: 2D-plot of 2D-GC analysis performed on sample liquid from an experiment at T = 460°C and residence time of 15 min.

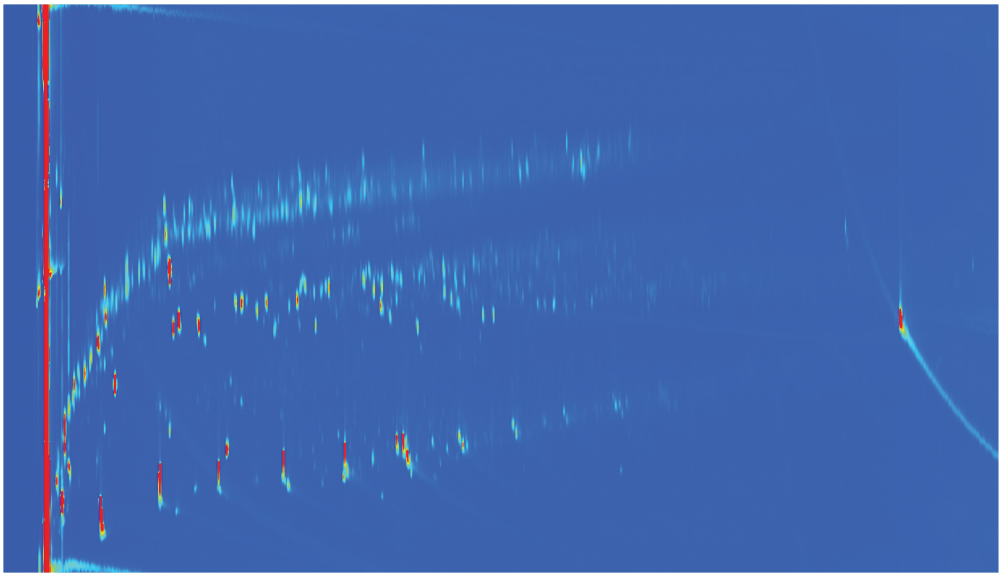

Figure C.10: 2D-plot of 2D-GC analysis performed on sample liquid from an experiment at T = 460°C and residence time of 35 min.

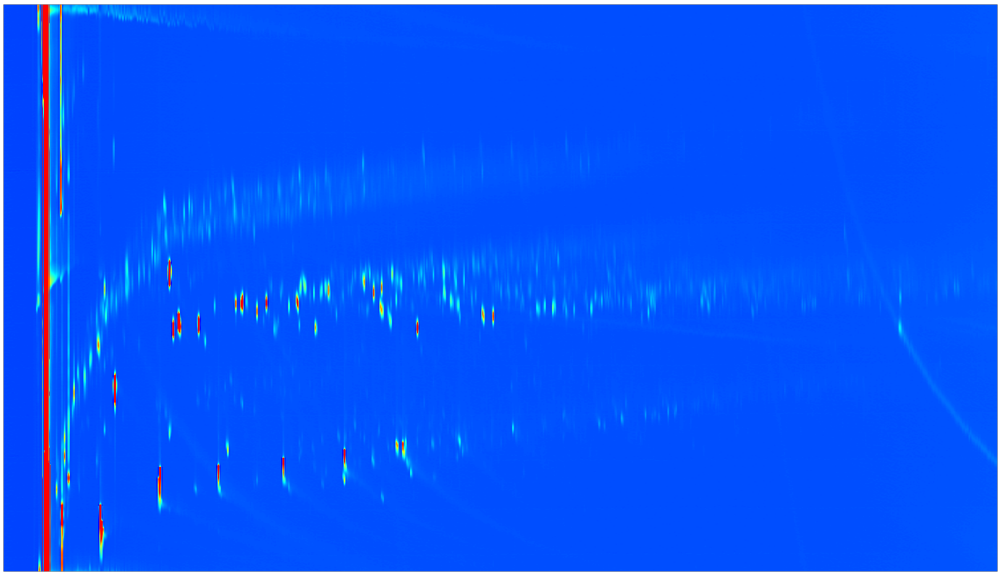

Figure C.11: 2D-plot of 2D-GC analysis performed on sample liquid from an experiment at T = 460°C and residence time of 65 min.

C.5.4. T = 520

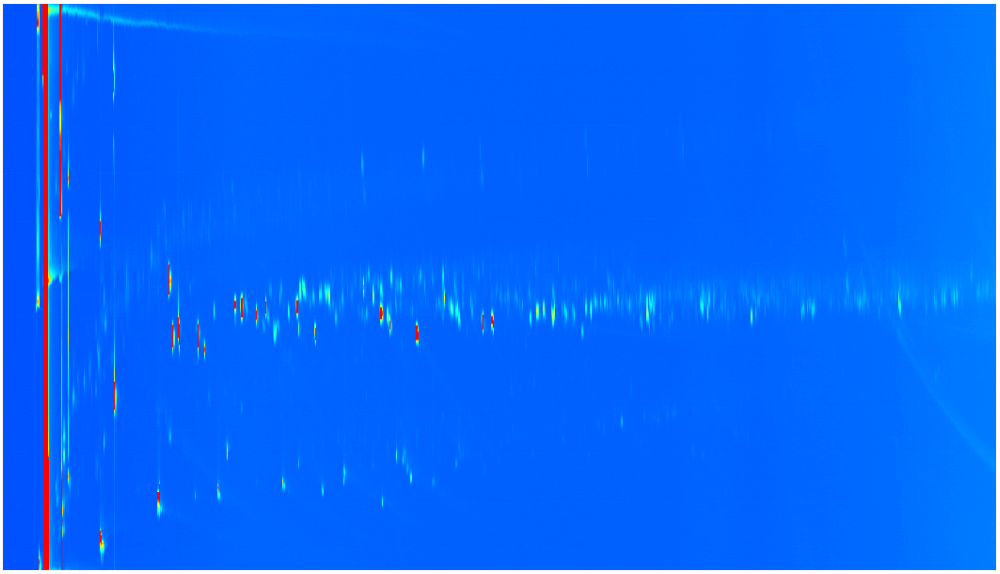

Figure C.12: 2D-plot of 2D-GC analysis performed on sample liquid from an experiment at T = 520°C and residence time of 15 min.

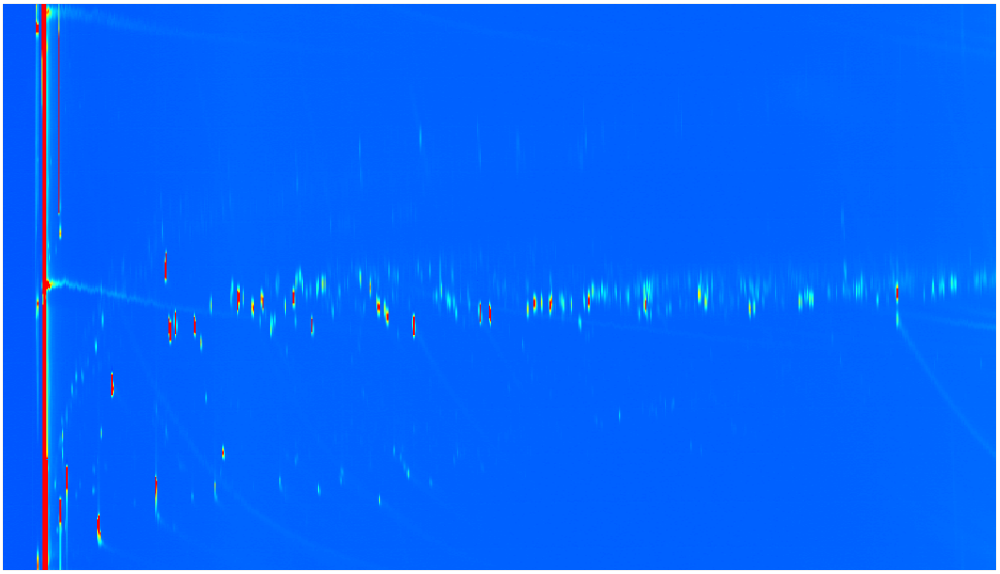

Figure C.13: 2D-plot of 2D-GC analysis performed on sample liquid from an experiment at T = 520°C and residence time of 35 min.

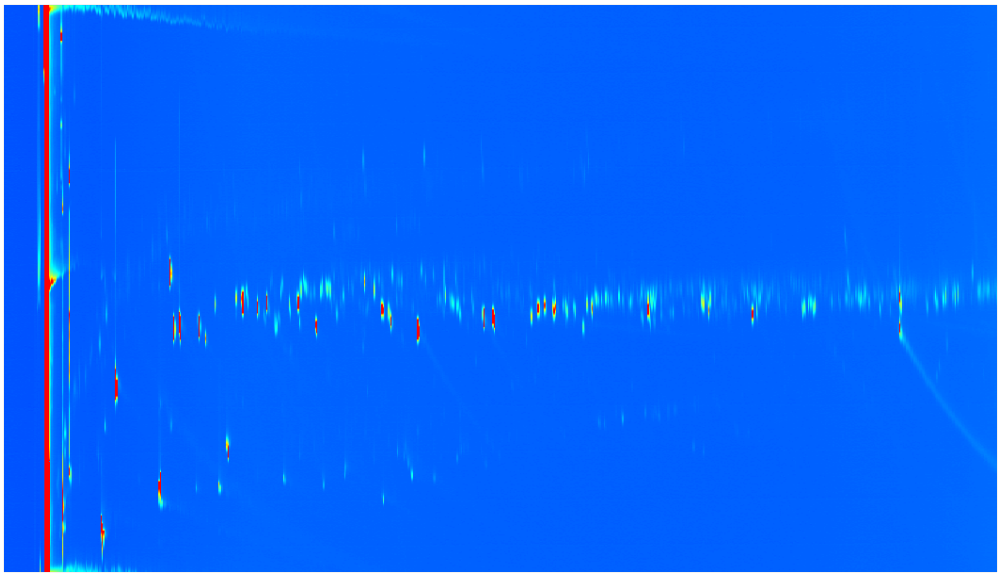

Figure C.14: 2D-plot of 2D-GC analysis performed on sample liquid from an experiment at T = 520°C and residence time of 35 min.

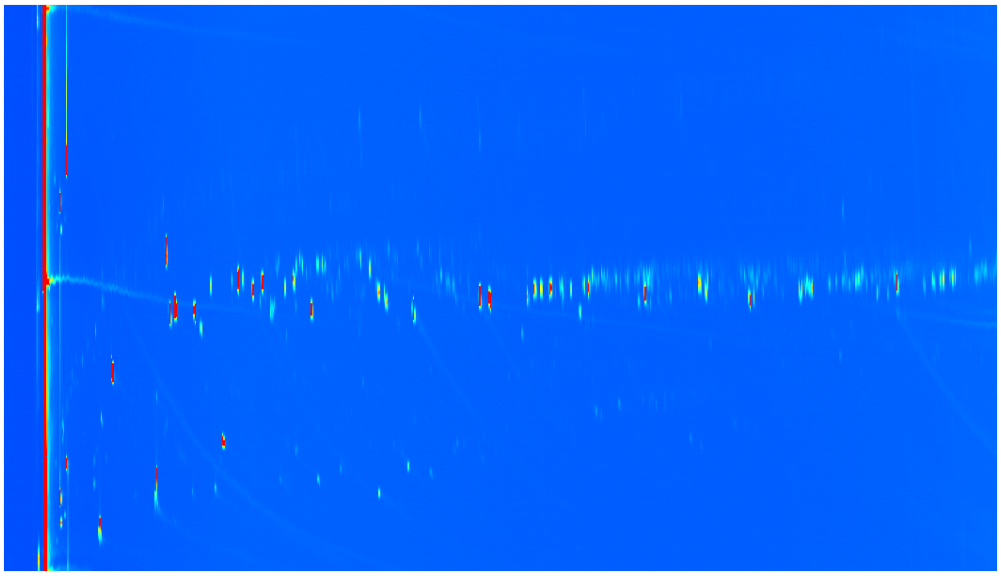

Figure C.15: 2D-plot of 2D-GC analysis performed on sample liquid from an experiment at T = 520°C and residence time of 65 min.

C.6. Oleic acid concentration results

Table C.10: Oleic acid concentration results from GC-MS analyses. Concentrations are in mmol/L

Time (min)	0	10	15	35	65
400°C	55.3	34.7	29.8	24.6	24.0 ±0.010
420°C	45.6	-	21.5	15.8	11.2
460°C	36.1	-	5.55 ±1.31	3.21	0.350
520°C	28.7	-	0.514	0.416 ±0.367	0.146

C.7. Assumed carbon weight percentages

Table C.11: Carbon weight percentages used for calculation of carbon mass balance. Weight percentages used for FAs were between the presented numbers in this table. Their exact value was the result of a weighed average of the fatty acids detected from GC-MS analysis.

Compound group	Carbon (wt%)
VFA	55-66
Small Aliphatic HC	85
Naphtalenes	94
Methylesters	67
LFA	67-76
Ketones & Alcohols	73
Large Aliphatic HC	85
Cycloalkanes	87
Aromatics	91

D

Kinetic model analysis

D.1. Sensitvity coefficients

Table D.1: Absolute sensitivity coefficients for T = 420°C. A value of 1 means that a 5% perturbation in the reaction rate results in a 5% change in product concentration

		[Oleic]	[Oxy]	[Aliph]	[Cyc]	[H_2]	[CH_4]	[C_aH_b]	[CO_2]	[CO]
5 min	k_1	0.195	0.900	0.893	0.932	0.705	0.932	0.932	0.934	0.932
60 min	k_1	2.220	0.123	0.260	0.344	0.095	0.355	0.344	0.439	0.303
5 min	k_2	0.000	0.023	0.024	0.015	0.012	0.014	0.015	0.968	0.016
60 min	k_2	0.000	0.342	0.277	0.150	0.080	0.109	0.150	0.690	0.243
5 min	k_3	0.000	0.005	0.005	0.003	0.008	0.003	0.003	0.013	0.996
60 min	k_3	0.000	0.075	0.061	0.033	0.162	0.024	0.033	0.077	0.944
5 min	k_4	0.000	0.000	0.013	0.991	0.988	0.008	0.009	0.000	0.000
60 min	k_4	0.001	0.000	0.066	0.950	0.829	0.042	0.048	0.000	0.001
5 min	k_6	0.000	0.001	0.000	0.000	0.000	0.056	0.000	0.001	0.001
60 min	k_6	0.000	0.012	0.005	0.001	0.001	0.120	0.001	0.006	0.008
5 min	k_8	0.000	0.000	0.014	0.009	0.007	0.935	0.009	0.000	0.000
60 min	k_8	0.000	0.000	0.071	0.051	0.011	0.831	0.051	0.000	0.000
5 min	k_9	0.000	0.000	0.212	0.140	0.109	0.133	0.853	0.000	0.000
60 min	k_9	0.001	0.000	1.019	0.742	0.164	0.652	0.221	0.000	0.000
5 min	k_{11}	0.000	0.000	0.000	0.000	0.231	0.000	0.000	0.000	0.000
60 min	k_{11}	0.001	0.000	0.000	0.000	0.930	0.000	0.000	0.000	0.000
5 min	k_{-12}	0.000	0.000	0.000	0.000	0.005	0.000	0.000	0.015	0.078
60 min	k_{-12}	0.000	0.000	0.000	0.000	0.053	0.000	0.000	0.053	0.717

Table D.2: Sensitivity coefficients for T= 460°C. A value of 1 means that a 5% perturbation in the reaction rate results in a 5% change in product concentration

		[Oleic]	[Oxy]	[Aliph]	[Cyc]	[H_2]	[CH_4]	[C_aH_b]	[CO_2]	[CO]
5 min	k_1	0.765	0.641	0.547	0.735	0.140	0.736	0.735	0.762	0.757
60 min	k_1	7.652	0.141	0.159	0.031	0.054	0.034	0.031	0.081	0.027
5 min	k_2	0.000	0.044	0.052	0.029	0.006	0.028	0.029	0.957	0.028
60 min	k_2	0.003	0.810	0.001	0.173	0.136	0.133	0.173	0.516	0.461
5 min	k_3	0.000	0.011	0.014	0.008	0.005	0.007	0.008	0.008	0.992
60 min	k_3	0.001	0.215	0.003	0.046	0.246	0.035	0.046	0.049	0.871
5 min	k_4	0.000	0.000	0.057	0.962	0.989	0.036	0.037	0.000	0.000
60 min	k_4	0.286	0.000	0.087	0.917	0.733	0.073	0.079	0.000	0.002
5 min	k_6	0.000	0.002	0.000	0.000	0.000	0.019	0.000	0.001	0.001
60 min	k_6	0.000	0.035	0.033	0.005	0.001	0.071	0.005	0.014	0.020
5 min	k_8	0.000	0.000	0.112	0.071	0.014	0.908	0.071	0.000	0.000
60 min	k_8	0.271	0.000	0.167	0.154	0.035	0.774	0.154	0.000	0.001
5 min	k_9	0.000	0.000	0.532	0.341	0.069	0.335	0.642	0.000	0.000
60 min	k_9	0.005	0.000	0.779	0.724	0.174	0.669	0.239	0.000	0.000
5 min	k_{11}	0.000	0.000	0.000	0.000	0.775	0.000	0.000	0.000	0.000
60 min	k_{11}	0.088	0.000	0.000	0.000	0.887	0.000	0.000	0.000	0.001
5 min	k_{-12}	0.000	0.000	0.000	0.000	0.003	0.000	0.000	0.014	0.059
60 min	k_{-12}	0.000	0.000	0.000	0.000	0.093	0.000	0.000	0.068	0.771

Table D.3: Sensitivity coefficients for T= 520°C. A value of 1 means that a 5% perturbation in the reaction rate results in a 5% change in product concentration

		[Oleic]	[Oxy]	[Aliph]	[Cyc]	[H_2]	[CH_4]	[C_aH_b]	[CO_2]	[CO]
5 min	k_1	4.987	0.021	0.537	0.050	0.007	0.052	0.050	0.189	0.182
60 min	k_1	10.403	0.042	0.042	0.001	0.005	0.001	0.001	0.004	0.011
5 min	k_2	0.001	0.141	0.526	0.093	0.005	0.091	0.093	0.911	0.072
60 min	k_2	15.224	1.935	1.249	0.072	0.090	0.045	0.072	0.261	0.731
5 min	k_3	0.000	0.048	0.179	0.032	0.010	0.031	0.032	0.009	0.974
60 min	k_3	0.160	0.680	0.431	0.025	0.269	0.016	0.025	0.034	0.734
5 min	k_4	0.002	0.000	0.110	0.897	0.985	0.097	0.098	0.000	0.000
60 min	k_4	0.550	0.000	0.101	0.896	0.711	0.095	0.099	0.000	0.002
5 min	k_6	0.000	0.008	0.006	0.001	0.000	0.013	0.001	0.004	0.004
60 min	k_6	0.020	0.113	0.112	0.015	0.000	0.024	0.015	0.032	0.042
5 min	k_8	0.011	0.000	0.500	0.447	0.031	0.524	0.447	0.000	0.000
60 min	k_8	7.829	0.003	0.464	0.453	0.057	0.503	0.453	0.000	0.001
5 min	k_9	0.006	0.000	0.471	0.421	0.029	0.415	0.558	0.000	0.000
60 min	k_9	2.840	0.001	0.435	0.427	0.053	0.409	0.552	0.000	0.000
5 min	k_{11}	0.000	0.000	0.000	0.000	0.888	0.000	0.000	0.000	0.000
60 min	k_{11}	0.001	0.000	0.000	0.000	0.786	0.000	0.000	0.000	0.002
5 min	k_{-12}	0.000	0.000	0.000	0.000	0.008	0.000	0.000	0.014	0.045
60 min	k_{-12}	0.417	0.000	0.000	0.000	0.149	0.000	0.000	0.094	0.743

D.2. Approximate confidence interval

This description of the approximate confidence interval method was previously made by Danon et al. [53].

The approximate method described by Smith et al. [55] is based on the comparison between two sets of predicted values. The first set is calculated with the kinetic parameters from the model. The second set is calculated with one of these parameters varied by a small step (1% in this case). The parameter sensitivity coefficient is then defined as,

$$\frac{\partial y_i^{mod}}{\partial p_i} = \frac{y_{p_i+\Delta p_i}^{mod} - y_{p_i}^{mod}}{\Delta p_i} \tag{D.1}$$

where p_i represents the i^{th} estimated parameter and Δp_i the variation in p_i.

The overall sensitivity of the model is then represented by a sensitivity matrix **A**, with size i by i, where the diagonal values are the squared sensitivity coefficients of the individual parameters. Next, the single-parameter standard error can be calculated from these diagonal values of the mean square error matrix V, which is related to the inverse of the sensitivity matrix **A**,

$$V = \sigma^2 A^{-1} \tag{D.2}$$

where σ^2 is the sum of square (absolute) errors. The 95% confidence interval is assumed to be approximately two times this single- parameter standard error.